# CORRELATION OF GEOTECHNICAL PROPERTIES OF BASALTS WITH ULTRASONIC VELOCITY IN GAZİANTEP REGION

M. Sc. Thesis

in

Civil Engineering

University of Gaziantep

Superviser

Assist. Prof. Dr. Hanifi ÇANAKCI

By

Teoman ERŞAN

July 2005

**ACKNOWLEDGEMENTS**

I express my sincere appreciation to my superviser Assist. Prof. Dr. Hanifi ÇANAKCI for his guidance and suggestions during the preparation of this thesis. My special thanks are extend to Assist. Prof. Dr. Hamza GÜLLÜ for his support and his suggestions.

I especially thank my friend Levent MARANGOZ for his self-sacrificing, support and suggestions.

Thanks also go to my mother, my father, my sister Emine, my sister Kübra and my brother Mahmut for their endurance, reassurance and support.

## ABSTRACT

### CORRELATION OF GEOTECHNICAL PROPERTIES OF BASALTS WITH ULTRASONIC VELOCITY IN GAZİANTEP REGION

ERŞAN, Teoman

M. Sc. in Civil Eng.

Supervisor: Assist. Prof. Dr. Hanifi ÇANAKCI

July 2005, 154 pages

The physical and mechanical properties of rocks are the most important concerns for geotechnical engineering. The properties of rocks and soil that the construction will be made on should be determined carefully. Large volume of basalt deposits dominantly exist in few areas of the Gaziantep Region. In this thesis, in order to remove the absence of studies about basalt in Gaziantep some rock mechanic tests were made with the exactly 179 samples collected from Gaziantep. Variety of basalt samples were taken as samples for each test. Ultrasonic Velocity, Brazillian Tensile, Direct Shear, Uniaxial Compressive Tests were performed and index properties such as dry-bulk-saturated densities, water absorbtion were determined on selected specimens in laboratory conditions. The tests were made according to International Society for Rock Mechanics ISRM (1981). The estimated ultrasonic velocity values were also correlated against the physical and mechanical properties of the Gaziantep basalt and multiple correlation coefficient up to a $R^2 \approx 0.67$ was obtained.



Key words: basalt, ultrasonic velocity, Brazillian tensile test, direct shear test, uniaxial compression test.

# ÖZET

## GAZİANTEP BÖLGESİNDEKİ BASALTLARIN GEOTEKNİK ÖZELLİKLERİYLE SONİK HIZ ARASINDA İLİŞKİNİN KURULMASI

ERŞAN, Teoman
Yüksek Lisans Tezi, İnş. Müh. Bölümü
Tez Yöneticisi: Yrd. Doç. Dr. Hanifi ÇANAKCI
Temmuz 2005, 154 Sayfa

Kayaların fiziksel ve mekanik özellikleri geoteknik mühendisliği açısından çok önemli bir konudur. Üzerine yapı inşa edilecek kayaların ve zeminlerin özellikleri dikkatlice belirlenmelidir. Büyük miktarlarda Bazalt yatakları Gaziantep yöresinin bazı alanlarında baskın bir şekilde yer almaktadır. Bu çalışmada, Gaziantep yöresindeki bazalt hakkındaki eksik çalışmaları ortadan kaldırmak için; Gaziantep' ten toplanan 179 numune üzerinde bazı mekanik kaya testleri yapıldı. Her bir deney için çeşitli bazalt numuneleri toplandı. Laboratuar koşullarında, seçilen numuneler üzerinde sonik hız, Brazil çekme, direkt kesme, tek eksenli basınç testleri ve kuru, ıslak yoğunluklar, su emme gibi indeks özellikler tespit edildi. Tüm deneyler uluslar arası kaya mekaniği deney standardı ISRM (1981)' ye uygun olarak yapılmıştır. Gaziantep bazaltının sonik hızı ile fiziksel ve mekanik özellikleri lineer korelasyon ve çoklu korelasyonla ilişkilendirildiğinde çoklu korelasyon katsayısı ($R^2 \approx 0.67$) ye varan değerler elde edilmiştir.

Anahtar kelimeler: bazalt, sonik hız, Brazil çekme deneyi, direkt kesme deneyi, tek eksenli basınç deneyi

**TABLE OF CONTENTS**

**LIST OF FIGURES**

## LIST OF SYMBOLS

Brz. = Brazillian tensile strength calculated with force divided by original area

Brz.$^{*}$ = Brazillian tensile strength calculated with force divided by fractured area

D. M. = Dry mass

Diam. = Diameter

L = Length

$l_o$ = Original measured axial length

$M_{sub}$ = Submerged mass of sample

$M_{sat}$ = Saturated mass of sample

$M_s$ = Dry mass of sample

N = Normal force

S. S. M. = Saturated – submerged – mass

S. S. D. M.= Saturated – surface – dried – mass

T = Shear force

Thick. = Thickness

Uni. Comp. Str. = Uniaxial Compressive Strength

$V_p$ = Velocity of the longitudinal wave

$V_s$ = Velocity of the shear wave

$W_{abs}$ = Water absorbtion

$\Delta L$ = Change in measured axial length

**LIST OF TABLES**

# CHAPTER 1

# INTRODUCTION

## 1.1. General

In order to remove the absence of studies about basalt in Gaziantep some rock mechanic tests were made with the samples collected from Gaziantep. Several tests such as uniaxial compression, direct shear, brazillian, ultrasonic velocity tests were performed. Also the parameters; water absorption, dry and saturated density, friction angle, cohesion were determined. The tests are made according to International Society for Rock Mechanics (ISRM), American Society for Testing and Materials (ASTM). This experimental studies were made to investigate some geotechnical properties of basalt which exist in Gaziantep city.

Reliable estimates of the strength and deformation characteristics of rock masses are required for almost any from of analysis used for the design of slopes, foundations and underground excavations. Large volume of basalt deposits dominantly exist in few areas of the Gaziantep Region. Industrial plants, residential house and highway construction increasing in Gaziantep in last two decades. Some of these activities take places on this large volume of basalt deposit. Therefore, for reliable design of foundation, slope and underground excavation geotechnical properties of this formation need to be determined.

Basalt occurring in Gaziantep region is called Yavuzeli Basalt. This extrusive and basic igneous rock is reddish dark brown; dark gray and blackish colored and very thick layered place to place. It has vesicular amygdaloidal texture. Some of the vesicles are filled with calcite. This unit was generally formed by flow of lava. It

overlies on some pyroclastic deposits. There are different ideas about the formation of this lava. Some groups explain this lava flow with the East Anatolian Fault and other faults related to main fault. Others explain it with the tectonic movements activated during Middle Miocene [9].

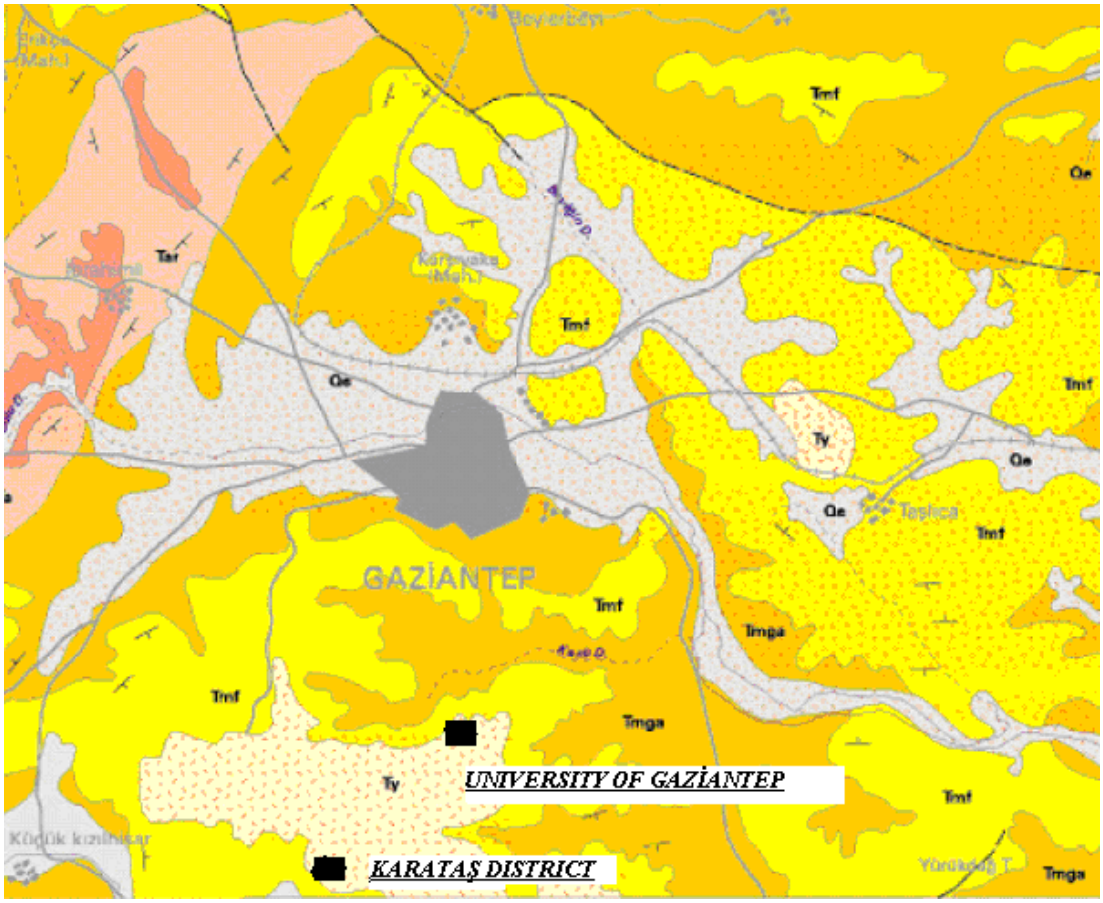


Figure 1.1a. Geologic map of the Gaziantep [50]

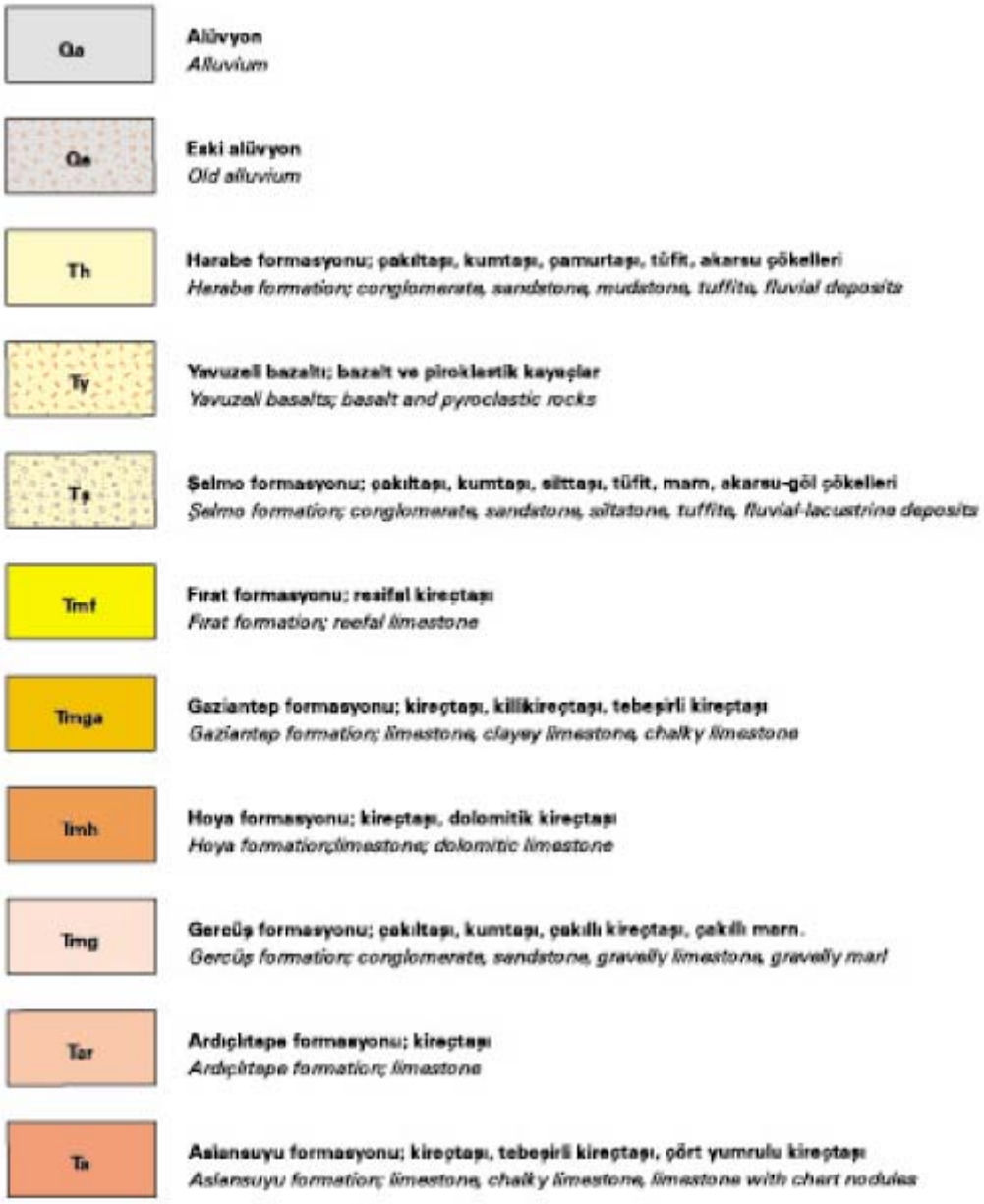


Figure 1.1b. Legend

This thesis contains a regional study. Study was done in Gaziantep region. Figure 1.1a shows the geologic map of the Gaziantep and Figure 1.1b shows the description of map units. In this region a study like in this thesis has not done before. All experiments have one repetition number.

The study aims to investigate the Physical and mechanical properties of basalt present in Gaziantep with rock mechanics tests to correlate rock properties of basalts with ultrasonic velocity in Gaziantep region. This is done for evaluating the

mechanical and physical properties of rock using nondestructive method (ultrasonic velocity test). Because ultrasonic test machine is portable and rechargeable. Ultrasonic test equipment can be used everywhere you want. It can be achieved many physical and mechanical properties of rock only performing the ultrasonic velocity test to calculate the sonic velocity of the specimen easily. because it is very easy to calculate the sonic velocity of a specimen.

Exactly 179 samples, taken from Karataş region, area which is on the way of the Gaziantep to Kilis and University of Gaziantep Campus, were used to determine the rock properties of basalt.

The experiments conducted are as follows :

Index properties :

- Dry and saturated densities
- Water absorption

Mechanical or strength properties :

- Ultrasonic velocity
- Uniaxial compressive
- Indirect tensile (Brazillian Test)
- Direct shear

## 1.2. Organization of The Thesis

The thesis is divided into 6 chapters, which are arranged as follows;

A literature review of the general properties of basalt is given in chapter 2.

In chapter 3, experimental studies are defined.

Chapter 4 includes the test results and correlations.

Chapter 5 includes the discussion

Chapter 6 contains the conclusions drawn from this research work and the recommendations for future study are given.

# CHAPTER 2

# LITERATURE SURVEY

## 2.1. Introduction

Basalt is an extrusive igneous rock. In this section a general information is given about igneous rocks and basalt. Additionally, preceding studies are have a part in.

## 2.2. Igneous Rocks

Geological Processes originate below the surface and these include the action of volcanoes, or volcanicity. Molten rock material which is generated within or below the earth's crust reaches the surface from time to time, and flows out from volcanic orifices as lava. Similar material may, on the other hand, be injected into the rocks of the crust, giving rise to a variety of igneous intrusions which cool slowly and solidify; many which were formed during past geological ages are now exposed to view after the removal of their covering rocks by denudation. The solidified lavas and intrusions constitute the igneous rocks.

The molten material from which igneous rocks have solidified is called magma. Natural magmas are hot, viscous siliceous melts with a gas content; the chief elements present are silicon and oxygen, and the metals potassium, sodium, calcium, magnesium, aluminium, and iron (in the order of their chemical activity). Together with these main constituents are small amounts of many other elements, and gases such as $CO_2$, $SO_2$, and $H_2O$. Magmas are thus complex bodies and the rocks derived from them have a wide variety of composition. Cooled quickly, a magma solidifies

as a rock-glass, without crystals; cooled slowly, rock-forming minerals crystallize out from it.

The content of silica ($SiO_2$) in igneous rocks varies from over 80 per cent to about 40 per cent. Magmas and rocks containing much silica (regarded as acid-forming oxide) were originally called acid, and those with less silica and correspondingly more of the basic oxides were called basic. This broad distinction is a useful one. Basic magmas are less viscous than acid magmas; the temperatures at which they exist in the crust are incompletely known, but measurements at volcanoes indicate values in the neighbourhood of $1000^0$C. For basic lavas, a figure which may be considerably lowered if fluex are present. (A flux lowers the melting point of substances with which it is mixed; the gases in magma, for example, act as fluxes).

Different styles of volcanic action may be distinguished, as follows:

1. Fissure eruptions, where lava issues quietly from lines of fracture at the earth, with little gas emission;

2. Shield Volcanoes, with large flat lava cones (Hawaiian Type) ;

3. Central Type volcanoes, which build cones around a central orifice with the emission of much gas, and are sometimes violently expllosive. In the waning stages of this type of volcanicity fumaroles (gas vents), geysers, and hot springs may be formed.

Igneous rocks are given names based upon two things. (how big the crystals are) and the composition of the magma. (The elements contained in the melt.)

1. Intrusive magma cools slowly giving the elements in the melt additional time to come together during the crystallization process. This results in larger minerals and a coarse texture. Extrusive magma cools quickly because of the rapid crystallization, elements have little time to form minerals this results in smaller minerals, and a fine grain texture.

2. The content of silica (SiO2) in igneous rocks varies from over 80 percent to about 40 percent. Magmas and rocks containing much silica called acid and less silica called basic [10].

Basalt is a fine-grained and a basic rock see in the 2.1., which is derived from below.

Table 2.1. Table of Igneous Rocks [10].

| | Acid | Intermediate | Basic | Ultrabasic |
|---|---|---|---|---|
| Coarse | Granite | Diorite | Gabbro | Peridotite |
| Intermediate | | Dacite | Diabase | |
| Fine | Rhyolite | Andesite | BASALT | |
| Frothy | Pumice | | Scoria | |
| Glassy | Obsidian | | | |

### 2.3. Basalt

Basalt is a dense-looking, black rock, often weathering to a brown colour, and is the commonest of all lavas. It is estimated that the basalt flows of the world have five times the volume of all other extrusive rocks together [10].

#### 2.3.1. Minerals

Essential minerals are plagioclase and augite. The normal feldspar of basalts is labradorite, but andesine, olioglase, or albite may occur in different varieties. Magnetite and ilmenite are common accessories; olivine occurs in many basalts and commonly shows alteration to serpentine; calcite, chlorite, zeolites, chalcedony, and

other secondary minerals may fill vesicles. Nepheline, leucite, and analcite are found in undersaturated types.

### 2.3.2. Texture

None seen in the hand specimen, unless the rock is porphyritic or vesicular. Under the microscope the texture is microcrystalline to cryptocrystalline or glassy, often with porphyritic crystals of olivine or augite which are too small to be visible without magnification. Basalt glass is called tachylite and is found as a chilled base to flows of basalt lava, or as the chilled margins of dykes. Vesicular and amygdaloidal textures are common. [10].

## 2.4. Preceding Studies About Basalt

- The porosity and engineering properties of vesicular basalt in Saudi Arabia.[1].

- Weathering effects on the strength and deformational behaviour of crystalline rocks under uniaxial compression state [16].

- Density of basalt core from hilo drill hole, Hawaii [34].

- Influence of thermal treatment on tensile failure of basalt fibers [33].

- Velocities of a natural mid – ocean ridge basalt glass [37].

- A geotechnical overview of Katse Dam and Transfer Tunnel Lesotho, with a note on basalt durability [4].

# CHAPTER 3

# EXPERIMENTAL STUDY

## 3.1. Introduction

The experimental work is directed mainly towards an determination of rock properties of basalt and correlation of rock properties of basalt with ultrasonic velocity.

First the following physical properties are calculated:

- Dry density
- Saturated density
- Bulk density
- Water absorption

After calculating the main index properties the following tests are performed:

- Ultrasonic velocity
- Brazillian indirect tensile strength
- Uniaxial compressive strength
- Shear strength

All this tests were performed according to ISRM (1981).

### 3.1.1. Equipments

Specimens are obtained from the collected rocks using the core machine and drilling machine (see in figure 3.1a, 3.1b). All tests were performed in the geotechnical laboratory of Civil Engineering Department of University of Gaziantep. This laboratory have many specific apparatus for different goals. Some of them were used during the thesis. These are;

1. Brazillian test apparatus : The critical dimensions of the apparatus are the radius of the curvature of the jaws, the clearance and length of the guide pins coupling the two curved jaws and the width of the jaws. These are as follows: Radius of jaws – 1.5 × specimen radius; guide pin clearance – permit rotation of one jaws relative to the other by $4 \times 10^{-3}$ rad out of plane of the apparatus (25 mm penetration of guide pin with 0.1 mm clearance); width of jaws – 1.1 × specimen thickness. The upper jaw contains a spherical seating conveniently formed by a 25-mm diameter half – ball bearing.

2. Uniaxial Test machine : The auto test range of concrete and mortar compression testing machine is 3000 kN capacity and has been designed for consistent, reliable testing. The automatic cycle enables high throughput of samples making this machine particularly suitable for central or commercial testing organizations. Technical Features of the machines are:

   - Overall dimensions ……length * width * height
     Compression frame ……..590 * 510 * 1215 mm
   - Console ……520 * 430 * 1215 mm
   - Max. Vertical Clearance ……340 mm
   - Max. Vertical Clearance (block tester) ……...260 mm
   - Max. Horizontal Clearance ……310 mm
   - Maximum ram travel ……50 mm
   - Approx. Weight of Console ……..145 kg
   - Approx. Weight of Compressive frame ……1270 kg
   - Approx. Weight of compressive frame for Block Teste……..1370 kg

**3.** Direct Shear test machine (MATEST COMPANY):

- Length…….. 770mm
- Width …….. 235mm
- Height ……..615mm
- Mass ……46kg
- max. load ……50 kN
- Allowed temperature ……. from -10 Cº to + 80 Cº
- Allowed humidity ……..……. from 30% to %95%
- max. height over sea level ……1000m.

Calibration: The machine is controlled and calibration by the manufacturer, using sampling tools, which are periodically checked by Official Institutions. A copy of the Calibration Certificate is delivered together with this literature. The gauges for pressure measurement should normally work without any maintenance. Anyway the calibration of every gauge should be checked periodically. This procedure can be done by using a dead weight pressure tester or any similar instrument which could induce in the gauge a known hydraulic pressure. The value got by the gauge should then be compared with the one corresponding to the given pressure**.** In case the gauge is out of range, damage, out of calibration or doesn't return to zero at pressure release, we recommend its replacement.

**4.** Ultrasonic Velocity test machine : The Ultrasonic tester model C 368 is an instrument to measure material characteristics by using ultrasonic pulses. Technical features of the machine are:

- Maximum measurable time ……..9999 microsec.
- Resolution ……..0,16 microsec.
- Accuracy ……...-/+0,16 microsec.
- Feeding ……12 Volt D.C.
- Consumption ...……...0,30 A
- Autonomy ……...5 h with battery 12 V 1,9 Ah

Figure 3.1a. The core machine

Figure 3.1b. The drilling machine

### 3.2. Determination of Index Properties

Determination of index properties were done according to ISRM (1981). Exactly 179 of basalt samples' index properties were determined in this thesis.

#### 3.2.1.Suggested method for density-water absorption and porositydetermination using saturation and buoyancy techniques

##### 3.2.1.1. Scope

**(a)** The test is intended to measure the dry density and related properties of a rock sample in the from of lumps or aggregate of irregular geometry. It may also be applied to a sample in the from of specimens of regular geometry.

**(b)** The method should only be used for rocks that do not appreciably swell or disintegrate when oven dried and immersed in water [8].

### 3.2.1.2. Apparatus

**(a)** An oven capable of maintaining a temperature of 105 $^{o}$C to within 3$^{o}$C for a period of at least 24 hr.

**(b)** A sample container of non-corrodible material, including an air-tight lid.

**(c)** A desiccator to hold sample containers during cooling.

**(d)** Vacuum saturation equipment such that the sample can be immersed in water under a vacuum of less than 800 Pa (6 torr) for a period of at least one hour.

**(e)** A balance of adequate capacity, capable of determining the mass of specimen to an accuracy of 0.01%.

**(f)** An immersion bath and a wire basket or perforated container, such that the sample immersed in water can be freely suspended from the stirrup of the balance to determine the saturated-submerged mass. The basket should be suspended from the balance by a fine wire so that only the wire intersects the water surface in the immersion bath.

### 3.2.1.3. Procedure

**(a)** A representative sample comprising at least 10 lumps of regular or irregular geometry, each having either a mass of at least 50g or a minimum dimension of at least 10 times the maximum grain size, whichever is the greater, is selected. The sample is washed in water to remove dust.

**(b)** The sample is saturated by water immersion in a vacuum of less than 800 Pa (6 torr) for a period of at least one hour, with periodic agitation to remove trapped air.

**(c)** The sample is then transferred under water to the basket in the immersion bath shown in figure 3.2. Its saturated-submerged mass $M_{sub}$ is determined to an accuracy of 0.1 g from the difference between the saturated-submerged mass of the basket plus sample and that of the basket alone.

Figure 3.2. An apparatus used for calculating the volume
by using the archimed's law

**(d)** The sample is removed from the immersion bath and surface-dried with a moist cloth, care being taken to remove only surface water and to ensure that no rock fragments are lost. The mass $M_{sat}$ of saturated-surface-dry sample determined.

**(e)** The sample dried to constant mass at a temperature of 105 $^{o}$C then the sample allowed to cool for 30 min in a desiccator. The mass $M_s$ of oven-dry sample is measured. An apparatus is shown in figure 3.3.

**(f)** $V_V$ volume of voids can be determined by the subtraction dry mass from the saturated mass dry. $V_d$ is a dimensional volume which is obtained from multiplying the dimensions each other.

Figure 3.3. A balance of adequate capacity, capable of determining the mass of specimen to an accuracy of 0.01%.

### 3.2.1.4. Calculations

- Saturated-surface dry mass $M_{sat}$
- Grain weight $M_s$
- Bulk volume $V = \frac{M_{sat} - M_{sub}}{\rho_w}$ (3.1)
- Pore volume $V = \frac{M_{sat} - M_s}{\rho_w}$ (3.2)
- Dry density $\rho_d = \frac{M_s}{V}$ (3.3)
- Saturated density $\rho_{sat} = \frac{M_{sat}}{V}$ (3.4)
- Water absorbtion $W_{abs} = \frac{M_{sat} - M_s}{M_s} \times 100$ (3.5)
- Porosity $n = \frac{V_v}{V_d}$ x 100 (3.6)

### 3.3. Determination of Strength Properties

All tests were done according to ISRM (1981). Exactly 179 of basalt samples used to perform this tests in this thesis. Out of this 179 specimens; 115 samples were used for Brazillian tensile strength, 52 samples were used for uniaxial compression test, 12 samples were used for direct shear test. Samples used for Brazillin test are core specimens which has a diameter of 54 mm and has a length of 30 mm. Samples used for uniaxial compression test are core specimens which has a diameter of 54 mm and has a length of 135 mm. Samples used for direct shear test are block samples which has a dimensions 50 mm * 50 mm.

#### 3.3.1. Ultrasonic velocity test

The ultrasonic velocities are measured and calculated on dry samples.

##### 3.3.1.1. Scope

This test is intended as a method to determine the velocity of propagation of elastic waves in laboratory rock testing. Three different variations of the method are given. Theese are the high frequency ultrasonic pulse technique, the low frequency ultrasonic pulse technique and the resonant method. In this thesis the low frequency ultrasonic pulse technique is used.

##### 3.3.1.2. Apparatus

Although there are three different methods, the electronic components should, as far as possible, be chosen so as to be applicable to all three methods. The same rock or even the same sample can be used for all three methods. Consideration should of course be given to the respective frequencies used for the different methods. The electronic components should be impedance matched and have shielded leads to ensure efficient energy transfer. To prevent damage to the system allowable voltage inputs should not be exceeded. An apparatus used for determining the ultrasonic velocity is shown in figure 3.4.

Figure 3.4. Ultrasonic velocity test equipment.

**(a)** Pulse generator unit (e.g. function generator): Frequency range: 2-30 kHz (if the generator mentioned in the first method has a low frequency range it can obviously be used here); repetition frequency: 10-100 repetitions per second; pulse voltage: same as first method.

**(b)** Transducers:

**(i)** Transmitter: piezo-electric ceramics or magnetostrictive elements, which are capable to generate high amplitude pulses (depending on the rock type and specimen dimensions) in the frequency range 2-30 kHz.

**(ii)** Receivers: piezo-electric ceramics with flat frequency response in the frequency range 2-30 kHz or magneto-strictive elements.

**(c)** Filters, amplifiers, CRO, time-marker analog to first method with consideration of the low frequency range.

### 3.3.1.3. Procedure

Care should be exercised in core drilling, handling, sawing, grinding and lapping the test specimen to minimize mechanical damage. The surface area under each transducer shall be sufficiently plane to provide good coupling.

Drying of specimens may be carried out by using a desiccator. Saturated specimens shall remain submerged in water up to the time of testing. If the velocity is to be determined with the in-situ condition, care must be exercised during the preparation procedure. It is also suggested that both the sample where the specimen is taken from as well as the specimen, be stored in moisture-proof bags. Dry surface-preparation procedures may be employed.

This test is for the determination of the velocity of dilatational and torsional waves in bar or rod-like rock specimens (bar waves, one-dimensional wave propagation). This method is suitable for specimens which are long compared to the diameter (length to diameter ratio >3) and the wave length of the pulse should be long compared to the diameter (wave length to diameter ratio >5).

**(a)** Dimensions should be as stated above. For the pulse transmission technique and the resonant frequency technique both the end planes of the specimen should be flat and parallel to within 0.005mm/mm of the lateral dimension.

**(b)** Rock cores are positioned on the sample holder of an acoustical bench. The cores have at least a length to diameter ratio of >3. The transmitter, generating a sine wave of a wave-length >5 times the core diameter, is pressed to a saw-cut flat end plane (normal to the core axis) by a stress of approx 10N/cm$^2$ for $V_p$ measurement.

**(c)** There are two possibilities in the positioning of the receiver (analog to (c) in first method):

**(i)** pulse transmission: the receiver is positioned at the opposite flat plane of the core is shown in figure 3.5. Both end planes should be parallel to within about one degree: ball joints may be used

**(ii)** seismic profiling: the receiver is moved along the surface of the core parallel to the core axis.

Figure 3.5a. The ultrasonic velocity test performed on core specimen for Brazillian test

Figure 3.5b. The ultrasonic velocity test performed on block specimen fordirect shear test

Figure 3.5c. The ultrasonic velocity test performed on core specimen for uniaxial compression test

### 3.3.1.4. Calculation

One or three-dimensional equations of wave propagation are used.

**(a)** Velocities are calculated from travel times measured and the distance, d, between transmitter and receiver by using the equations:

$$V_p = d \times t_p^{-1} \quad (3.7)$$

$$V_s = d \times t_s^{-11} \quad (3.8)$$

where $V_p$ is the velocity of the longitudinal wave, $V_s$ is the velocity of the shear wave, $t_p$ and $t_s$ are the times which the P and S wave, respectively, took to travel the distance d.

**(b)** If seismic profiling technique was used the velocities are given by the slope of the curve travel time Vs distance d.

### 3.3.2. Brazil test

Brazillian tensile test was performed according to ISRM (1981). 115 samples were used for Brazillian tensile strength. Samples used for Brazillin test are core specimens which has a diameter of 54 mm and has a length of 30 mm.

#### 3.3.2.1. Scope

This test is intended to measure the uniaxial tensile strength of prepared rock specimens indirectly by the brazil test. The justification for the test is based on the experimental fact that most rocks in biaxial stress fields fail in tension at their uniaxial tensile strength when one principal stress is tensile and the other finite principal stress is compressive with a magnitude not exceeding three times that of the tensile principal stress [8].

#### 3.3.2.2. Apparatus

**(a)** Two steel loading jaws designed so as to contact a disc-shaped rock sample at diametrically-opposed surfaces over an arc of contact of approx $10^0$ at a failure. The suggested apparatus to achieve this is illustrated in figure 3.6a and figure 3.6b The critical dimensions of the apparatus are the radius of the curvature of the jaws, the clearance and length of the guide pins coupling the two curved jaws and the width of the jaws. These are as follows: Radius of jaws – 1.5 × specimen radius; guide pin clearance – permit rotation of one jaws relative to the other by $4 \times 10^{-3}$ rad out of plane of the apparatus (25 mm penetration of guide pin with 0.1 mm clearance); width of jaws – 1.1 × specimen thickness. The upper jaw contains a spherical seating conveniently formed by a 25-mm diameter half – ball bearing ISRM (1981).

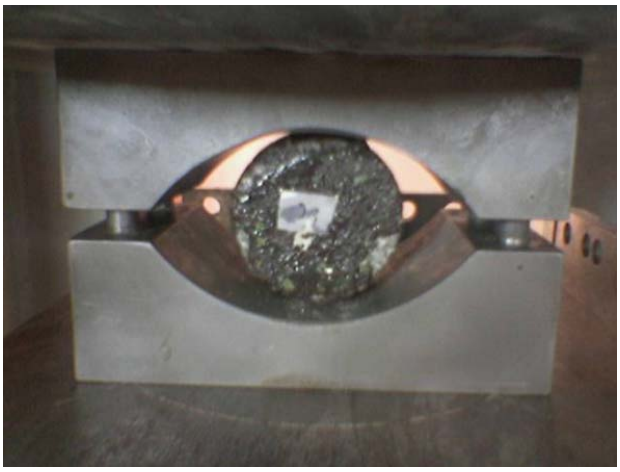

Figure 3.6a. The suggested apparatus for Brazil Test (ISRM 1981)

Figure 3.6b. The suggested apparatus for Brazil Test (ISRM 1981)

**(b)** Double thickness (0.2 – 0.4 mm) adhesive paper strip (masking tape) with a width equal to or slightly greater than the specimen thickness.

**(c)** A suitable machine for applying and measuring compressive loads to the specimen can be seen in figure 3.7. It shall be of sufficient capacity and be capable of applying load at a rate conforming to the requirements set out in section 3.

Figure 3.7. A suitable machine for applying and measuring compressive loads to the specimen

**(d)** A spherical seat, if any, of the testing machine crosshead shall be placed in a locked position, the two loading surfaces of the machine being parallel to each other.

**(e)** It is a preferable but not obligatory that the testing machine be fitted with a chart recorder to record load against displacement to aid in the measurement of the failure load.

### 3.3.2.3. Procedure

**(a)** the test specimens should be cut and prepared using clean water. The cylindrical surfaces should be free from obvious tool marks and any irregularities across the thickness of the specimen should not exceed 0.025 mm. End faces shall be flat to with 0.25 mm and square and parallel to within $0.25^{\circ}$.

**(b)** specimen orientation shall be known and the water content controlled or measured and reported in accordance with the 'suggested method for the determination of the water content of rock sample.

**(c)** The specimen diameter shall not be less than NX core size, approximately 54 mm, and the thickness should be approximately equal to the specimen radius.

**(d)** The test specimen shall be wrapped around its periphery with one layer of the masking tape and mounted squarely in the test apparatus such that the curved platens load the specimen diametrally with the axes of rotation for specimen and apparatus coincident.

**(e)** Load on the specimen shall be applied continuously at a constant rate such that the failure in the weakest rocks occurs within 15-30s. A loading rate of 200 N / s is recommended.

### 3.3.2.4. Calculations

The tensile strength of the specimen $\sigma_t$, shall be calculated by the following formula:

$$\sigma_t = 0.636\ P / (D.t)\ \ (MPa) \qquad (3.9)$$

where P is the load at failure (kN), D is the diameter of the test specimen (mm), t is the thickness of the test specimen measured at the center (mm).

### 3.3.3. Uniaxial compression test and determination of young's modulus

Uniaxial compression test was performed according to ISRM (1981). 52 samples were used for uniaxial compression test. Samples used for uniaxial compression test are core specimens which has a diameter of 54 mm and has a length of 135 mm.

### 3.3.3.1. Scope

This method of test is intended to determine stress-strain curves and young's modulus and Poisson's ratio in uniaxial compression of a rock specimen of regular geometry. The test is mainly intended for classification and characterization of intact rock.

### 3.3.3.2. Apparatus

**(a)** A suitable machine shall be used for applying and measuring axial load to the specimen which is shown in figure 3.8. It shall be of sufficient capacity and capable of applying load at a rate conforming to the requirements set in section 3.


Figure 3.8. A suitable machine shall be used for applying and measuring axial load to the specimen

**(b)** A spherical seat, if any, of the testing machine, if not complying with spesification 2(d) below, shall be removed or placed in a locked position, the two loading faces of the machine being parallel to each other.

**(c)** Steel platens in the form of discs and having a Rockwell hardness of not less than HRC58 shall be placed at the specimen ends. The diameter of the platens shall be between D and D + 2 mm where D is the diameter of the specimen. The thickness of the platens shall be at least 15 mm or D / 3. surfaces of the discs should be ground and their flatness should be better than 0.005 mm.

**(d)** One of the two platens shall incorporate a spherical seat. The spherical seat should be placed on the upper and of the specimen. It should be lightly lubricated with mineral oil so that it locks after the deadweight of the cross-head has been picked up. The specimen, the platens and spherical seat shall be accurately centered with respect to one another and to the loading machine. The curvature centre of the seat surface should coincide with the centre of the top end of the specimen.

**(e)** Electrical resistance strain gauges, linear variable differential transformers, compressometers, optical devices or other suitable measuring devices. Their design shall be such that the average of two circumferential and two axial strain measurements, equally spaced, can be determined for each increment of load. The devices should be robust and stable, with strain sensitivity of the order of $5x10^{-6}$.

Both axial and circumferential strains shall be determined within an accuracy of 2% of the reading and a precision of 0.2 percent of full scale.

If electrical resistance strain gauges are used, the length of gauges over which axial and circumferential strains are determined shall be at least ten grain diameters in magnitude and the gauges should not encroach within D/2 of the specimen ends, where D is diameter of the specimen.

If micrometers of LVDT's are used for measuring axial deformation due to loading, these devices should be graduated to read in 0.002mm units and accurate within 0.002mm in any 0.02mm range and within 0.005mm in any

0.25 range. The dial micrometer or LVDT's should not encroach within D/2 of the specimen ends.

**(f)** An apparatus for recording the loads and deformations; preferably an X-Y recorder capable of direct plotting of load-deformation curves.

### 3.3.3.3. Procedure

**(a)** Test specimens shall be right circular cylinders having a height to diameter ratio of 2.5 – 3 and a diameter preferably of not less than NX core size, approximately 54 mm . Figure 3.9. shows the specimens that can be used for calculating the uniaxial compressive strength. The diameter of the specimen should be related to the size of the largest grain in the rock by the ratio of at least 10 : 1.

Figure 3.9. Specimens for uniaxial compressive strength.

**(b)** The ends of the specimen shall be flat to 0.02 mm and shall not depart from perpendicularly to the axis of the specimen by more than 0.001 radian (about 3.5 min) or 0.05 mm in 50 mm.

**(c)** The sides of the specimen shall be smooth and free of abrupt irregularities and straight to within 0.3 mm over the full length of the specimen.

**(d)** The use of the capping materials or end surface treatments other than machining is not permitted.

**(e)** The diameter of the test specimen shall be measured to the nearest 0.1 mm by averaging two diameters measured at right angles to each other at about the upper height, the mid-height and the lower height of the specimen. The average diameter shall be used for calculating the cross-sectional area. The height of the specimen shall be determined to the nearest 1.0 mm.

**(f)** Moisture can have a significant effect on the deformability of the test specimen. When possible, in situ moisture conditions should be preserved until the time of the test. When the characteristic of the rock material under conditions varying from saturation to dry is required, proper note shall be made of moisture conditions so that correlation between deformability and moisture content can be made. Excess moisture can create a problem of adhesion of strain gauges which may require making a change in moisture content of the require making a change in moisture content of the sample. The moisture condition shall be reported in accordance with Suggested method for determination of the water content of a rock sample.

**(g)** Load on the specimen shall be applied continuously at a constant stress rate such that failure will occur within 5-10 min of loading, alternatively the stress rate shall be within the limits of 0.5-10 MPa/s.

**(h)** Load and axial and circumferential strains or deformations shall be recorded at evenly spaced load intervals during the test, if not continually recorded. At least ten readings should be taken over the load range to define the axial and diametric stress-strain curves.

**(i)** It is sometimes advisable for a few cycles of loading and unloading to be performed.

**(j)** The number of specimens instrumented and tested under a specified set of conditions shall be governed by practical considerations but at least five are preferred.

### 3.3.3.4. Calculations

**(a)** Axial strain, $\varepsilon_a$, and diametric strain, $\varepsilon_{\mathrm{d}}$, may be recorded directly from strain indicating equipment or may be calculated from strain indicating equipment or may be calculated from deformation readings depending upon the type of instrumentation such as discussed in 3.3.3.2. apparatus (e).

**(b)** Axial strain is calculated from the equation

$$\varepsilon_a = \frac{\Delta l}{l_0} \tag{3.10}$$

Where

$l_0$ = original measured axial length

$\Delta l$ = change in measured axial length (defined to be positive for a decrease in length)

**(c)** Diametric strain may be determined either by measuring the changes in specimen diameter or by measuring the circumferential strain. In the case of measuring the changes in diameter, the diametric strain is calculated from the equation.

$$\varepsilon_{\mathrm{d}} = \frac{\Delta d}{d_0} \tag{3.11}$$

Where

$d_0$ = original undeformed diameter of the specimen

$\Delta d$ = change in diameter (defined to be negative for an increase in diameter)

In the case of measuring the circumferential strain $\varepsilon_d$, the circumference is C = πd, thus the change in circumference is $\Delta C = \pi \Delta d$. Consequently, the circumferential strain, $\varepsilon_c$, is related to diametric strain, $\varepsilon_d$, by

$$\varepsilon_c = \frac{\Delta C}{C_0} = \frac{\Delta d}{d_0} \tag{3.12}$$

So that

$$\varepsilon_c = \varepsilon_d$$

Where $C_0$ and $d_0$ are original specimen circumference and diameter, respectively.

**(d)** The compressive stress in the test specimen, σ, is calculated by dividing the compressive load P on the specimen by the initial cross-sectional area, $A_0$.

Thus $$\sigma = \frac{P}{A_0} \tag{3.13}$$

where in this test procedure, compressive stresses and strains are considered positive.

**(e)** Fig. 3.10 illustrates typical plot of axial stress versus axial and diametric strains. These curves show typical behaviour of rock materials from zero stress up to ultimate strength, $\sigma_u$, The complete curves give the best description of the deformation behaviour of rocks having non-linear stress-strain behaviour at low and high stress levels.

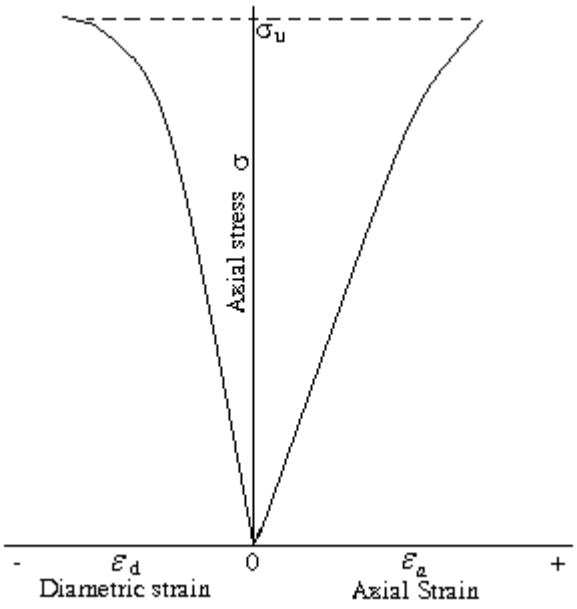


Figure. 3.10. Format for graphical presentation of axial and diametric stress-strain curves.

**(f)** Axial Young's modulus, E (defined as the ratio of the axial stress change to axial strain produced by the stress change) of the specimen may be calculated using any one of several methods (in this thesis tangent modulus is used) employed in accepted engineering practice. The most common methods, listed in figure 3.11 are as follows:

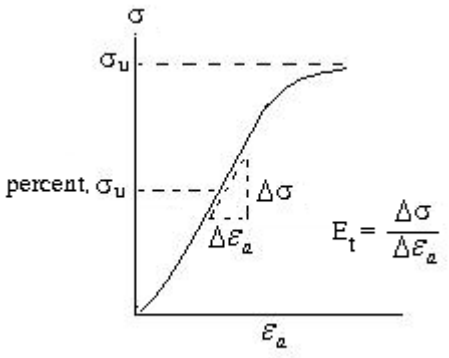


Figure. 3.11a. tangent modulus measured at a fixed percentage of ultimate strength

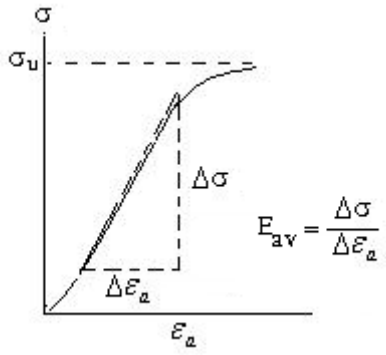


Figure. 3.11b. Average modulus of linear portion of the stress-strain curve

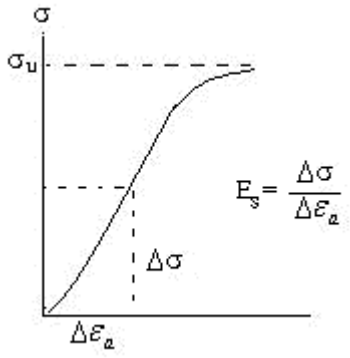


Figure. 3.11c. Secant modulus measured up to a fixed percentage of ultimate strength

**(1)** Tangent Young's modulus, $E_t$, is measured at a stress level which is some fixed percentage of the ultimate strength (figure 3.10a). It is generally taken at a stress level equal to 50% of the ultimate uniaxial compressive strength [8].

**(2)** Average Young's modulus, $E_{av}$, is determined from the average slopes of the more-or-less straight line portion of the axial stress-axial strain curve (figure 3.10b).

**(3)** Secant Young's modulus, $E_t$, is usually measured from zero stress to some fixed percentage of the ultimate strength (figure 3.10c), generally at 50%.

Axial Young's modulus E is expressed in units of stress i.e. pascal (Pa) but the most appropriate multiple is the gigapascal (GPa = $10^9$ Pa).

**(g)** Poisson's ratio, $\nu$, may be calculated from the equation. (ISRM 1981)

$$\nu = - \frac{\text{slope of axial stress - strain curve}}{\text{slope of diametric stress - strain curve}} \qquad (3.14)$$

$$= - \frac{E}{\text{slope of diametric curve}} \qquad (3.15)$$

where the slope of the diametric curve is calculated in the same manner for either of the three ways discussed for Young's modulus in paragraph 3.3.3.4.(f). Note that Poisson's ratio in this equation has a positive value, since the slope of the diametric curve is negative by the conventions used in this procedure.

**(h)** The volumetric strain, $\varepsilon_v$, for a given stress level is calculated from the equation.

$$\varepsilon_v = \varepsilon_a + 2\varepsilon_d \qquad (3.16)$$

### 3.3.4. Direct shear test

Direct shear test was performed according to ISRM (1981). 12 samples were used for direct shear test. Samples used for direct shear test are block samples which has a dimensions 50 mm * 50 mm.

#### 3.3.4.1. Scope

**(a)** This test measures peak and residual direct shear strength as a function of stress normal to the sheared plane. Results are employed, for example, in the limiting equilibrium analysis of slope stability problems or for the stability analysis of dam foundations.

**(b)** The inclination of the test specimen with respect to the rock mass, and its direction of mounting in the testing machine are usually selected so that the sheared plane coincides with a plane of weakness in the rock, for example a joint, plane of bedding, schistosity or cleavage, or with the interface between soil and rock or concrete and rock.

**(c)** A shear strength determination should preferably comprise at least five tests on the same test horizon with each specimen tested at a different but constant normal stress.

**(d)** In applying the results of the test, the pore-water pressure conditions and the possibility of progressive failure must be assessed for the design case as they may differ from the test conditions.

### 3.3.4.2. Apparatus

Equipment for taking specimens of rock, including:

**(a)** Equipment for cutting the specimen; for example a large-diameter core drill, percussive drills, rock saws or hammers and chisels, also equipment for measuring the dip, dip direction, roughness and other characteristic features of the test horizon.

**(b)** Materials for holding the specimen together, for example binding wire or metal bands.

**(c)** Materials to protect the specimen against mechanical damage and change in water content both during cutting and transit to the laboratory, example protective packing and wax or similar waterproofing material.

Equipment for mounting the specimen including:

**(a)** Specimen carriers, forming a dismountable part of the test equipment.

**(b)** Cement, plaster, resin or similar strong encapsulating materials together with appropriate mixing utensils.

Testing equipment (a shear box, for example Figure 3.12.) incorporating:

**(a)** A means of applying the normal load, typically a hydraulic, pneumatic or dead-weight mechanical system, designed to ensure that the load is uniformly

distributed over the plane to be tested. The resultant force should act normal to the shear plane, passing through its centre of area. The system should have a travel greater than the amount of dilation or consolidation to be expected, and should be capable of maintaining normal load to within 2% of a selected value throughout the test.

Figure 3.12. Arrangement for laboratory direct shear test.

**(b)** A means of applying the shear force, typically a hydraulic jack or a mechanical gear-drive system, designed so that the load is distributed uniformly along one half-face of the specimen with the resultant applied shear force acting in the plane of shearing. The equipment should be designed for a shear travel greater than 10% of the specimen length. It should include rollers, cables or a similar low friction device to ensure that resistance of the equipment to shear displacement is less than 1% of the maximum shear force applied in the test.

**(c)** Equipment for independent measurement of the applied shear and normal forces, with an accuracy better than +-2% of the maximum forces reached in the test. Recent calibration data applicable to the range of testing should be appended to the test report.

**(d)** Equipment for measuring shear, normal and lateral displacement, for example micrometer dial gauges or electric transducers or the four normal displacement gauges may be replaced by a single gauge mounted centrally. The shear displacement measuring system should have a travel greater than 10% of the specimen length and an accuracy better 0.1 mm. The normal and lateral displacement measuring systems should have a travel greater than 20 mm and an accuracy better than 0.05 mm. Resetting of gauges during the test should if possible be avoided. If electric calibration should be included in the report.

### 3.3.4.3. Procedure

Preparation:

**(a)** The test horizon is selected and dip, dip direction and other relevant geological characteristic are recorded. Block or core specimens containing the test horizon are collected using methods selected to minimize disturbance, if possible in such a way as to retain natural water content. The specimen dimensions and the location of the test horizon within the block or core should if possible allow mounting without further trimming in the laboratory, and with sufficient clearance for adequate encapsulation. The test plane should preferable be square with a minimum area of 2500mm$^2$. The mechanical integrity with wire or tape which is to be left in position until immediately before testing [8].

**(b)** Specimens that are not encapsulated immediately for testing should be given a waterproof coating, labeled and packaged to avoid damage in transit to the laboratory. Fragile specimens require special treatment, for example packaging in polyurethane foam.

**(c)** The protective packaging, with the exception of the steel wire, is removed and the block supported in one of the carriers so that the horizon to be tested is secured in the correct position and orientation. The encapsulating material

is poured and, after this has set, the other half-specimen is encapsulated in a similar manner (see in figure 3.13). A zone at least 5mm either side of the shear horizon should be free from encapsulating material.

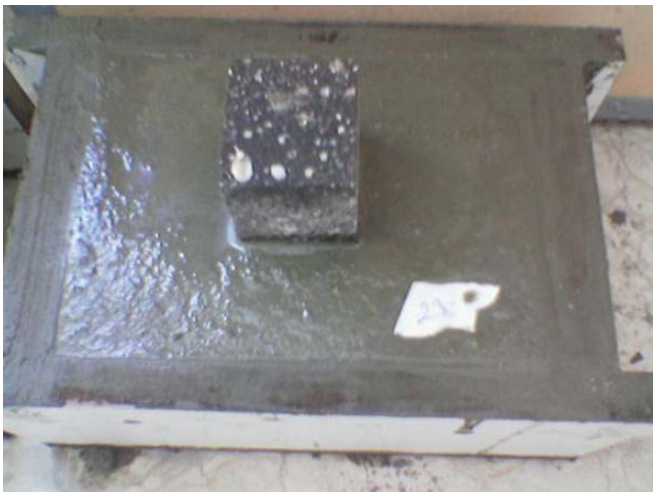

Figure 3.13 shows the encapsulating material as concrete

Shearing:

**(a)** the propose of shearing is to establish values for the peak and residual direct shear strengths of the test horizon.

**(b)** The shear force may be applied in increments but is usually applied continuously in such a way as to control the rate of shear displacement.

**(c)** Approximately 10 sets of readings should be taken before reaching peak strength. The rate of shear displacement should be less than 0.1 mm/min in the 10-minute period before taking a set of readings. This rate may be increased to not more than 0.5 mm/min between sets of readings provided that the peak strength itself is adequately recorded. For a 'drained' test particularly when testing clay-filled discontinuities, the total time to reach peak strength should exceed $6t_{100}$ as determined from the consolidation curve. If necessary the rate of the shear should be reduced or the application of later shear force increments delayed to meet this requirement.

**(d)** After reaching peak strength, readings should be taken at increments of from 0.5 to 5 mm shear displacement as required to adequately define the force-displacement curves. The rate of the shear displacement should be 0.002-0.2 mm/min in the 10-minute period before a set o readings is taken, and may be increased to not more than 1 mm/min between sets of readings.

**(e)** It may be possible to establish a residual strength value when the sample is sheared at constant normal stress and at least four consecutive sets of readings are obtained which show not more than 5% variation in shear stress over a shear displacement of 1 cm.

**(f)** Having established a residual strength the normal stress may be increased or reduced and shearing continued to obtain additional residual strength values. The specimen should be reconsolidated under each new normal stress.

**(g)** After the test the shear plane should be exposed and fully described. The area of the shear surface is measured and photographs may be also be required. Samples of rock, infilling and shear debris should be taken for index testing.

**3.3.4.4. Calculations**

**(a)** Shear and normal stress are computed as follows:

$$\text{Normal stress } \tau = \frac{Ps}{A} \tag{3.17}$$

$$\text{Shear stress } \sigma_n = \frac{Pn}{A} \tag{3.18}$$

Where

$P_s$ = Total shear force;

$P_n$ =Total normal force;

A = Area of shear surface overlap (corrected to account for shear displacement).

**(b)** For each test specimen graphs of shear stress (or shear force) and normal displacement vs. shear displacement are plotted. Annotated to show the nominal normal stress and any change in normal stress during shearing. Values of peak and residual shear strength and the normal stresses, shear and normal displacement at which these occur are abstracted from these graphs.

**(c)** Graphs of peak and residual shear strength vs. normal stress are plotted from the combined results for all test specimens. Shear strength parameters Ø, $Ø_r$, and c are abstracted from figure 3.14 [8].

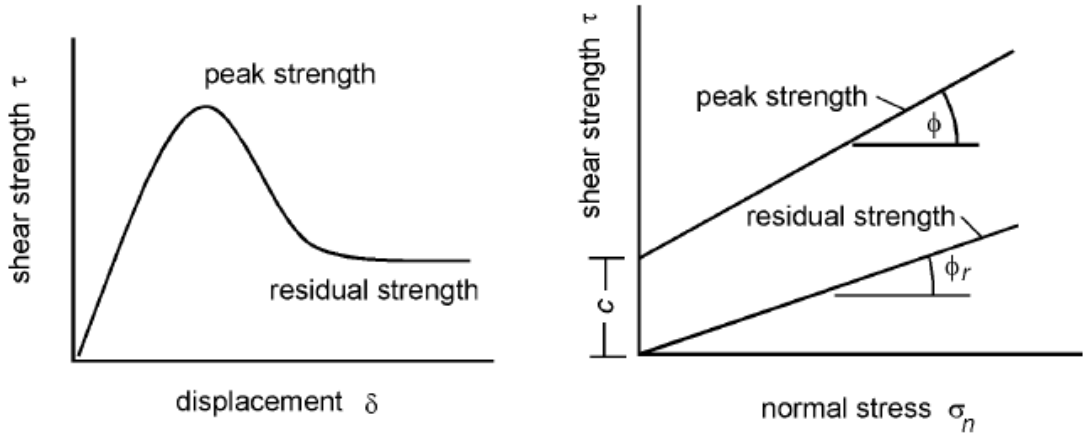


Figure 3.14. Shear testing of discontinuities [51].

### 3.4. Sources of Error In Strength Tests

In assessing the scope and method of testing appropriate for a particular project it is important that the likely errors be properly taken into account. These come from two sources, namely: (i) bias in sample selection; and (ii) errors resulting from inappropriate sample preparation, test apparatus or test procedure.

The substantial variability which is usually found in rocks in engineering projects means that critical appraisal must be made of errors which may occur in testing but which may have an effect substantially less than the inherent variability. This does not mean that a casual attitude to laboratory testing should be condoned, but it does mean that there is little point in spending time and money in chasing a 1% error in the laboratory tests when there is a 40% variability in the results due to natural variability, sample selection bias, etc. [22].

### 3.5. Factors Influencing The Measurement of Strength

Many factors influence the measurement and determination of rock strength such as uniaxial compressive strength tensile strength shear strength etc. The most important factors are briefly reviewed here.

The rock specimen tested in the laboratory is considered to be an element of the field and to contain properties that are representative of the rock mass from which it is taken. However, depending on a number of factors to which the specimen is exposed in the laboratory test, the specimen may not yield properties that are directly applicable to the field. An appreciation of the limitations of the laboratory tests may provide guidance in selecting appropriate properties for use in analyses of rock structures [25].

#### 3.5.1.Specimen shape

The rock specimens tested in uniaxial and triaxial compression are most often cylindrical The height : diameter ratio of the specimen influences the measured strength. Typically the strength decreases with increasing height : diameter ratio , but it tends to become constant for ratios in the order of 2:1 to 3: [23,35]. For higher ratios the specimen strength may be influenced by buckling.

### 3.5.2. Specimen size

The specimen size may influence the measured strength. According to Weibull [45] a large specimen contains more flaws than a small specimen. The large specimen therefore also has more flaws with critical orientation relative to the applied shear stresses than the small specimen. A large specimen with a given shape is therefore likely to fail and exhibit lower strength than a small specimen with the same shape. This type of behaviour is observed for most brittle materials, including many rocks [5, 15, 26].

### 3.5.3. Platen friction

The end of platens through which the specimen is loaded may apply frictional forces directed towards the center of the specimen as it begins to expand laterally during axial compression. This results in apparent higher confining pressure near the ends of the specimen, and it will consequently exhibit higher strength. This effect is more pronounced and is directly responsible for the higher strength observed in shorter specimens as discussed above [35]. Procedures involving brush platens or fluid cushions may be employed to reduce the platen friction and improve the test results significantly [2, 3, 7, 18, 28, 32].

### 3.5.4. Rate of loading

Experimental observations show that the strength decreases with decreasing rate of loading or strain rate [2, 3, 7, 15, 18, 26, 28, 32, 43]. This is due to effects of creep that are present in all materials. Longer times to peak failure allow greater amounts of creep to occur, and this plays a role in the measured strength. Some rock types are known to creep more (e.g. rock salt) than others (e.g. granite), and the creep behaviour has a dominant influence on the design of structures in such rocks [11].

### 3.5.5. Presence of water

Water may have two effects on the behaviour: (i) chemical or physical effects that will cause the rock to be altered simply due to the presence of moisture; and (ii) a

mechanical effect when the water is under pressure. Some rocks may be weaker by addition of water, either by deterioration of cementing agents or by swelling and consequent reduction in strength [20, 40]. The effects of water under pressure can be accounted for by Terzaghi's effective stress principle [6, 14, 20, 40].

The presence of moisture in a rock body can influence the rupture behaviour of the rock in two important ways:

**a)** The moisture can reduce the strenght of the rock by chemical or physical alteration of its inherent properties. This strength reduction can be very important.

**b)** If the moisture is present under pressure, the strength of rock is further reduced [42].

### 3.5.6. Temperature

Increasing temperature will cause a reduction in strength. [12, 13, 27]. This strength reduction may not be pronounced until the rock begins to recrystallize or melt at relatively high temperatures. Experiments at increasingly high temperatures indicate reductions in both tensile and compressive strengths, as well in the overall three-dimensional strength properties of rocks.

### 3.5.7. Stiffness of the testing

The stiffness of the testing machine controls the measured stress-strain-strength behaviour, especially in the softeing portion of the curve for brittle rocks [15, 24, 26]. Stiff testing machines prevent a sudden release of energy and consequent rapid, uncontrolled decline in the stress-strain relation past peak failure. This may not affect the peak failure value substantially, but it may have an effect on the residual strength of the rock.

# CHAPTER 4

# TEST RESULTS AND CORRELATIONS

## 4.1. Introduction

This chapter contains the test results and correlations obtained from the test results. All physical and mechanical properties of Gaziantep basalts are correlated with ultrasonic velocity. In addition, Some physical and mechanical properties of Gaziantep basalts correlated with each other. This correlations were done by linear correlation method (Least square method) and multiple correlation method. The accuracy of correlations were checked by correlation coefficient of $R^2$ since higher correlation coefficients.

$R^2$ was calculated by

$$R^2 = SSR / SST \qquad (4.1.)$$

SSR : Sum of square regression
SST : Sum of the square total

## 4.2. Brazil Test

Brazillian tensile test was performed according to ISRM (1981). 115 samples were used for Brazillian tensile strength. Samples used for Brazillin test are core specimens which has a diameter of 54 mm and has a length of 30 mm.

### 4.2.1. Results

Results obtained from Brazillian tensile test were plotted on graphics

#### 4.2.1.1. Dry density versus ultrasonic velocity for samples of Brazil test

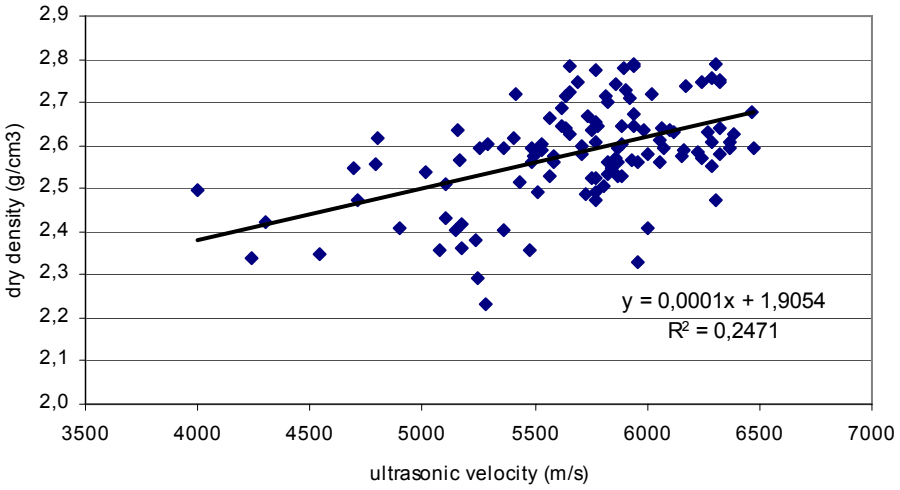


Figure 4.1. Ultrasonic Velocity – Dry density diagram

Table 4.1. Equation and $R^2$ values for Ultrasonic Velocity – Dry density

| TRENDLINE TYPE | $R^2$ | EQUATION |
|---|---|---|
| LINEAR | 0,2471 | $y = 0,0001x + 1,9054$ |
| POWER | 0,2485 | $y = 0,2907x^{0,2526}$ |
| EXPONENTIAL | 0,2461 | $y = 1,9754e^{5E-0,5x}$ |

Figure 4.1 shows the highest $R^2$ for test results of the dry density of basalts versus ultrasonic velocity. Other trends of correlation are also given in table 4.1. 115 specimens are used to perform this test. It can be seen clearly from figure 4.1, dry density of basalt increases as ultrasonic velocity increase. Dry density of basalts reach the maximum value at 6478,3 m/s ultrasonic velocity and it reaches the minimum value at 4000,0 m/s ultrasonic velocity. Maximum and minimum dry density values are 2,79 g/cm$^3$ and 2,23 g/cm$^3$.

Rock samples were selected different from each other much possible. However, rock samples are concentrated dense between 5436,4 m/s and 6387,8 m/s ultrasonic velocities. If the rock samples were selected between maximum and minimum ultrasonic velocity values equally, it would be seen clearer increase in the figure 4.1.

In this graphic the relationship follows a linear law with a reasonable squared regression coefficient R-square is 0,2471 and equation is y = 0,0001x + 1,9054.

#### 4.2.1.2. Bulk density versus ultrasonic velocity for samples of Brazil test

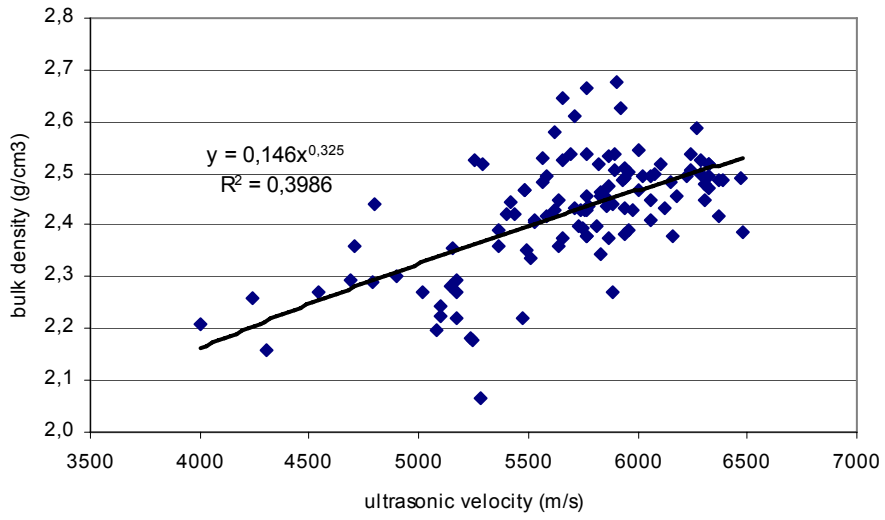


Figure 4.2. Ultrasonic velocity – Bulk density diagram

Table 4.2. Equation and $R^2$ values for Ultrasonic velocity – Bulk density

| TRENDLINE TYPE | $R^2$ | EQUATION |
|---|---|---|
| LINEAR | 0,3881 | y = 0,0001x + 1,6181 |
| POWER | 0,3986 | $y = 0,146x^{0,325}$ |
| EXPONENTIAL | 0,2491 | $y = 1,9754e^{5E-0,5x}$ |

Figure 4.2 shows the highest $R^2$ for test results of the bulk density of basalts versus ultrasonic velocity. Other trends of correlation are also given in table 4.2. 115 specimens are used to perform this test. It can be seen clearly from figure 4.2.

bulk density of basalt increases as ultrasonic velocity increase. Bulk density of basalts reach the maximum value at 6478,3 m/s ultrasonic velocity and it reaches the minimum value at 4000,0 m/s ultrasonic velocity. Maximum and minimum bulk density values are 2,68 g/cm$^3$ and 2,07 g/cm$^3$.

Rock samples were selected different from each other much possible. However, rock samples are concentrated between 5363,6 m/s and 6387,8 m/s ultrasonic velocities. If the rock samples were selected between maximum and minimum ultrasonic velocity values equally, ıt would be seen clearer increase in the figure 4.2.

In this graphic the relationship follows a power law with a reasonable squared regression coefficient R-square is 0,3986 and equation is $y = 0{,}146x^{0{,}325}$ .

### 4.2.1.3. Saturated density versus ultrasonic velocity for samples of Brazil test

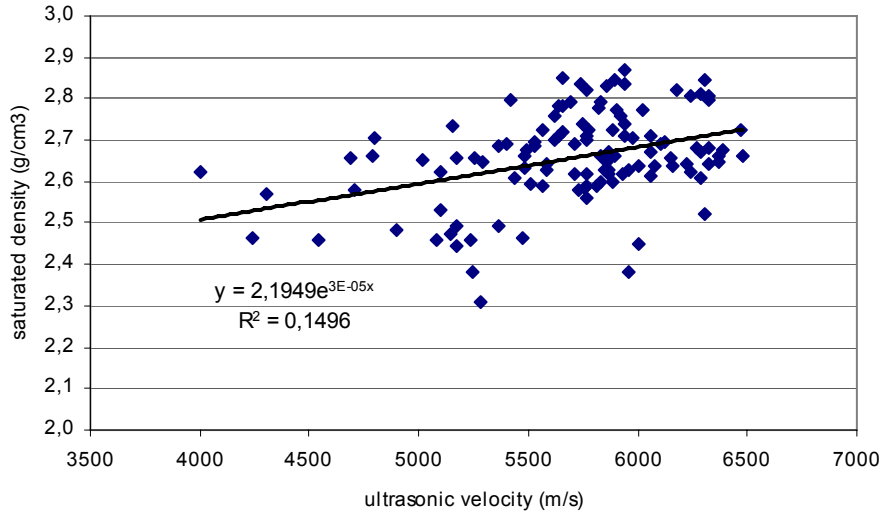


Figure 4.3. Ultrasonic Velocity – Saturated density diagram

Table 4.3. Equation and $R^2$ values for Ultrasonic Velocity – Saturated density

| TRENDLINE TYPE | $R^2$ | EQUATION |
|---|---|---|
| LINEAR | 0,1489 | y = 9E-05x + 2,1593 |
| POWER | 0,1488 | $y = 0{,}5906x^{0{,}1799}$ |
| EXPONENTIAL | 0,1496 | $y = 2{,}1949e^{3E\text{-}0{,}5x}$ |

Figure 4.3 shows the highest $R^2$ for test results of the saturated density of basalts versus ultrasonic velocity. Other trends of correlation are also given in table 4.3. 115 specimens are used to perform this test. It can be seen clearly from figure 4.3. saturated density of basalt increases as ultrasonic velocity increase. Saturated density of basalts reach the maximum value at 6478,3 m/s ultrasonic velocity and it reaches the minimum value at 4000,0 m/s ultrasonic velocity. Maximum and minimum saturated density values are 2,87 g/cm$^3$ and 2,31 g/cm$^3$.

Rock samples were selected different from each other much possible. However, rock samples are concentrated between 5436,4 m/s and 6387,8 m/s ultrasonic velocities. If the rock samples were selected between maximum and minimum ultrasonic velocity values equally, ıt would be seen clearer increase in the figure 4.3.

In this graphic the relationship follows an exponential law with a reasonable squared regression coefficient R-square is 0,1496 and equation is $y = 2{,}1949e^{3E\text{-}0{,}5x}$.

#### 4.2.1.4. Water absorption versus ultrasonic velocity for samples of Brazil test

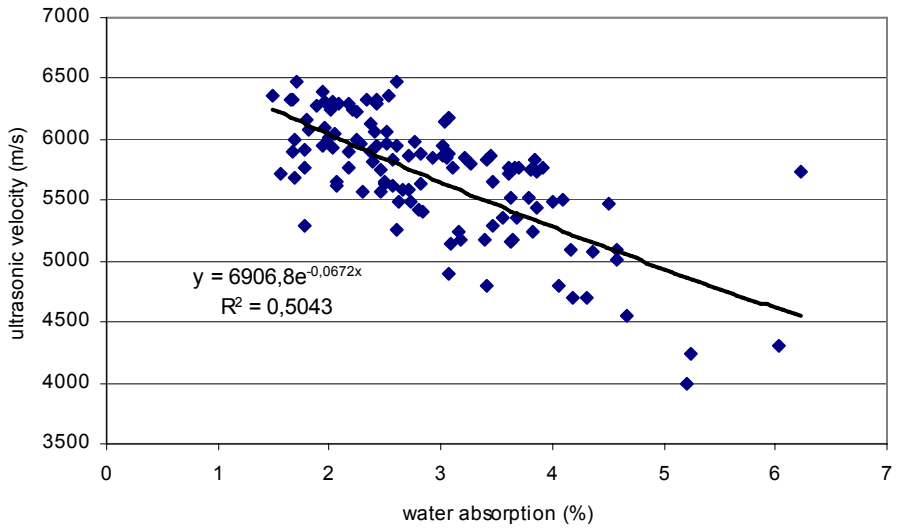


Figure 4.4. Ultrasonic velocity – Water absorption diagram

Table 4.4. Equation and $R^2$ values for Ultrasonic velocity – Water absorption

| TRENDLINE TYPE | $R^2$ | EQUATION |
|---|---|---|
| LINEAR | 0,5022 | $y = -0,0014x + 10,842$ |
| POWER | 0,4683 | $y = 0,6938,9x^{0,1965}$ |
| EXPONENTIAL | 0,5043 | $y = 6,9068e^{-0,0672x}$ |

Figure 4.4 shows the highest $R^2$ for test results of the water absorption of basalts versus ultrasonic velocity. Other trends of correlation are also given in table 4.4. 115 specimens are used to perform this test. It can be seen clearly from figure 4.4, water absorption of basalt decreases as ultrasonic velocity increase. Water absorption of basalts reach the maximum value at 6478,3 m/s ultrasonic velocity and it reaches the minimum value at 4000,0 m/s ultrasonic velocity. Maximum and minimum water absorption values are 6,22 % and 1,50 %.

Rock samples were selected different from each other much possible. However, rock samples are concentrated between 5152,5 m/s and 6326,5 m/s ultrasonic velocities. If the rock samples were selected between maximum and minimum ultrasonic velocity values equally, ıt would be seen clearer increase in the figure 4.4.

In this graphic the relationship follows an exponential law with a reasonable squared regression coefficient R-square is 0,5043 and equation is $y = 6,9068e^{-0,0672x}$.

### 4.2.1.5. Porosity versus ultrasonic velocity for samples of Brazil test

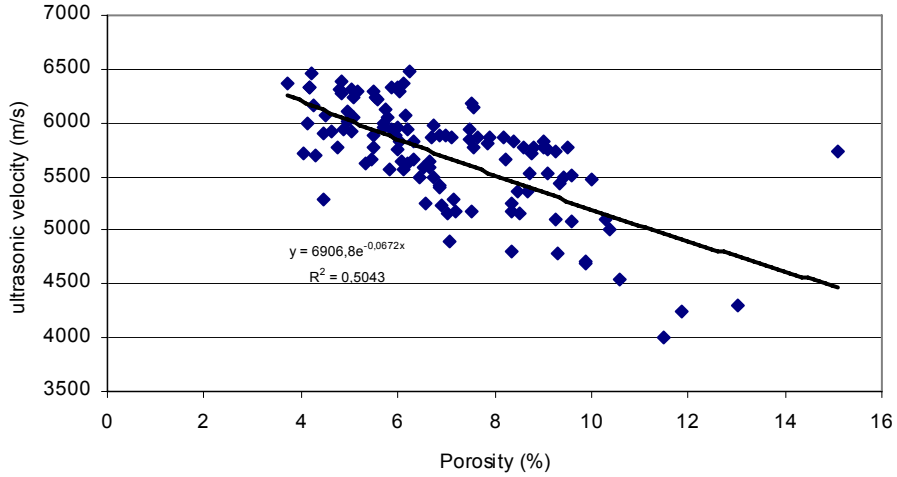


Figure 4.5. Ultrasonic velocity – Porosity diagram

Table 4.5. Equation and $R^2$ values for Ultrasonic velocity – Water absorption

| TRENDLINE TYPE | $R^2$ | EQUATION |
|---|---|---|
| LINEAR | 0,4506 | y = -159,48x + 6816,6 |
| POWER | 0,4348 | $y = 8493,7x^{-0,2113}$ |
| EXPONENTIAL | 0,5043 | $y = 6,9068e^{-0,0672x}$ |

Figure 4.5 shows the highest $R^2$ for test results of the porosity of basalts versus ultrasonic velocity. Other trends of correlation are also given in table 4.5. 115 specimens are used to perform this test. It can be seen clearly from figure 4.5, porosity of basalt increases as ultrasonic velocity increase. porosity of basalts reach the maximum value at 6478,3 m/s ultrasonic velocity and it reaches the minimum value at 4000,0 m/s ultrasonic velocity. Maximum and minimum porosity values are 3,72 MPa and 15,10 MPa.

Rock samples were selected different from each other much possible. However, rock samples are concentrated between 5152,5 m/s and 6326,5 m/s ultrasonic velocities. If the rock samples were selected between maximum and minimum ultrasonic velocity values equally, it would be seen clearer increase in the figure 4.5.

In this graphic the relationship follows an exponential law with a reasonable squared regression coefficient R-square is 0,5043 and equation is $y = 6,9068e^{-0,0672x}$.

#### 4.2.1.6. Brazillian tensile strength versus ultrasonic velocity for samples of Brazil test

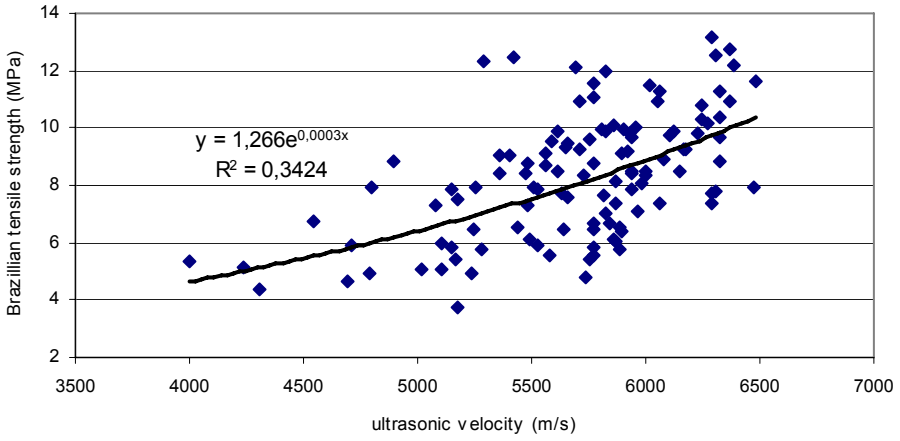


Figure 4.6. Ultrasonic velocity – Brazillian tensile strength diagram

Table 4.6.Equation and $R^2$ values for Ultrasonic velocity – Brazillian tensile strength

| TRENDLINE TYPE | $R^2$ | EQUATION |
|---|---|---|
| LINEAR | 0,3139 | y = -0,0025x + 5,6989 |
| POWER | 0,3378 | $y = 2E-06x^{1,738}$ |
| EXPONENTIAL | 0,3424 | $y = 1,266e^{0,0003x}$ |

Figure 4.6 shows the highest $R^2$ for test results of the Brazillian tensile strength of basalts versus ultrasonic velocity. Other trends of correlation are also given in table 4.6. 115 specimens are used to perform this test. It can be seen clearly from figure 4.6, brazillian tensile strength of basalt increases as ultrasonic velocity increase. Brazillian tensile strength of basalts reach the maximum value at 6478,3 m/s ultrasonic velocity and it reaches the minimum value at 4000,0 m/s ultrasonic velocity. Maximum and minimum brazillian tensile strength values are 13,16 MPa and 3,71 MPa.

Rock samples were selected different from each other much possible. However, rock samples are concentrated between 5152,5 m/s and 6326,5 m/s ultrasonic velocities. If the rock samples were selected between maximum and minimum ultrasonic velocity values equally, ıt would be seen clearer increase in the figure 4.6.

In this graphic the relationship follows an exponential law with a reasonable squared regression coefficient R-square is 0,3424 and equation is $y = 1{,}266e^{0{,}0003x}$.

#### 4.2.1.7. Dry density versus Brazillian tensile strength

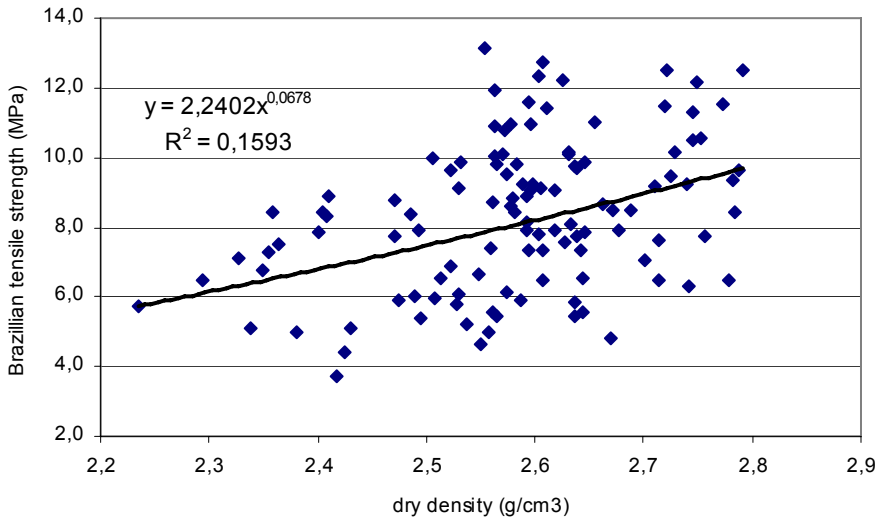


Figure 4.7. Dry density – Brazillian tensile strength diagram

Table 4.7. Equation and $R^2$ values for Dry density – Brazillian tensile strength

| TRENDLINE TYPE | $R^2$ | EQUATION |
|---|---|---|
| LINEAR | 0,1571 | y = 0,0216x + 2,4031 |
| POWER | 0,1593 | $y = 2{,}2402x^{0{,}0678}$ |
| EXPONENTIAL | 0,1574 | $y = 2{,}4042e^{0{,}0085x}$ |

Figure 4.7 shows the highest $R^2$ for test results of the dry density of basalts versus Brazillian tensile strength. Other trends of correlation are also given in table 4.7. 115

specimens are used to perform this test. It can be seen clearly from figure 4.7, dry density of basalt increases as Brazillian tensile strength increase. Dry density of basalts reach the maximum value at 13,16 Mpa Brazillian tensile strength and it reaches the minimum value at 3,71 Mpa Brazillian tensile strength. Maximum and minimum dry density values are 2,79 g/cm$^3$ and 2,23 g/cm$^3$.

Rock samples were selected different from each other much possible. Rock samples are concentrated dense between 3,71 Mpa and 13,16 Mpa Brazillian tensile strengths.

In this graphic the relationship follows a power law with a reasonable squared regression coefficient R-square is 0,1593 and equation is $y = 0{,}2402x^{0{,}0678}$.

#### 4.2.1.8. Bulk density versus Brazillian tensile strength

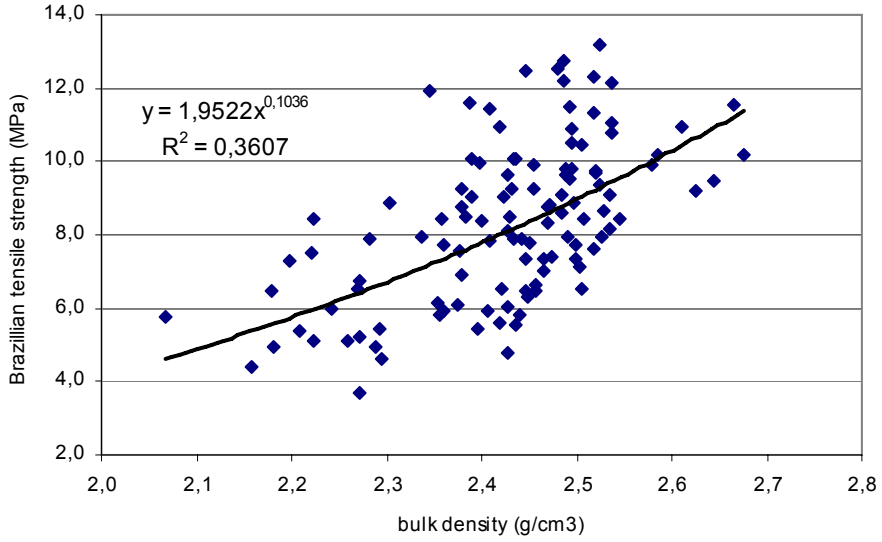


Figure 4.8. Bulk density – Brazillian tensile strength diagram

Table 4.8. Equation and $R^2$ values for Bulk density – Brazillian tensile strength

| TRENDLINE TYPE | $R^2$ | EQUATION |
|---|---|---|
| LINEAR | 0,3313 | $y = 0{,}0298x + 2{,}1772$ |
| POWER | 0,3607 | $y = 1{,}9522x^{0{,}1036}$ |
| EXPONENTIAL | 0,3302 | $y = 2{,}1836e^{0{,}0125x}$ |

Figure 4.8 shows the highest $R^2$ for test results of the bulk density of basalts versus Brazillian tensile strength. Other trends of correlation are also given in table 4.8. 115 specimens are used to perform this test. It can be seen clearly from figure 4.8. bulk density of basalt increases as Brazillian tensile strength increase. Bulk density of basalts reach the maximum value at 13,16 Mpa Brazillian tensile strength and it reaches the minimum value at 3,71 Mpa Brazillian tensile strength. Maximum and minimum bulk density values are 2,68 g/cm$^3$ and 2,07 g/cm$^3$.

Rock samples were selected different from each other much possible. However, rock samples are concentrated between 3,71 Mpa and 13,16 Mpa Brazillian tensile strengths.

In this graphic the relationship follows a power law with a reasonable squared regression coefficient R-square is 0,3607 and equation is $y = 1{,}9522x^{0{,}1036}$.

#### 4.2.1.9. Saturated density versus Brazillian tensile strength

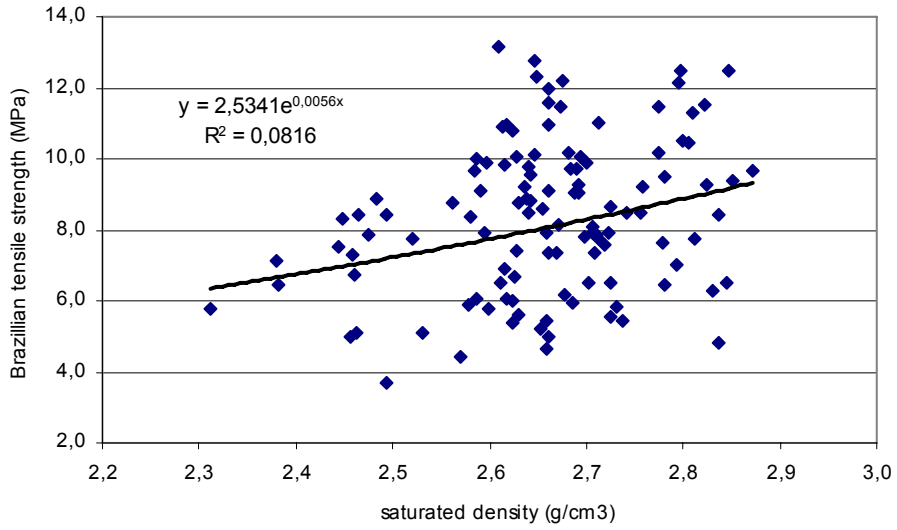


Figure 4.9. Saturated density- Brazillian tensile strength diagram

Table 4.9.Equation and $R^2$ values for Saturated density – Brazillian tensile strength

| TRENDLINE TYPE | $R^2$ | EQUATION |
|---|---|---|
| LINEAR | 0,0804 | $y = 0,0146x + 2,536$ |
| POWER | 0,0806 | $y = 2,421x^{0,0444}$ |
| EXPONENTIAL | 0,0816 | $y = 2,5341e^{0,0056x}$ |

Figure 4.9 shows the highest $R^2$ for test results of the saturated density of basalts versus Brazillian tensile strength. Other trends of correlation are also given in table 4.9. 115 specimens are used to perform this test. It can be seen clearly from figure 4.9. saturated density of basalt increases as Brazillian tensile strength increase. Saturated density of basalts reach the maximum value at 13,16 Mpa Brazillian tensile strength and it reaches the minimum value at 3,71 Mpa Brazillian tensile strength. Maximum and minimum saturated density values are 2,87 g/cm$^3$ and 2,31 g/cm$^3$.

Rock samples were selected different from each other much possible. However, rock samples are concentrated between 3,71 Mpa and 13,16 Mpa Brazillian tensile strengths.

In this graphic the relationship follows an exponential law with a reasonable squared regression coefficient R-square is 0,0816 and equation is $y = 2,5341e^{0,0056x}$.

#### 4.2.1.10. Water absorption versus Brazillian tensile strength

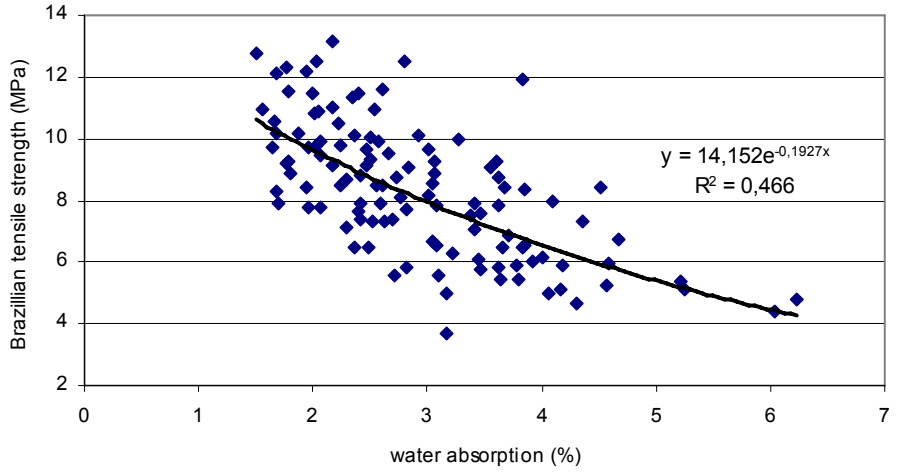


Figure 4.10. Water absorption- Brazillian tensile strength diagram

Table 4.10. Equation and $R^2$ values for Water absorption – Brazillian tensile strength

| TRENDLINE TYPE | $R^2$ | EQUATION |
|---|---|---|
| LINEAR | 0,438 | y = -0,2953x + 5,3884 |
| POWER | 0,4657 | $y = 14{,}655x^{-0{,}5849}$ |
| EXPONENTIAL | 0,466 | $y = 14{,}152e^{-0{,}1927x}$ |

Figure 4.10 shows the highest $R^2$ for test results of the water absorption of basalts versus Brazillian tensile strength. Other trends of correlation are also given in table 4.10. 115 specimens are used to perform this test. It can be seen clearly from figure 4.10, water absorption of basalt decreases as Brazillian tensile strength increase. Water absorption of basalts reach the maximum value at 13,16 MPa Brazillian tensile strength and it reaches the minimum value at 3,71 MPa Brazillian tensile strength. Maximum and minimum water absorption values are 6,22 % and 1,50 %.

Rock samples were selected different from each other much possible. However, rock samples are concentrated between 3,71 MPa and 13,76 MPa Brazillian tensile strengths.

In this graphic the relationship follows an exponential law with a reasonable squared regression coefficient R-square is 0,466 and equation is $y = 14{,}152\ e^{-0{,}1927x}$

#### 4.2.1.11. Porosity versus Brazillian tensile strength

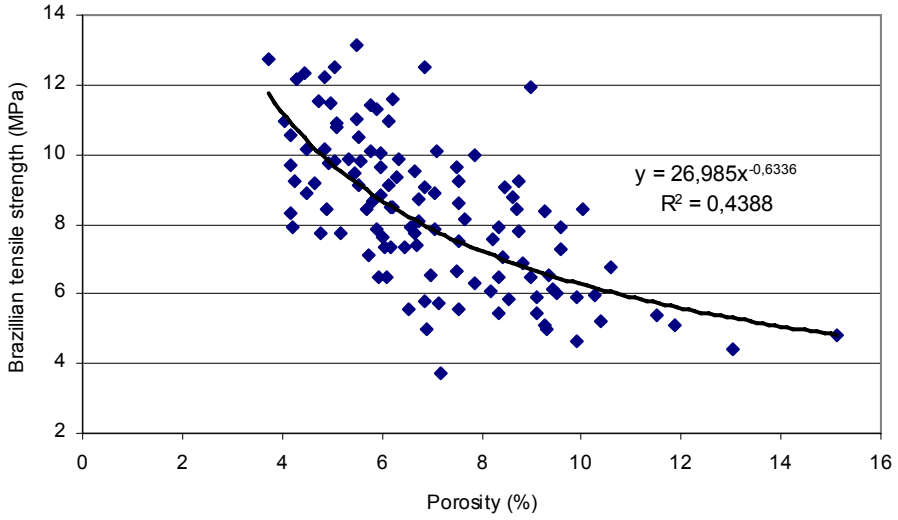


Figure 4.11. Porosity - Brazillian tensile strength diagram

Table 4.11. Equation and $R^2$ values for Porosity – Brazillian tensile strength

| TRENDLINE TYPE | $R^2$ | EQUATION |
|---|---|---|
| LINEAR | 0,4167 | $y = -0{,}674x + 13{,}072$ |
| POWER | 0,4388 | $y = 26{,}985x^{-0{,}6336}$ |
| EXPONENTIAL | 0,4387 | $y = 14{,}843e^{-0{,}0871x}$ |

Figure 4.11 shows the highest $R^2$ for test results of the porosity of basalts versus Brazillian tensile strength. Other trends of correlation are also given in table 4.11. 115 specimens are used to perform this test. It can be seen clearly from figure 4.11, porosity of basalt decreases as Brazillian tensile strength increase. porosity of basalts reach the maximum value at 13,16 MPa Brazillian tensile strength and it reaches the minimum value at 3,71 MPa Brazillian tensile strength. Maximum and minimum porosity values are 15,10 % and 3,72 %.

Rock samples were selected different from each other much possible. However, rock samples are concentrated between 3,71 MPa and 13,76 MPa Brazillian tensile strengths.

In this graphic the relationship follows a power law with a reasonable squared regression coefficient R-square is 0,466 and equation is $y = 26{,}985x^{-0{,}6336}$.

### 4.3. Direct Shear Test

Direct shear test was performed according to ISRM (1981). 12 samples were used for direct shear test. Samples used for direct shear test are block samples which has a dimensions 50 mm * 50 mm. This test is not confidental, Because of the lack of the specimen and the friction between the concretes after the sample was broken.

#### 4.3.1. Results

Results obtained from direct shear test were plotted on graphics

##### 4.3.1.1. Dry density versus ultrasonic velocity for samples of direct shear test

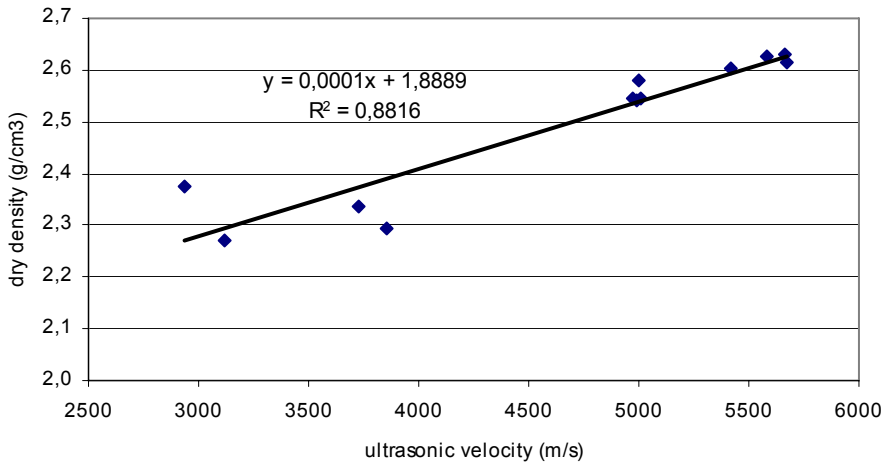


Figure 4.12. Ultrasonic velocity – Dry density diagram

Table 4.12. Equation and $R^2$ values for Ultrasonic velocity – Dry density

| TRENDLINE TYPE | $R^2$ | EQUATION |
|---|---|---|
| LINEAR | 0,8816 | $y = 0,0001x + 1,8889$ |
| POWER | 0,8445 | $y = 0,392x^{0,2196}$ |
| EXPONENTIAL | 0,8768 | $y = 1,9468e^{5E-05x}$ |

Figure 4.12 shows the highest $R^2$ for test results of the dry density of basalts versus Ultrasonic velocity. Other trends of correlation are also given in table 4.12. 12 specimens are used to perform this test. It can be seen clearly from figure 4.12, dry density of basalt increases as ultrasonic velocity increase. Dry density of basalts reach the maximum value at 5670,5 m/s ultrasonic velocity and it reaches the minimum value at 2939,8 m/s ultrasonic velocity. Maximum and minimum dry density values are 2,63 g/cm$^3$ and 2,27 g/cm$^3$.

In this graphic the relationship follows a linear law with a reasonable squared regression coefficient R-square is 0,8816 and equation is y = 0,0001x + 1,8889.

#### 4.3.1.2. Bulk density versus ultrasonic velocity for samples of direct shear test

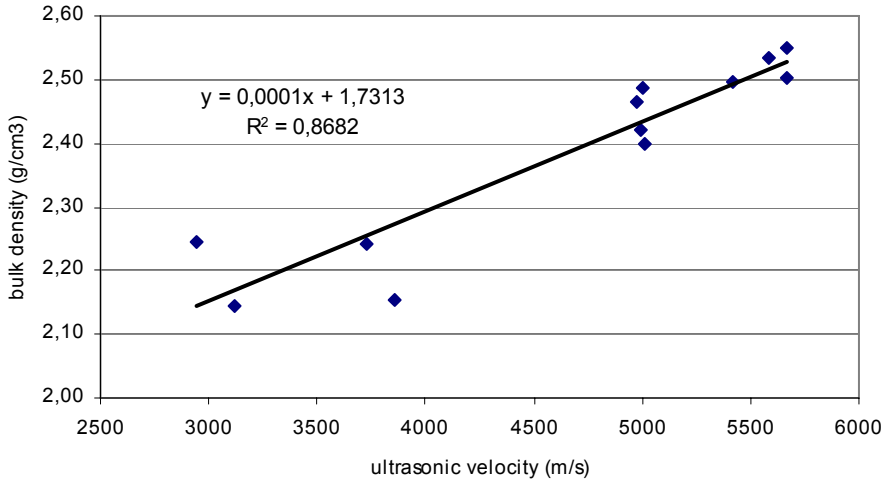


Figure 4.13. Ultrasonic velocity – Bulk density diagram

Table 4.13. Equation and $R^2$ values for Ultrasonic velocity – Bulk density

| TRENDLINE TYPE | $R^2$ | EQUATION |
|---|---|---|
| LINEAR | 0,8682 | $y = 0,0001x + 1,7313$ |
| POWER | 0,8331 | $y = 0,2943x^{0,2483}$ |
| EXPONENTIAL | 0,864 | $y = 1,8015e^{6E-05x}$ |

Figure 4.13 shows the highest $R^2$ for test results of the bulk density of basalts versus ultrasonic velocity. Other trends of correlation are also given in table 4.13. 12 specimens are used to perform this test. It can be seen clearly from figure 4.13, bulk density of basalt increases as ultrasonic velocity increase. Bulk density of basalts reach the maximum value at 5670,5 m/s ultrasonic velocity and it reaches the minimum value at 2939,8 m/s ultrasonic velocity. Maximum and minimum bulk density values are 2,55 g/cm$^3$ and 2,15 g/cm$^3$.

In this graphic the relationship follows a linear law with a reasonable squared regression coefficient R-square is 0,8682 and equation is y = 0,0001x + 1,7313.

#### 4.3.1.3. Saturated density versus ultrasonic velocity for samples of direct shear test

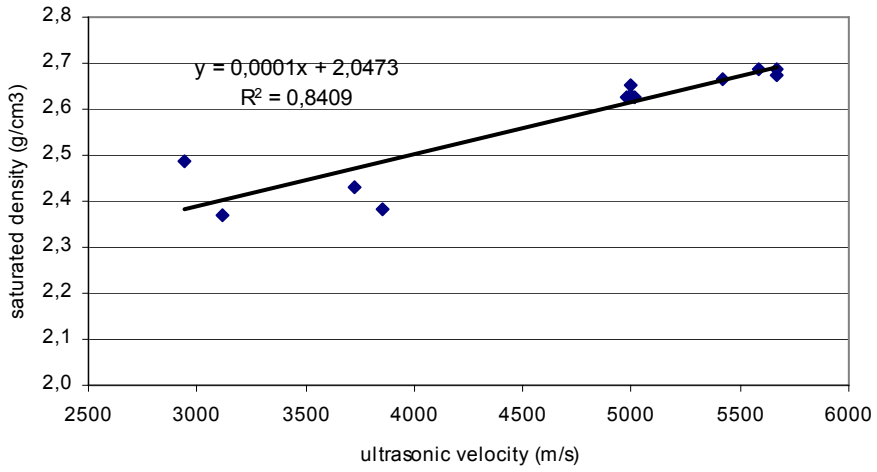


Figure 4.14. Ultrasonic velocity – Saturated density diagram

Table 4.14. Equation and $R^2$ values for Ultrasonic velocity – Saturated density

| TRENDLINE TYPE | $R^2$ | EQUATION |
|---|---|---|
| LINEAR | 0,8409 | $y = 0,0001x + 2,0473$ |
| POWER | 0,8024 | $y = 0,5418x^{0,185}$ |
| EXPONENTIAL | 0,8346 | $y = 2,0895e^{4E-05x}$ |

Figure 4.14 shows the highest $R^2$ for test results of the saturated density of basalts versus ultrasonic velocity. Other trends of correlation are also given in table 4.14. 12 specimens are used to perform this test. It can be seen clearly from figure 4.14, saturated density of basalt increases as ultrasonic velocity increase. Saturated density of basalts reach the maximum value at 5670,5 m/s ultrasonic velocity and it reaches the minimum value at 2939,8 m/s ultrasonic velocity. Maximum and minimum saturated density values are 2,69 g/cm$^3$ and 2,37 g/cm$^3$.

In this graphic the relationship follows a linear law with a reasonable squared regression coefficient R-square is 0,8409 and equation is y = 0,0001x + 2,0473.

#### 4.3.1.4. Water absorption versus ultrasonic velocity for samples of direct shear test

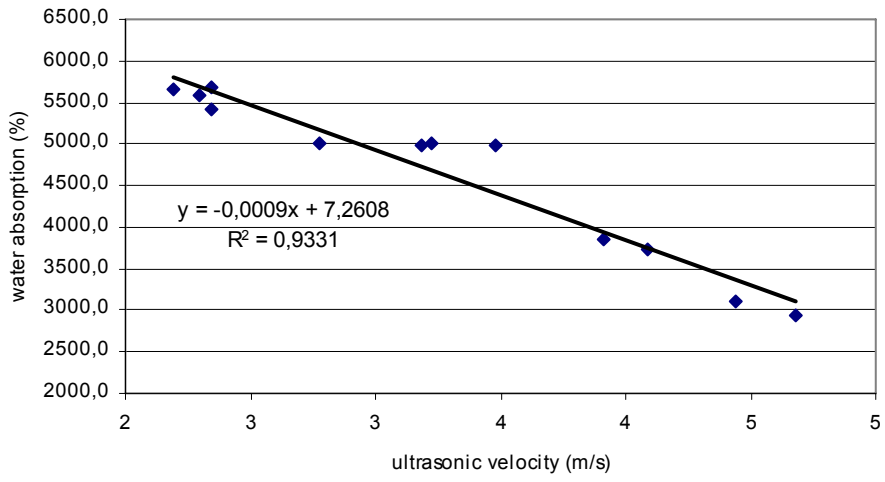


Figure 4.15. Ultrasonic velocity – Water absorption diagram

Table 4.15. Equation and $R^2$ values for Ultrasonic velocity – Water absorption

| TRENDLINE TYPE | $R^2$ | EQUATION |
|---|---|---|
| LINEAR | 0,9331 | $y = -0,0009x + 7,2608$ |
| POWER | 0,852 | $y = 11279x^{-0,7927}$ |
| EXPONENTIAL | 0,9082 | $y = 10378e^{-0,2536x}$ |

Figure 4.15 shows the highest $R^2$ for test results of the water absorption of basalts versus ultrasonic velocity. Other trends of correlation are also given in table 4.15. 12 specimens are used to perform this test. It can be seen clearly from figure 4.15, water absorption of basalt decreases as ultrasonic velocity increase. Water absorption of basalts reach the maximum value at 5670,5 m/s ultrasonic velocity and it reaches the minimum value at 2939,8 m/s ultrasonic velocity. Maximum and minimum water absorption values are 4,68 % and 2,19 %.

In this graphic the relationship follows a linear law with a reasonable squared regression coefficient R-square is 0,9331 and equation is y = -0,0009x + 7,2608.

### 4.3.2. Determination of friction angle and cohesion of basalt samples by direct shear test

In this part friction angle and cohesion of basalt samples were determined. Basalt samples are divided into three groups according to their visual variation. Four different samples selected out of variety of basalt samples that represent each group. Results are found out and represented as figures and tables.

- Vesicular basalt
- Vesicular basalt with calcite
- Basalt with no vesicle and calcite

#### 4.3.2.1. Vesicular basalt

Table 4.16. Direct Shear Test Results (vesicular basalt)

| Sample no | N (Kn) | T (Kn) | Size A (mm) | Size B (mm) | Area (m2) | Shear strength (kPa) | Normal stress (kPa) |
|---|---|---|---|---|---|---|---|
| 21 | 5 | 28,5 | 46,8 | 50,3 | 0,00235 | 12106,85 | 2124,01 |
| 32 | 10 | 32,0 | 46,1 | 51,0 | 0,00235 | 13610,65 | 4253,33 |
| 37 | 10 | 33,0 | 46,4 | 49,8 | 0,00231 | 14281,26 | 4327,66 |
| 4 | 15 | 38,5 | 48,8 | 49,6 | 0,00242 | 15905,94 | 6197,12 |

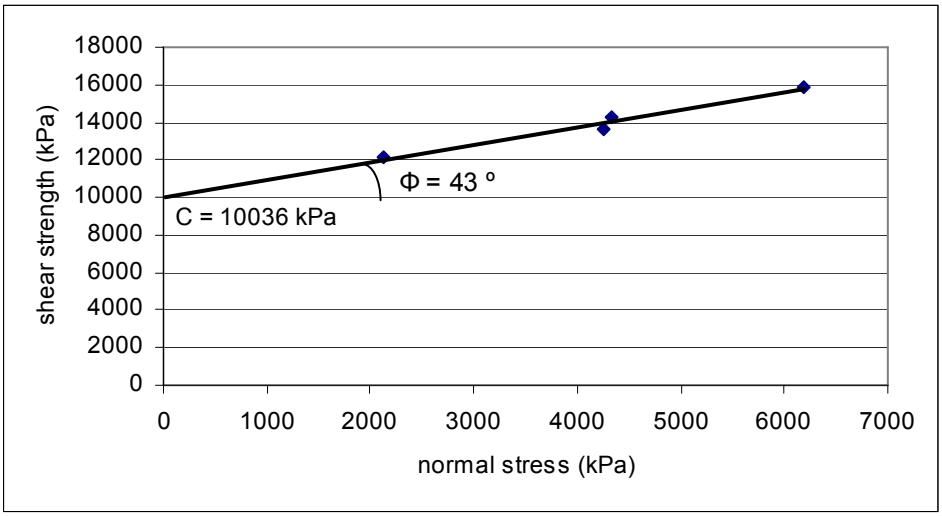


Figure 4.16. Shear Strength – Normal stress diagram (vesicular basalt)

Figure 4.16 shows the shear strength – normal stress diagram of the vesicular basalt samples. Other values which was obtained from the test is given in table 4.16. 4 specimens are used to perform this test. As can be seen from figure 4.16, shear strength increases as normal strength increase. From this figure friction angle and cohesion can be determined. The cohesion of this group determined from the graphic is 10036 kPa and the friction angle is $43^0$.

### 4.3.2.2. Vesicular basalt with calcite

Table 4.17. Direct Shear Test Results (Vesicular basalt with calcite)

| Sample no | N (Kn) | T (Kn) | Size A (mm) | Size B (mm) | Area (m2) | shear strength (kPa) | normal stress (kPa) |
|---|---|---|---|---|---|---|---|
| 33 | 5 | 11,0 | 50,1 | 52,9 | 0,00265 | 4150,49 | 1886,59 |
| 55 | 10 | 14,0 | 45,2 | 50,0 | 0,00226 | 6194,69 | 4424,78 |
| 59 | 10 | 18,5 | 50,0 | 53,1 | 0,00266 | 6967,98 | 3766,48 |
| 57 | 15 | 24,5 | 46,3 | 50,1 | 0,00232 | 10562,03 | 6466,55 |

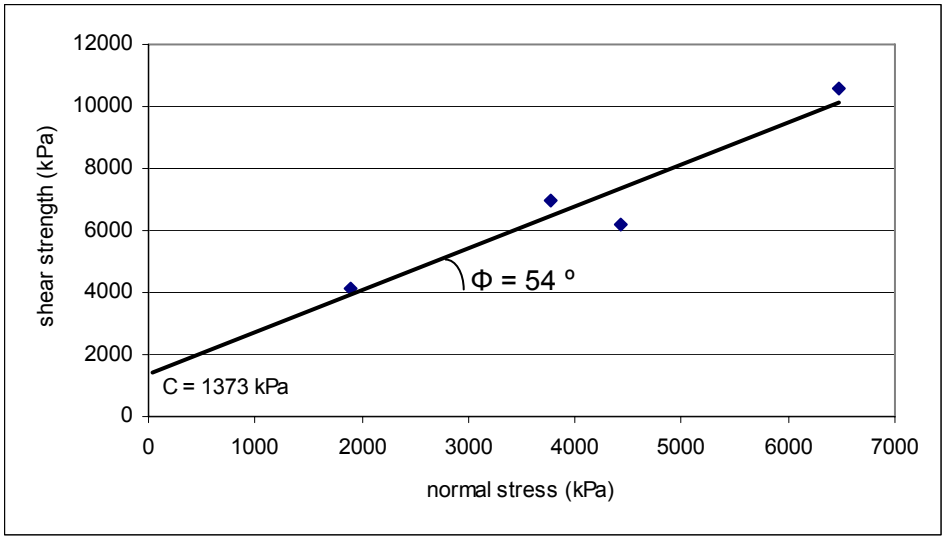


Figure 4.17. Shear Strength – Normal stress diagram (Vesicular basalt with calcite)

Figure 4.17 shows the shear strength – normal stress diagram of the vesicular basalt with calcite samples. Other values which was obtained from the test is given in table 4.17. 4 specimens are used to perform this test. As can be seen from figure 4.17, shear strength increases as normal strength increase. From this figure friction angle and cohesion can be determined. The cohesion of this group determined from the graphic is 1373 kPa and the friction angle is $54^0$.

### 4.3.2.3. Basalt with no vesicle and calcite

Table 4.18. Direct Shear Test Results (Basalt with no vesicle and calcite)

| Sample no | N (Kn) | T (Kn) | Size A (mm) | Size B (mm) | Area (m2) | Shear strength (kPa) | Normal stress (kPa) |
|---|---|---|---|---|---|---|---|
| 16 | 5 | 20 | 47,3 | 51,0 | 0,002412 | 8290,84 | 2072,71 |
| 46 | 5 | 16 | 46,6 | 52,3 | 0,002437 | 6564,96 | 2051,55 |
| 13 | 10 | 28 | 48,4 | 48,7 | 0,002357 | 11879,10 | 4242,54 |
| 38 | 15 | 34 | 46,3 | 51,5 | 0,002384 | 14259,05 | 6290,76 |

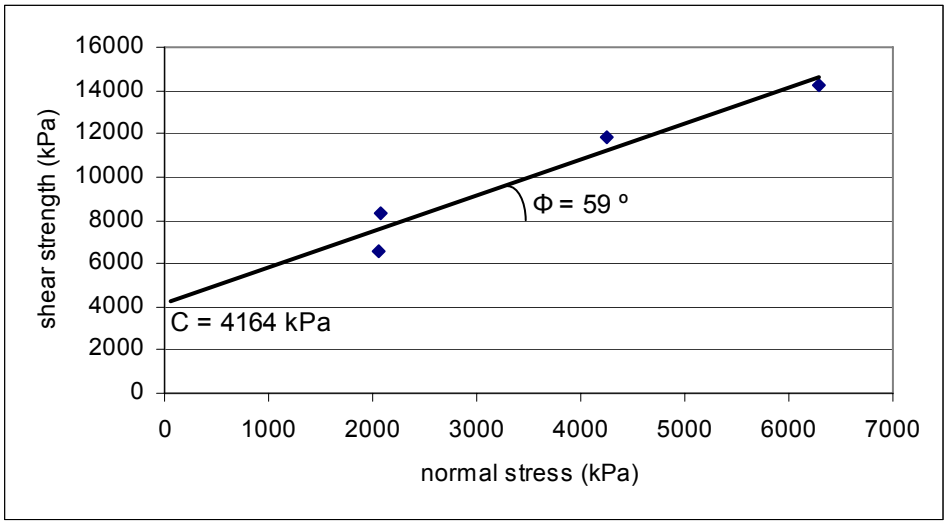


Figure 4.18 Shear Strength–Normal stress diagram
(Basalt with no vesicle and calcite)

Figure 4.18 shows the shear strength – normal stress diagram of the vesicular basalt samples. Other values which was obtained from the test is given in table 4.18. 4 specimens are used to perform this test. As can be seen from figure 4.18, shear strength increases as normal strength increase. From this figure friction angle and cohesion can be determined. The cohesion of this group determined from the graphic is 4164 kPa and the friction angle is $59^0$.

### 4.3.2.4. Graphics ultrasonic velocity versus friction angle and cohesion.

Table 4.19. Friction angle and cohesion values for each group

| Sample no | Cohesion kPa | Angle Φ | Average velocity m/s |
|---|---|---|---|
| 33-55-57-59 | 1373 | 54 | 3409,991 |
| 16-46-13-38 | 4164 | 59 | 5584,870 |
| 21-32-37-4 | 10036 | 43 | 4994,872 |

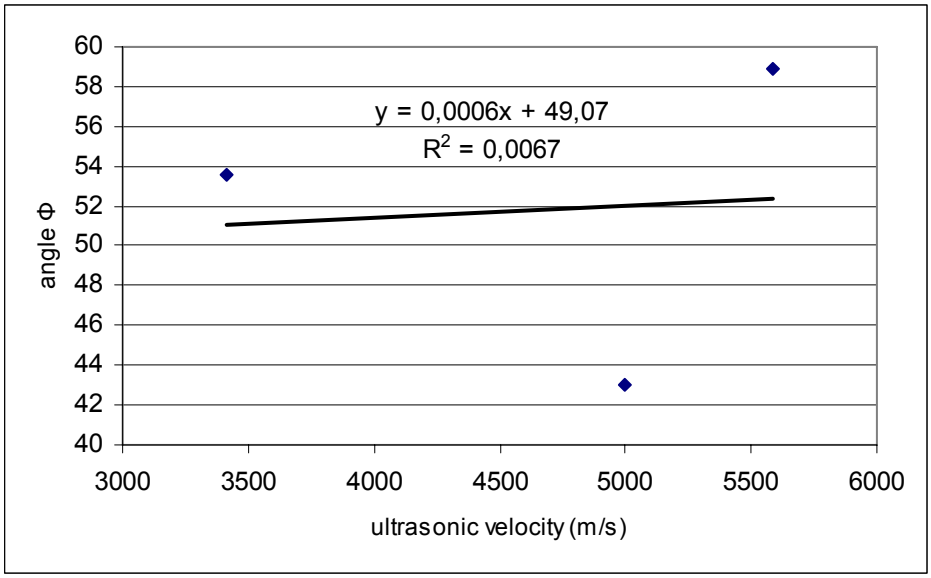


Figure 4.19 Friction angle – Ultrasonic velocity diagram

Table 4.20. Equation and $R^2$ values for Friction angle – Ultrasonic velocity

| TRENDLINE TYPE | $R^2$ | EQUATION |
|---|---|---|
| LINEAR | 0,0067 | $y = 0,0006x + 49,07$ |
| POWER | 1E-05 | $y = 52,369x^{-0,0023}$ |
| EXPONENTIAL | 0,002 | $y = 49,882e^{6E-06x}$ |

Figure 4.19 shows the highest $R^2$ for test results of the friction angle of basalts versus ultrasonic velocity. Other trends of correlation are also given in table 4.20 and table 4.19 shows the friction angle, cohesion and ultrasonic velocity values for each group. 12 specimens are used to perform this test. As can be seen from the figure 4.19 friction angle increases as ultrasonic velocity increase.

In this graphic the relationship follows a linear law with a reasonable squared regression coefficient R-square is 0,9331 and equation is y = 0,0006x + 49,07.

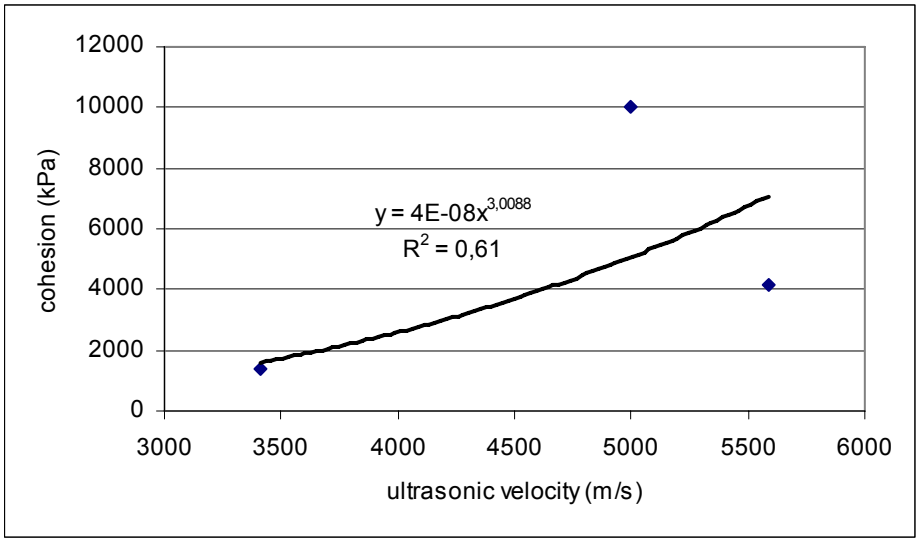


Figure 4.20 Cohesion – Ultrasonic velocity diagram

Table 4.21. Equation and $R^2$ values for Cohesion – Ultrasonic velocity

| TRENDLINE TYPE | $R^2$ | EQUATION |
|---|---|---|
| LINEAR | 0,2997 | y = 2,1522x – 4844,8 |
| POWER | 0,61 | $y = 4E\text{-}08x^{3,0088}$ |
| EXPONENTIAL | 0,5628 | $y = 173,77e^{0,0007x}$ |

Figure 4.20 shows the highest $R^2$ for test results of the cohesion of basalts versus ultrasonic velocity. Other trends of correlation are also given in Table 4.21. 12 specimens are used to perform this test. As can be seen from the figure cohesion increases as ultrasonic velocity increase.

In this graphic the relationship follows an exponential law with a reasonable squared regression coefficient R-square is 0,9331 and equation is $y = 173,77e^{0,0007x}$.

### 4.3.3. Determination of residual friction angle and cohesion of basalt samples by Direct Shear Test

In this part residual friction angle and cohesion of basalt samples were determined. Basalt samples are divided into three groups according to their visual variation. Four different samples selected out of variety of basalt samples that represent each group. Results are found out and represented as figures and tables.

- Vesicular basalt
- Vesicular basalt with calcite
- Basalt with no vesicle and calcite
-

#### 4.3.3.1. Vesicular basalt

Table 4.22.Direct Shear Test Results obtained for residual strength (vesicular basalt)

| Sample no | N (Kn) | T (Kn) | Size A (mm) | Size B (mm) | Area (m2) | shear strength (kPa) | normal stress (kPa) |
|---|---|---|---|---|---|---|---|
| 21 | 5 | 10 | 46,8 | 50,3 | 0,00235 | 4248,02 | 2124,01 |
| 32 | 10 | 15 | 46,1 | 51 | 0,00235 | 6379,99 | 4253,33 |
| 37 | 10 | 15 | 46,4 | 49,8 | 0,00231 | 6491,48 | 4327,66 |
| 4 | 15 | 27 | 48,8 | 49,6 | 0,00242 | 11154,81 | 6197,12 |

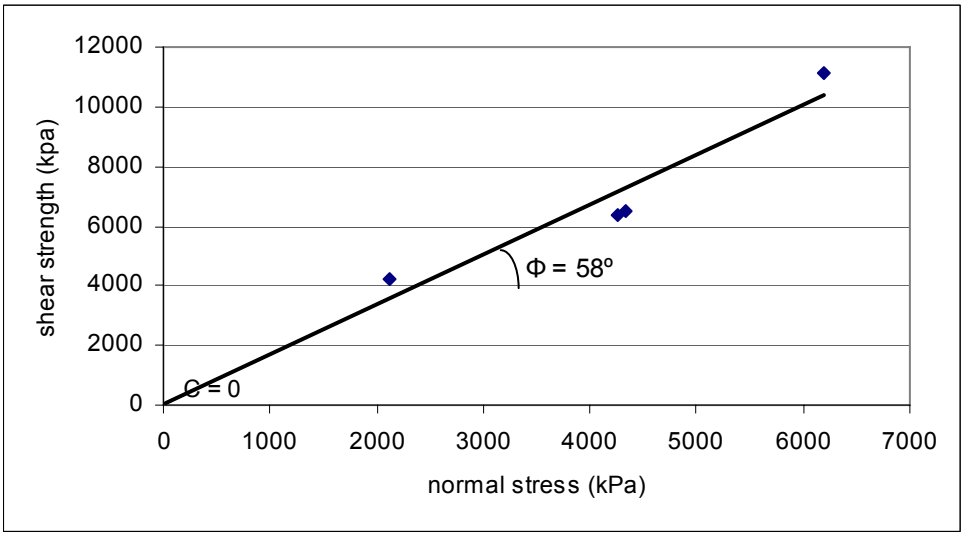


Figure 4.21. Shear Strength – Normal stress diagram for residual strength (vesicular basalt)

Figure 4.21 shows the shear strength – normal stress diagram of the vesicular basalt samples. Other values which was obtained from the test is given in table 4.22. 4 specimens are used to perform this test. As can be seen from figure 4.21, shear strength increases as normal strength increase. From this figure friction angle and cohesion can be determined. The cohesion of this group determined from the graphic is 0 kPa and the friction angle is $58^0$.

### 4.3.3.2. Vesicular basalt with calcite

Table 4.23. Direct Shear Test Results obtained for residual strength (Vesicular basalt with calcite)

| Sample no | N (Kn) | T (Kn) | Size A (mm) | Size B(mm) | Area (m2) | shear strength (kPa) | normal stress (kPa) |
|---|---|---|---|---|---|---|---|
| 33 | 5 | 5 | 50,1 | 52,9 | 0,00265 | 1886,59 | 1886,59 |
| 55 | 10 | 9,5 | 45,2 | 50 | 0,00226 | 4203,54 | 4424,78 |
| 59 | 10 | 12 | 50 | 53,1 | 0,00266 | 4519,77 | 3766,48 |
| 57 | 15 | 16 | 46,3 | 50,1 | 0,00232 | 6897,65 | 6466,55 |

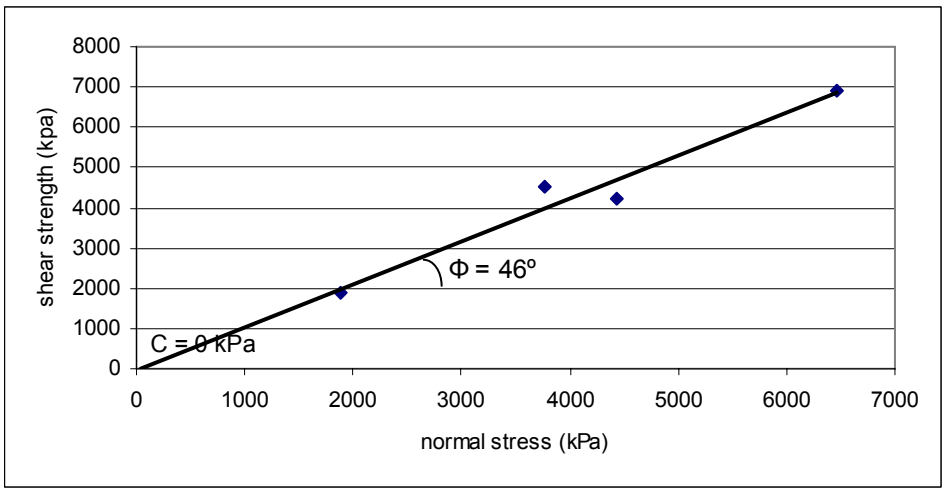


Figure 4.22 Shear Strength – Normal stress diagram for residual strength (Vesicular basalt with calcite)

Figure 4.22 shows the shear strength – normal stress diagram of the vesicular basalt samples. Other values which was obtained from the test is given in table 4.23. 4 specimens are used to perform this test. As can be seen from figure 4.22, shear

strength increases as normal strength increase. From this figure friction angle and cohesion can be determined. The cohesion of this group determined from the graphic is 0 kPa and the friction angle is $46^0$.

#### 4.3.3.3. Basalt with no vesicle and calcite

Table 4.24. Direct Shear Test Results obtained for residual strength (Basalt with no vesicle and calcite)

| Sample no | N (Kn) | T (Kn) | Size A (mm) | Size B (mm) | Area (m2) | shear strength (kPa) | normal stress (kPa) |
|---|---|---|---|---|---|---|---|
| 16 | 5 | 8 | 47,3 | 51 | 0,00241 | 3316,34 | 2072,71 |
| 46 | 5 | 7,5 | 46,6 | 52,3 | 0,00244 | 3077,33 | 2051,55 |
| 13 | 10 | 15 | 48,4 | 48,7 | 0,00236 | 6363,81 | 4242,54 |
| 38 | 15 | 23 | 46,3 | 51,5 | 0,00238 | 9645,83 | 6290,76 |

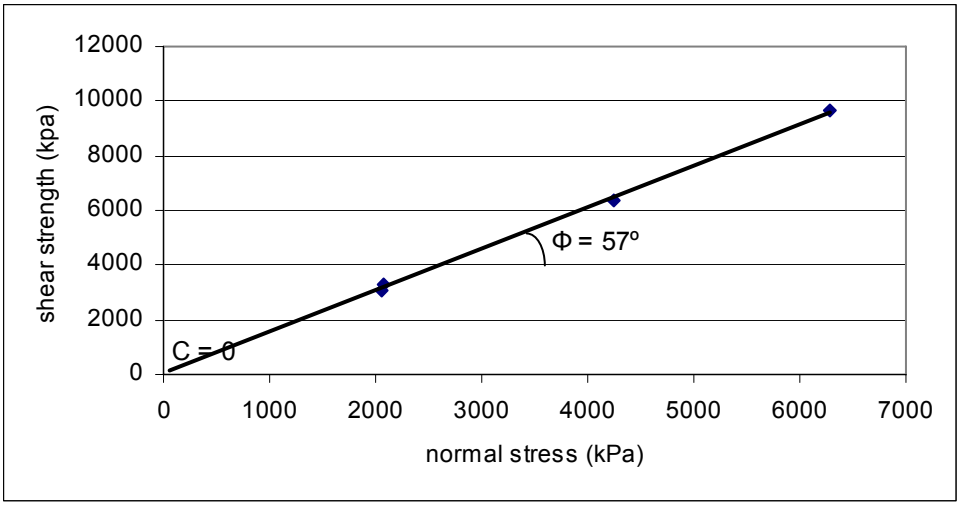


Figure 4.23 Shear Strength–Normal stress diagram for residual strength (Basalt with no vesicle and calcite)

Figure 4.23 shows the shear strength – normal stress diagram of the vesicular basalt samples. Other values which was obtained from the test is given in table 4.24. 4 specimens are used to perform this test. As can be seen from figure 4.23, shear strength increases as normal strength increase. From this figure friction angle and

cohesion can be determined. The cohesion of this group determined from the graphic is 0 kPa and the friction angle is $57^0$.

#### 4.3.3.4. Graphics ultrasonic velocity versus residual friction angle and cohesion.

Table 4.25. Friction angle and cohesion values for each group obtained for residual shear strength

| Sample no | Cohesion (kPa) | Angle Φ | Average Velocity (m/s) |
|---|---|---|---|
| 33-55-57-59 | 0 | 46 | 3409,991 |
| 16-46-13-38 | 38,81 | 57 | 5584,870 |
| 21-32-37-4 | 1,72 | 58 | 4994,872 |

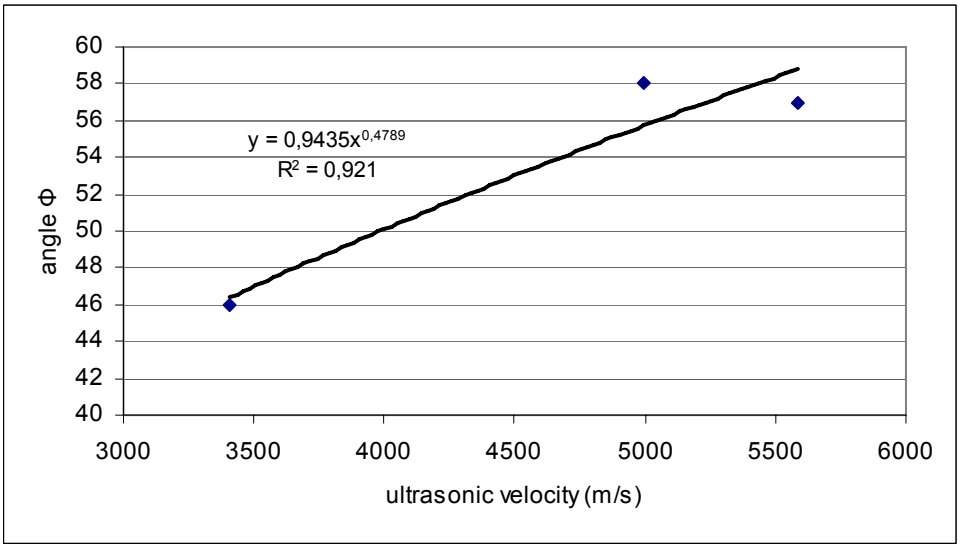


Figure 4.24 Residual friction angle – Ultrasonic velocity diagram

Table 4.26. Equation and $R^2$ values for Residual friction angle – Ultrasonic velocity

| TRENDLINE TYPE | $R^2$ | EQUATION |
|---|---|---|
| LINEAR | 0,8884 | $y = 0,0056x + 27,646$ |
| POWER | 0,921 | $y = 0,9435x^{0,4789}$ |
| EXPONENTIAL | 0,8933 | $y = 32,184e^{0,0001x}$ |

Figure 4.24 shows the highest $R^2$ for test results of the residual friction angle of basalts versus ultrasonic velocity. Other trends of correlation are also given in

table 4.26 and table 4.25 shows the residual friction angle, residual cohesion and ultrasonic velocity values for each group. 12 specimens are used to perform this test. As can be seen from the figure 4.24 friction angle increases as ultrasonic velocity increase. But two of the residual friction angle is bigger than the normal friction angle, but not. Because of the friction between the concretes after the sample was broken.

In this graphic the relationship follows an exponential law with a reasonable squared regression coefficient R-square is 0,9331 and equation is $y = 32{,}184e^{0{,}0001x}$.

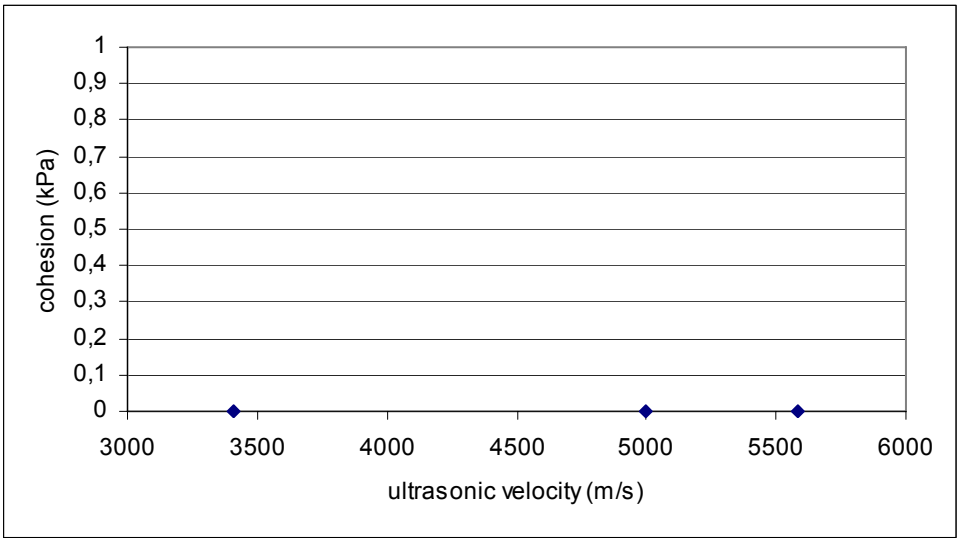


Figure 4.25 Residual cohesion – Ultrasonic velocity diagram

Figure 4.25 shows the ultrasonic velocity – residual cohesion diagram. 12 specimens are used to perform this test. In the case of the residual strength, the cohesion *c* has dropped to zero and the relationship between $\phi_r$ and $\sigma_n$ can be represented by:

$\tau_r = \sigma_n \tan\phi_r$, where $\phi_r$ is the residual angle of friction [51].

As can be seen from the figure; the cohesion of the samples approximate zero.

### 4.4. Uniaxial Compression Test

Uniaxial compression test was performed according to ISRM (1981). 52 samples were used for uniaxial compression test. Samples used for uniaxial compression test are core specimens which has a diameter of 54 mm and has a length of 135 mm.

#### 4.4.1. Results

Results obtained from Uniaxial compression test were plotted on graphics

##### 4.4.1.1. Dry density versus ultrasonic velocity for samples of uniaxial compression test

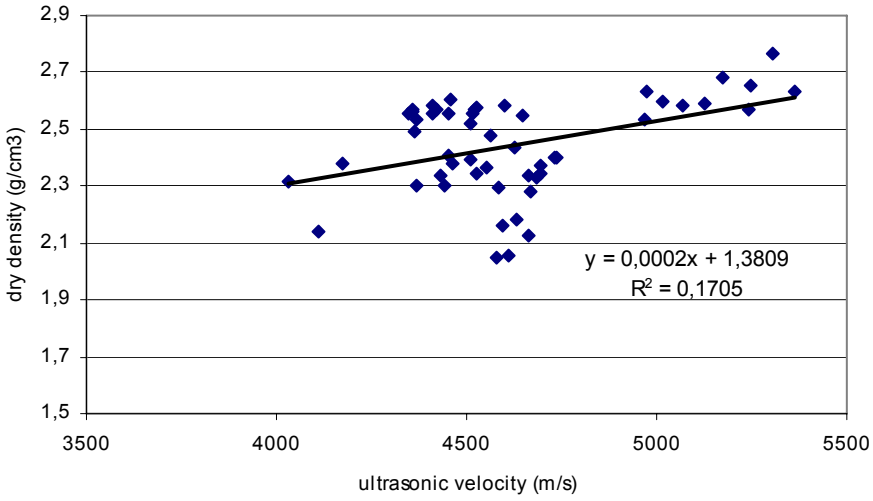


Figure 4.26. Ultrasonic velocity – Dry density diagram

Table 4.27. Equation and $R^2$ values for Ultrasonic velocity – Dry density

| TRENDLINE TYPE | $R^2$ | EQUATION |
|---|---|---|
| LINEAR | 0,1705 | y = 0,0002x + 1,3809 |
| POWER | 0,1505 | $y = 0,0662x^{0,4275}$ |
| EXPONENTIAL | 0,1575 | $y = 1,5886e^{9E-05x}$ |

Figure 4.26 shows the highest $R^2$ for test results of the dry density of basalts versus ultrasonic velocity. Other trends of correlation are also given in table 4.27. 52 specimens are used to perform this test. It can be seen clearly from figure 4.26, dry density of basalt increases as ultrasonic velocity increase. Dry density of basalts reach the maximum value at 5363,2 m/s ultrasonic velocity and it reaches the minimum value at 4032,1 m/s ultrasonic velocity. Maximum and minimum dry density values are 2,77 g/cm$^3$ and 2,05 g/cm$^3$.

Rock samples were selected different from each other much possible. However, rock samples are concentrated dense between 4368,2 m/s and 4649,1 m/s ultrasonic velocities. If the rock samples were selected between maximum and minimum ultrasonic velocity values equally, it would be seen clearer increase in the figure 4.26.

In this graphic the relationship follows a linear law with a reasonable squared regression coefficient R-square is 0,1705 and equation is y = 0,0002x + 1,3809.

#### 4.4.1.2. Bulk density versus ultrasonic velocity for samples of uniaxial compression test

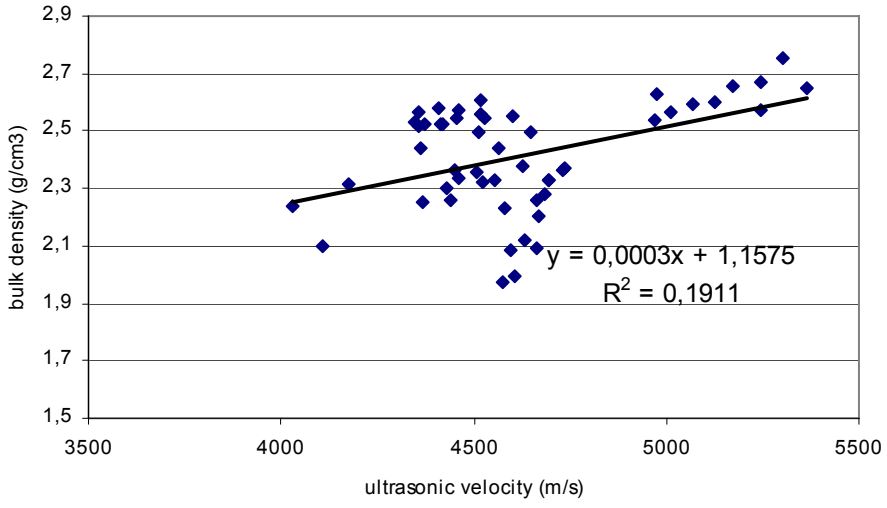


Figure 4.27. Ultrasonic velocity – Bulk density diagram

Table 4.28. Equation and $R^2$ values for Ultrasonic velocity – bulk density

| TRENDLINE TYPE | $R^2$ | EQUATION |
|---|---|---|
| LINEAR | 0,1911 | $y = 0,0003x + 1,1575$ |
| POWER | 0,168 | $y = 0,0324x^{0,5106}$ |
| EXPONENTIAL | 0,1753 | $y = 1,4429e^{0,0001x}$ |

Figure 4.27 shows the highest $R^2$ for test results of the bulk density of basalts versus ultrasonic velocity. Other trends of correlation are also given in table 4.28. 52 specimens are used to perform this test. It can be seen clearly from figure 4.27, bulk density of basalt increases as ultrasonic velocity increase. Bulk density of basalts reach the maximum value at 5363,2 m/s ultrasonic velocity and it reaches the minimum value at 4032,1 m/s ultrasonic velocity. Maximum and minimum bulk density values are 2,75 g/cm$^3$ and 1,97 g/cm$^3$.

Rock samples were selected different from each other much possible. However, rock samples are concentrated between 4368,2 m/s and 4649,1 m/s ultrasonic velocities. If the rock samples were selected between maximum and minimum ultrasonic velocity values equally, ıt would be seen clearer increase in the figure 4.27.

In this graphic the relationship follows a linear law with a reasonable squared regression coefficient R-square is 0,1911 and equation is $y = 0,0003x + 1,1575$.

#### 4.4.1.3. Saturated density versus ultrasonic velocity for samples of uniaxial compression test

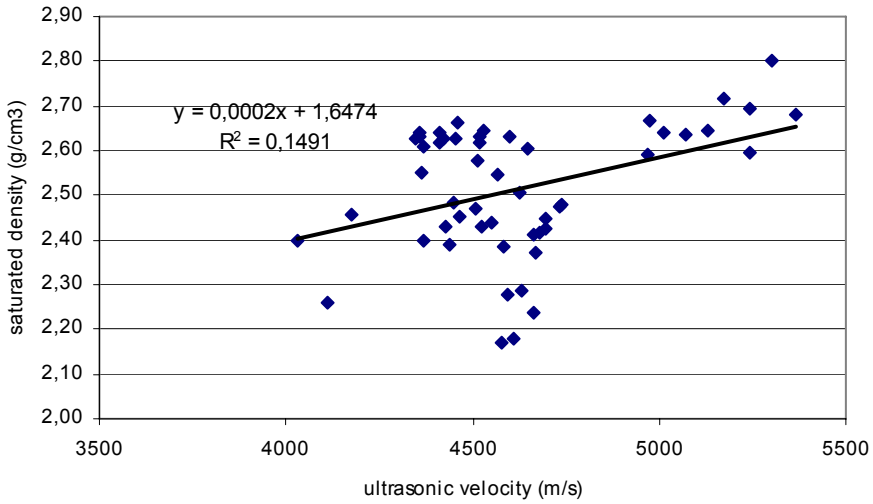


Figure 4.28 Ultrasonic velocity – Saturated density diagram

Table 4.29. Equation and $R^2$ values for Ultrasonic velocity – saturated density

| TRENDLINE TYPE | $R^2$ | EQUATION |
|---|---|---|
| LINEAR | 0,1491 | $y = 0,0002x + 1,6474$ |
| POWER | 0,1334 | $y = 0,1428x^{0,3398}$ |
| EXPONENTIAL | 0,14 | $y = 1,7858e^{7E-05x}$ |

Figure 4.28 shows the highest $R^2$ for test results of the saturated density of basalts versus ultrasonic velocity. Other trends of correlation are also given in table 4.29. 52 specimens are used to perform this test. It can be seen clearly from figure 4.28, saturated density of basalt increases as ultrasonic velocity increase. Saturated density of basalts reach the maximum value at 5363,2 m/s ultrasonic velocity and it reaches the minimum value at 4032,1 m/s ultrasonic velocity. Maximum and minimum saturated density values are 2,80 g/cm$^3$ and 2,17 g/cm$^3$.

Rock samples were selected different from each other much possible. However, rock samples are concentrated between 4368,2 m/s and 4649,1 m/s ultrasonic velocities.

If the rock samples were selected between maximum and minimum ultrasonic velocity values equally, ıt would be seen clearer increase in the figure 4.28.

In this graphic the relationship follows a linear law with a reasonable squared regression coefficient R-square is 0,1491 and equation is y = 0,0002x + 1,6474.

#### 4.4.1.4. Water absorption versus ultrasonic velocity for samples of uniaxial compression test

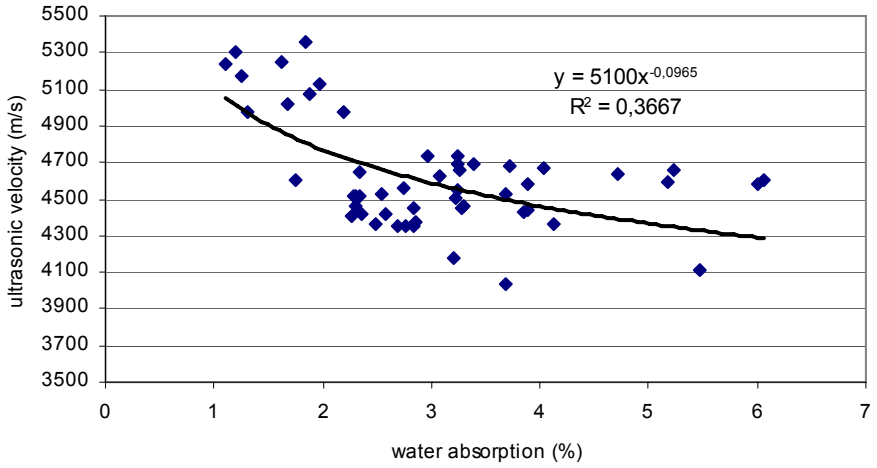


Figure 4.29. Ultrasonic velocity – Water absorption diagram

Table 4.30. Equation and $R^2$ values for Ultrasonic velocity – Water absorption

| TRENDLINE TYPE | $R^2$ | EQUATION |
|---|---|---|
| LINEAR | 0,245 | y = -126,51x + 5008,4 |
| POWER | 0,3667 | $y = 5100x^{-0,0965}$ |
| EXPONENTIAL | 0,237 | $y = 4999,4e^{-0,0263x}$ |

Figure 4.29 shows the highest $R^2$ for test results of the water absorption of basalts versus ultrasonic velocity. Other trends of correlation are also given in table 4.30. 52 specimens are used to perform this test. It can be seen clearly from figure 4.29, water absorption of basalt decreases as ultrasonic velocity increase. Water absorption of basalts reach the maximum value at 5363,2 m/s ultrasonic velocity and it reaches

the minimum value at 4032,1 m/s ultrasonic velocity. Maximum and minimum water absorption values are 6,07 % and 1,10 %.

Rock samples were selected different from each other much possible. However, rock samples are concentrated between 4368,2 m/s and 4649,1 m/s ultrasonic velocities. If the rock samples were selected between maximum and minimum ultrasonic velocity values equally, it would be seen clearer increase in the figure 4.29.

In this graphic the relationship follows a power law with a reasonable squared regression coefficient R-square is 0,3667 and equation is $y = 5100x^{-0,0965}$.

#### 4.4.1.5. Porosity versus ultrasonic velocity for samples of uniaxial compression Test

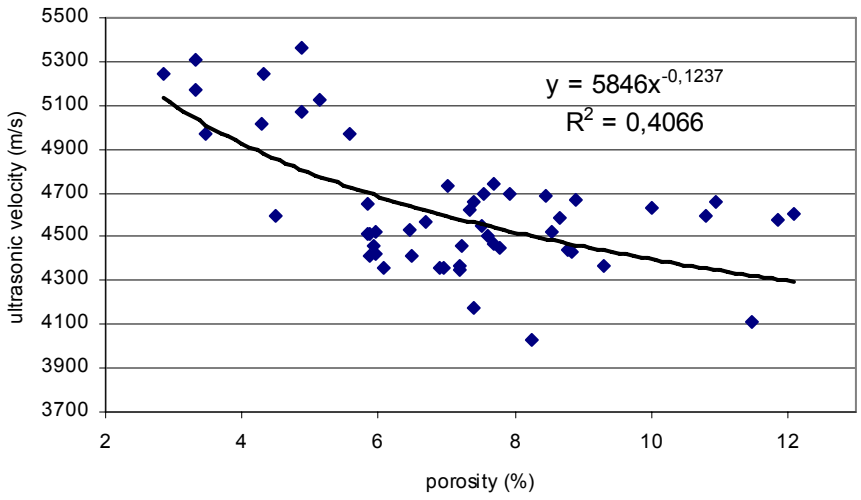


Figure 4.30. Ultrasonic velocity – Porosity diagram

Table 4.31. Equation and $R^2$ values for Ultrasonic velocity – Porosity

| TRENDLINE TYPE | $R^2$ | EQUATION |
|---|---|---|
| LINEAR | 0,316 | y = -77,992x + 5178,8 |
| POWER | 0,4066 | $y = 5846x^{-0,1237}$ |
| EXPONENTIAL | 0,3062 | $y = 5180,5e^{-0,0163x}$ |

Figure 4.30 shows the highest $R^2$ for test results of the porosity of basalts versus ultrasonic velocity. Other trends of correlation are also given in table 4.31. 52 specimens are used to perform this test. It can be seen clearly from figure 4.30, porosity of basalt decreases as ultrasonic velocity increase. porosity of basalts reach the maximum value at 5363,2 m/s ultrasonic velocity and it reaches the minimum value at 4032,1 m/s ultrasonic velocity. Maximum and minimum porosity values are 2,8 % and 12,1 %.

Rock samples were selected different from each other much possible. However, rock samples are concentrated between 4368,2 m/s and 4649,1 m/s ultrasonic velocities. If the rock samples were selected between maximum and minimum ultrasonic velocity values equally, ıt would be seen clearer increase in the figure 4.30.

In this graphic the relationship follows a power law with a reasonable squared regression coefficient R-square is 0,4066 and equation is $y = 5846x^{-0,1237}$.

#### 4.4.1.6. Uniaxial compressive strength versus ultrasonic velocity for samples of uniaxial compression test

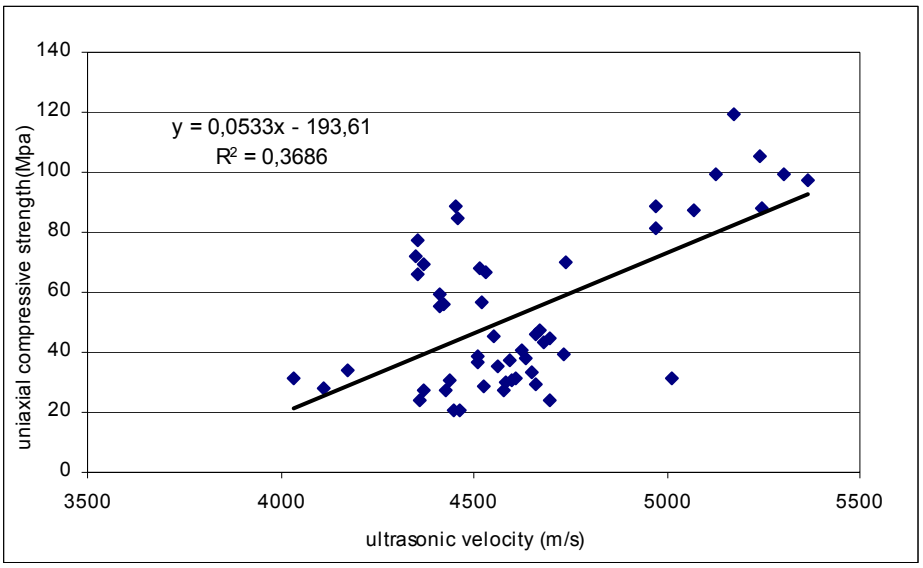


Figure 4.31. Ultrasonic velotiy – Uniaxial compressive strength diagram

Table 4.32. Equation and $R^2$ values for Ultrasonic velotciy – Uniaxial compressive strength

| TRENDLINE TYPE | $R^2$ | EQUATION |
|---|---|---|
| LINEAR | 0,3686 | y = 0,0533x - 193,61 |
| POWER | 0,2823 | $y = 5E\text{-}14x^{4,0897}$ |
| EXPONENTIAL | 0,2926 | $y = 0,7982e^{0,0009x}$ |

Figure 4.31 shows the highest $R^2$ for test results of the ultrasonic velocity of basalts versus uniaxial compressive strength. Other trends of correlation are also given in table 4.32. 52 specimens are used to perform this test. It can be seen clearly form figure 4.31, uniaxial compressive strength of basalt increases as ultrasonic velocity increase. Uniaxial compressive strength of basalts reach the maximum value at 5363,2 m/s ultrasonic velocity and it reaches the minimum value at 4032,1 m/s ultrasonic velocity. Maximum and minimum uniaxial compressive strength values are 119,366 MPa and 20.428 MPa.

Rock samples were selected different from each other much possible. However, rock samples are concentrated between 4368,2 m/s and 4649,1 m/s ultrasonic velocities. If the rock samples were selected between maximum and minimum ultrasonic velocity values equally, ıt would be seen clearer increase in the figure 4.31.

In this graphic the relationship follows a linear law with a reasonable squared regression coefficient R-square is 0,3686 and equation is y = 0,0533x – 193,61.

### 4.4.1.7. Dry density versus uniaxial compressive strength

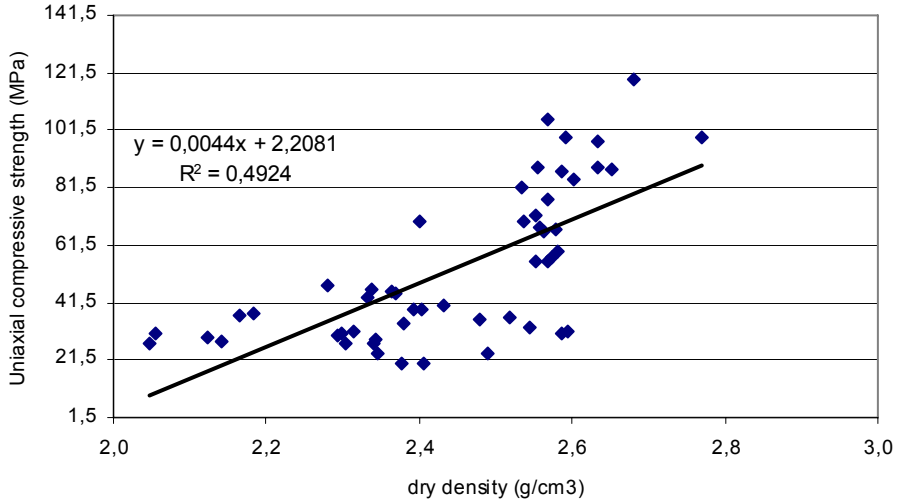


Figure 4.32. Dry density – Uniaxial Compressive strength diagram

Table 4.33. Equation and $R^2$ values for Dry density – Uniaxial Compressive strength

| TRENDLINE TYPE | $R^2$ | EQUATION |
|---|---|---|
| LINEAR | 0,4924 | $y = 0,0044x + 2,2081$ |
| POWER | 0,4609 | $y = 1,6766x^{0,0972}$ |
| EXPONENTIAL | 0,4728 | $y = 2,213e^{0,0018x}$ |

Figure 4.32 shows the highest $R^2$ for test results of the dry density of basalts versus uniaxial compressive strength. Other trends of correlation are also given in table 4.33. 52 specimens are used to perform this test. It can be seen clearly from figure 4.32, dry density of basalt increases as Uniaxial compressive strength increase. Dry density of basalts reach the maximum value at 119,37 Mpa Uniaxial compressive strength and it reaches the minimum value at 20,43 Mpa Uniaxial compressive strength. Maximum and minimum dry density values are 2,77 g/cm$^3$ and 2,05 g/cm$^3$.

Rock samples were selected different from each other much possible. However, rock samples are concentrated dense between 20,43 Mpa and 119,37 Mpa Uniaxial compressive strengths.

In this graphic the relationship follows a linear law with a reasonable squared regression coefficient R-square is 0,4924 and equation is y = 0,0044x + 1,2081.

#### 4.4.1.8. Bulk density versus uniaxial compression strength

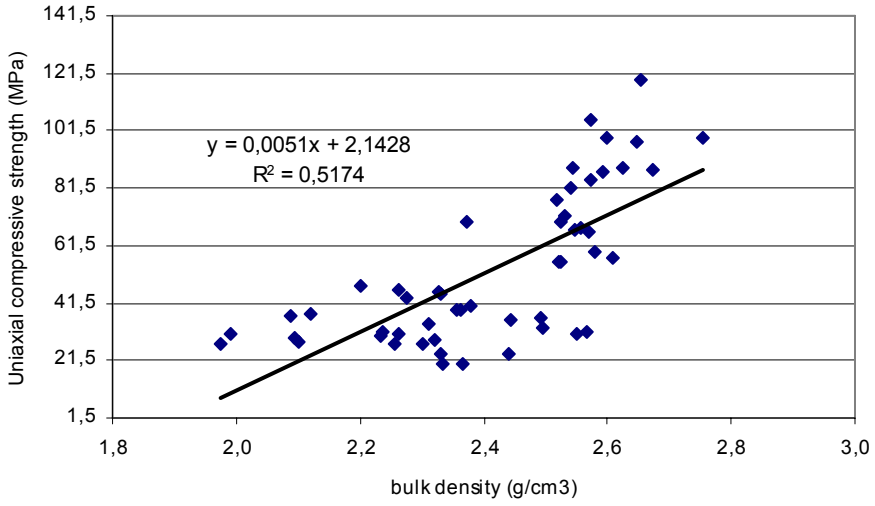


Figure 4.33. Bulk density – Uniaxial Compressive strength diagram

Table 4.34.Equation and $R^2$ values for Bulk density – Uniaxial Compressive strength

| TRENDLINE TYPE | $R^2$ | EQUATION |
|---|---|---|
| LINEAR | 0,5174 | y = 0,0051x + 2,1428 |
| POWER | 0,4795 | y = 1,5617x0,1121 |
| EXPONENTIAL | 0,4945 | $y = 2,1501e^{0,0021x}$ |

Figure 4.33 shows the highest $R^2$ for test results of the bulk density of basalts versus uniaxial compressive strength. Other trends of correlation are also given in table 4.34. 52 specimens are used to perform this test. It can be seen clearly from figure 4.33, bulk density of basalt increases as Uniaxial compressive strength increase. Bulk density of basalts reach the maximum value at 119,37 Mpa Uniaxial compressive strength and it reaches the minimum value at 20,43 Mpa Uniaxial compressive strength. Maximum and minimum bulk density values are 2,75 $g/cm^3$ and 1,97 $g/cm^3$.

Rock samples were selected different from each other much possible. However, rock samples are concentrated between 20,43 Mpa and 119,37 Mpa Uniaxial compressive strengths.

In this graphic the relationship follows a linear law with a reasonable squared regression coefficient R-square is 0,5174 and equation is y = 0,0051x + 2,1428.

#### 4.4.1.9. Saturated density versus uniaxial compression strength

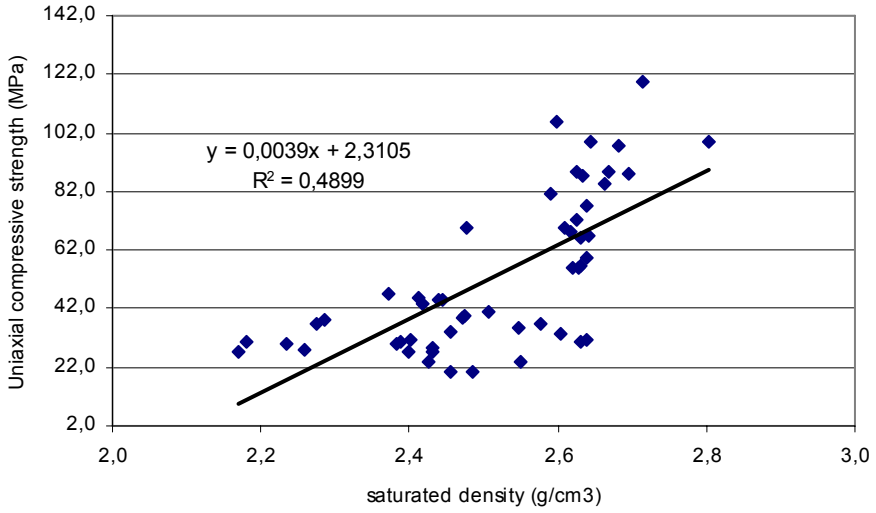


Figure 4.34. Saturated density – Uniaxial Compressive strength diagram

Table 4.35. Equation and $R^2$ values for Saturated density – Uniaxial Compressive strength

| TRENDLINE TYPE | $R^2$ | EQUATION |
|---|---|---|
| LINEAR | 0,4899 | y = 0,0051x + 2,3105 |
| POWER | 0,4649 | $y = 1,8277x^{0,0825}$ |
| EXPONENTIAL | 0,4741 | $y = 2,3141e^{0,0015x}$ |

Figure 4.34 shows the highest $R^2$ for test results of the saturated density of basalts versus uniaxial compressive strength. Other trends of correlation are also given in table 4.35. 52 specimens are used to perform this test. It can be seen clearly from figure 4.34, saturated density of basalt increases as Uniaxial compressive strength

increase. Saturated density of basalts reach the maximum value at 119,37 Mpa Uniaxial compressive strength and it reaches the minimum value at 20,43 Mpa Uniaxial compressive strength. Maximum and minimum saturated density values are 2,80 g/cm$^3$ and 2,17 g/cm$^3$.

Rock samples were selected different from each other much possible. However, rock samples are concentrated between 20,43 Mpa and 119,37 Mpa Uniaxial compressive strengths.

In this graphic the relationship follows a linear law with a reasonable squared regression coefficient R-square is 0,4899 and equation is y = 0,0039x + 2,3105.

#### 4.4.1.10. Water absorption versus uniaxial compression strength

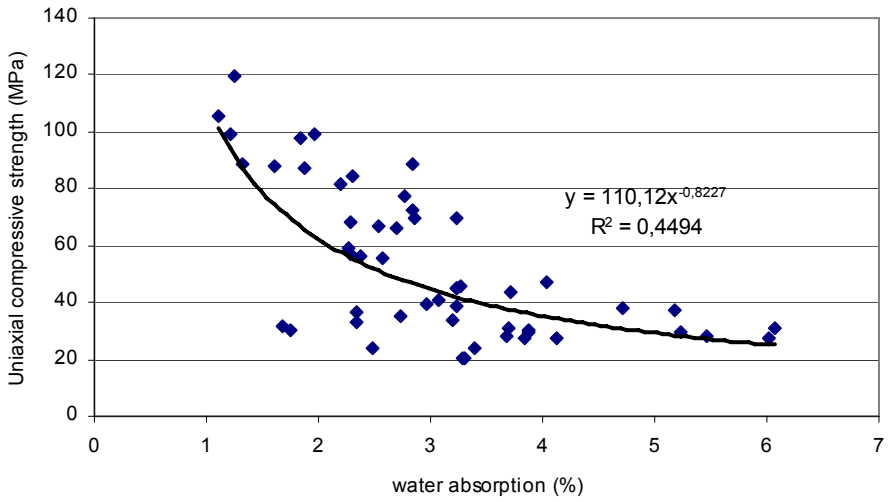


Figure 4.35. Water absorption – Uniaxial Compressive strength diagram

Table 4.36. Equation and $R^2$ values for Water absorption – Uniaxial Compressive strength

| TRENDLINE TYPE | $R^2$ | EQUATION |
|---|---|---|
| LINEAR | 0,4257 | y = -14,644x + 97,319 |
| POWER | 0,4494 | $y = 110,12x^{-0,8227}$ |
| EXPONENTIAL | 0,3976 | $y = 104,29e^{-0,2627x}$ |

Figure 4.35 shows the highest $R^2$ for test results of the water absorption of basalts versus uniaxial compressive strength. Other trends of correlation are also given in table 4.36. 52 specimens are used to perform this test. It can be seen clearly from figure 4.35, water absorption of basalt decreases as Uniaxial compressive strength increase. Water absorption of basalts reach the maximum value at 119,37 MPa Uniaxial compressive strength and it reaches the minimum value at 20,43 MPa Uniaxial compressive strength. Maximum and minimum water absorption values are 6,07 % and 1,10 %.

Rock samples were selected different from each other much possible. However, rock samples are concentrated between 20,43 MPa and 119,37 MPa Uniaxial compressive strengths.

In this graphic the relationship follows a power law with a reasonable squared regression coefficient R-square is 0,4494 and equation is $y = 110,12x^{-0,8227}$

#### 4.4.1.11. Porosity versus uniaxial compression strength

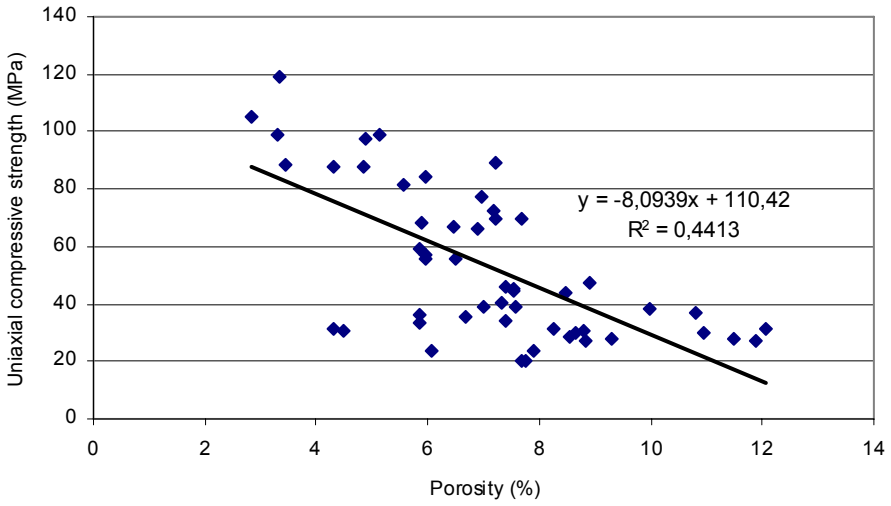


Figure 4.36. Porosity – Uniaxial compressive strength diagram

Table 4.37. Equation and $R^2$ values for Porosity – Uniaxial Compressive strength

| TRENDLINE TYPE | $R^2$ | EQUATION |
|---|---|---|
| LINEAR | 0,4413 | y= -8,0939x + 110,42 |
| POWER | 0,4202 | $y = 298{,}97x^{-0{,}9677}$ |
| EXPONENTIAL | 0,4001 | $y = 129{,}93e^{-0{,}143x}$ |

Figure 4.36 shows the highest $R^2$ for test results of the porosity of basalts versus uniaxial compressive strength. Other trends of correlation are also given in table 4.37. 52 specimens are used to perform this test. It can be seen clearly from figure 4.36, porosity of basalt decreases as Uniaxial compressive strength increase. porosity of basalts reach the maximum value at 119,37 MPa Uniaxial compressive strength and it reaches the minimum value at 20,43 MPa Uniaxial compressive strength. Maximum and minimum porosity values are 2,8 % and 12,1 %.

Rock samples were selected different from each other much possible. However, rock samples are concentrated between 20,43 MPa and 119,37 MPa Uniaxial compressive strengths.

In this graphic the relationship follows a linear law with a reasonable squared regression coefficient R-square is 0,4413 and equation is y= -8,0939x + 110,42

### 4.4.2. Determination of young's modulus

In this part young's modulus of specimens were determined. Results were presented as figures and tables. Basalt specimens were divided into three groups according to their visual variation. Two different samples selected out of variety of basalt samples that represent each group.

- Vesicular basalt
- Vesicular basalt with calcite
- Basalt with no vesicle and calcite

#### 4.4.2.1. Vesicular basalt

Table 4.38. Young's Modulus Test Results (sample no: 59)

| Sample No: 59 | | | | | |
|---|---|---|---|---|---|
| Δ.L. (mm) | L (mm) | Strain (E-3) | Load (kN) | Diam(cm) | Stress (MPa) |
| 0,1 | 140 | 0,714 | 16,6 | 5,38 | 7,306 |
| 0,2 | 140 | 1,429 | 19,8 | 5,38 | 8,714 |
| 0,3 | 140 | 2,143 | 33,5 | 5,38 | 14,744 |
| 0,35 | 140 | 2,500 | 42,2 | 5,38 | 18,573 |
| 0,4 | 140 | 2,857 | 54,6 | 5,38 | 24,030 |
| 0,45 | 140 | 3,214 | 65,1 | 5,38 | 28,651 |
| 0,5 | 140 | 3,571 | 74,9 | 5,38 | 32,965 |
| 0,55 | 140 | 3,929 | 82,8 | 5,38 | 36,441 |
| 0,6 | 140 | 4,286 | 86 | 5,38 | 37,850 |

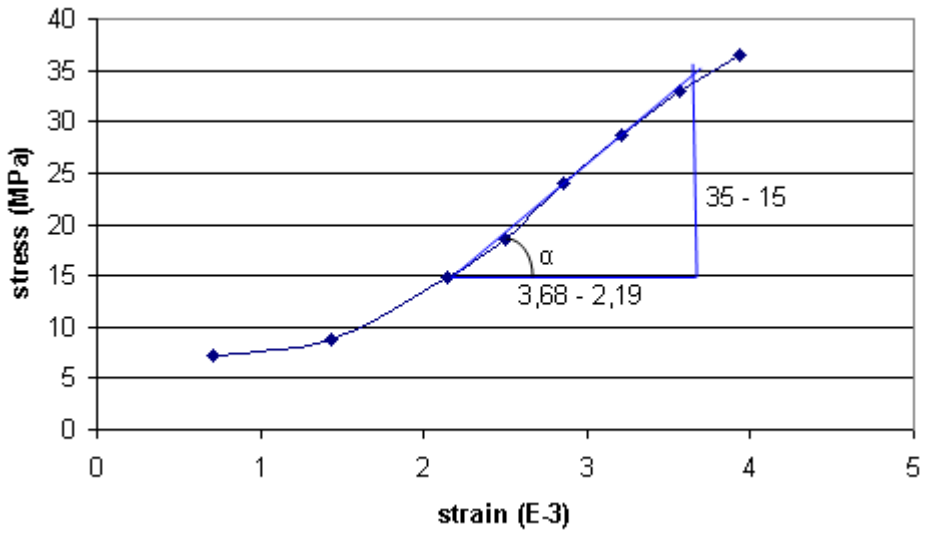


Figure 4.37. Stress-strain diagram (sample no: 59)

Figure 4.37 shows the stress-strain diagram of basalt sample with a number 59. Other values which was obtained from the test is given in table 4.38. As can be seen from figure 4.37, uniaxial compressive stress increases as strain increase. From this figure young's modulus of this sample was determined according to Tangent modulus measured at a fixed percentage of ultimate strength. The young's modulus of the sample 59 is 13,42 GPa.

Table 4.39. Young's Modulus Test Results (sample no: 60)

| Sample No: 60 | | | | | |
|---|---|---|---|---|---|
| Δ.L. (mm) | L (mm) | Strain (E-3) | Load (Kn) | Diam(cm) | Stress (Mpa) |
| 0,05 | 137,8 | 0,363 | 16,3 | 5,35 | 7,255 |
| 0,1 | 137,8 | 0,726 | 23,9 | 5,35 | 10,637 |
| 0,15 | 137,8 | 1,089 | 32,8 | 5,35 | 14,598 |
| 0,2 | 137,8 | 1,451 | 41,2 | 5,35 | 18,337 |
| 0,25 | 137,8 | 1,814 | 48,2 | 5,35 | 21,452 |
| 0,3 | 137,8 | 2,177 | 49,8 | 5,35 | 22,164 |
| 0,35 | 137,8 | 2,540 | 51,9 | 5,35 | 23,099 |
| 0,4 | 137,8 | 2,903 | 55,6 | 5,35 | 24,746 |
| 0,45 | 137,8 | 3,266 | 64,9 | 5,35 | 28,885 |
| 0,5 | 137,8 | 3,628 | 69,7 | 5,35 | 31,021 |

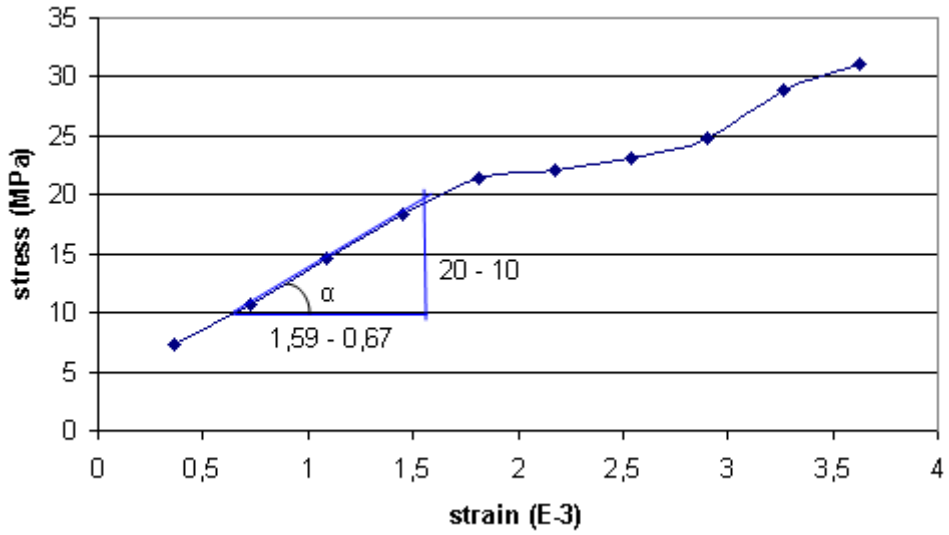


Figure 4.38. Stress-strain diagram (sample no: 60)

Figure 4.38 shows the stress-strain diagram of basalt sample with a number 60. Other values which was obtained from the test is given in table 4.39. As can be seen from figure 4.38, uniaxial compressive stress increases as strain increase. From this figure young's modulus of this sample was determined according to Tangent modulus measured at a fixed percentage of ultimate strength. The young's modulus of the sample 60 is 10,87 GPa.

The same two vesicular basalts in the above are has an average 12.15 GPa young's modulus.

#### 4.4.2.2 Vesicular basalt with calcite

Table 4.40. Young's Modulus Test Results (sample no: 5)

| Sample No: 5 | | | | | |
|---|---|---|---|---|---|
| Δ.L. (mm) | L (mm) | Strain (E-3) | Load (Kn) | Diam(cm) | Stress (Mpa) |
| 0,05 | 148,2 | 0,337 | 13,2 | 6,2 | 4,374 |
| 0,1 | 148,2 | 0,675 | 18,3 | 6,2 | 6,065 |
| 0,15 | 148,2 | 1,012 | 24,7 | 6,2 | 8,185 |
| 0,2 | 148,2 | 1,350 | 31,9 | 6,2 | 10,572 |
| 0,25 | 148,2 | 1,687 | 40 | 6,2 | 13,256 |
| 0,3 | 148,2 | 2,024 | 47,4 | 6,2 | 15,708 |
| 0,35 | 148,2 | 2,362 | 56,8 | 6,2 | 18,823 |
| 0,4 | 148,2 | 2,699 | 67,9 | 6,2 | 22,502 |
| 0,45 | 148,2 | 3,036 | 80,1 | 6,2 | 26,545 |
| 0,5 | 148,2 | 3,374 | 90,8 | 6,2 | 30,091 |
| 0,55 | 148,2 | 3,711 | 99,8 | 6,2 | 33,073 |
| 0,6 | 148,2 | 4,049 | 102,6 | 6,2 | 34,001 |

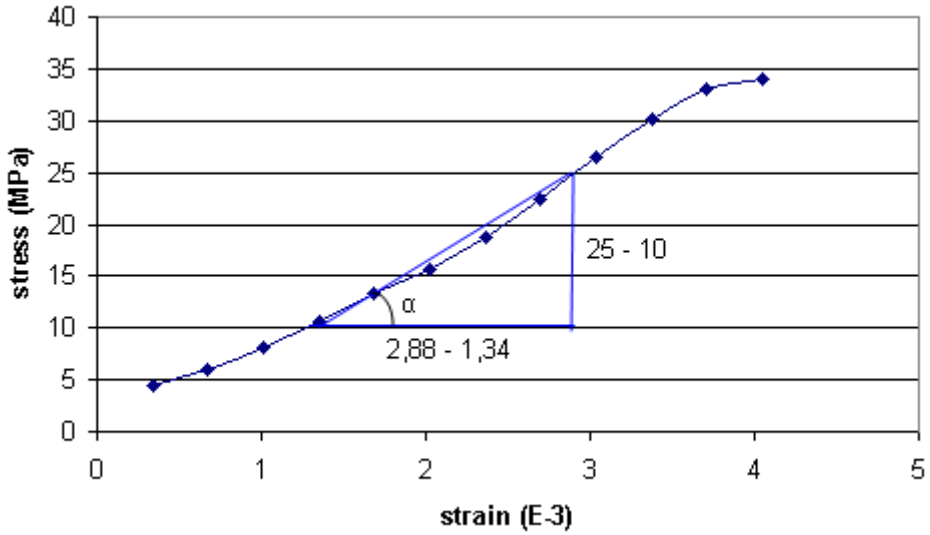


Figure 4.39. Stress-strain diagram (sample no: 5)

Figure 4.39 shows the stress-strain diagram of basalt sample with a number 5. Other values which was obtained from the test is given in table 4.40. As can be seen from figure 4.39, uniaxial compressive stress increases as strain increase. From this figure young's modulus of this sample was determined according to Tangent modulus measured at a fixed percentage of ultimate strength. The young's modulus of the sample 5 is 9,74 GPa.

Table 4.41. Young's Modulus Test Results (sample no: 17)

| Sample No: 17 | | | | | |
|---|---|---|---|---|---|
| Δ.L. (mm) | L (mm) | Strain (E-3) | Load (Kn) | Diam(cm) | Stress (Mpa) |
| 0,05 | 150,8 | 0,332 | 13,2 | 6,17 | 4,417 |
| 0,1 | 150,8 | 0,663 | 16,1 | 6,17 | 5,387 |
| 0,15 | 150,8 | 0,995 | 20,8 | 6,17 | 6,960 |
| 0,2 | 150,8 | 1,326 | 26,2 | 6,17 | 8,767 |
| 0,25 | 150,8 | 1,658 | 32 | 6,17 | 10,708 |
| 0,3 | 150,8 | 1,989 | 37,9 | 6,17 | 12,682 |
| 0,35 | 150,8 | 2,321 | 45 | 6,17 | 15,058 |
| 0,4 | 150,8 | 2,653 | 52,8 | 6,17 | 17,668 |
| 0,45 | 150,8 | 2,984 | 58,4 | 6,17 | 19,542 |
| 0,5 | 150,8 | 3,316 | 64,8 | 6,17 | 21,684 |
| 0,55 | 150,8 | 3,647 | 72,7 | 6,17 | 24,327 |
| 0,6 | 150,8 | 3,979 | 80,2 | 6,17 | 26,837 |
| 0,65 | 150,8 | 4,310 | 86,6 | 6,17 | 28,979 |
| 0,7 | 150,8 | 4,642 | 92 | 6,17 | 30,786 |

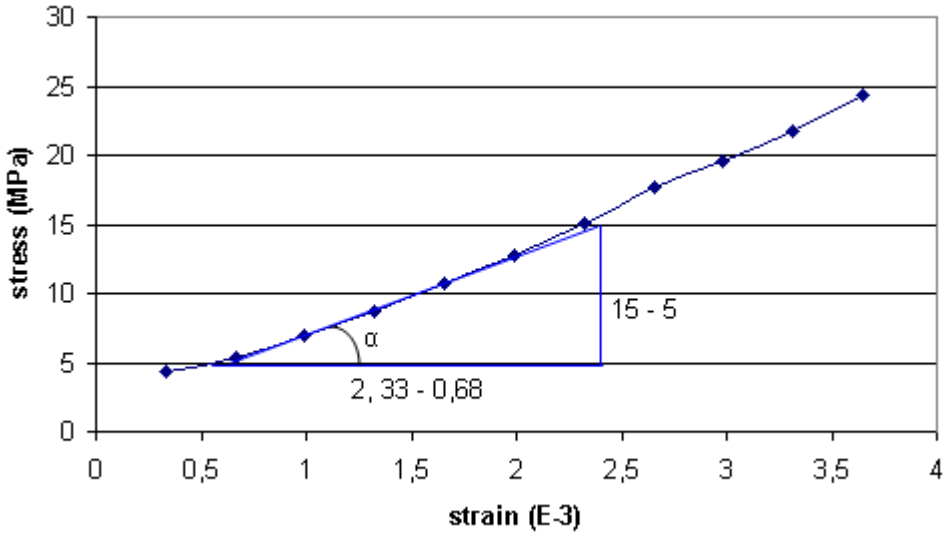


Figure 4.40. Stress-strain diagram (sample no:17)

Figure 4.40 shows the stress-strain diagram of basalt sample with a number 17. Other values which was obtained from the test is given in table 4.41. As can be seen from figure 4.40, uniaxial compressive stress increases as strain increase. From this figure young's modulus of this sample was determined according to Tangent modulus measured at a fixed percentage of ultimate strength. The young's modulus of the sample 17 is 6,06 GPa.

The same two vesicular basalts with calcite in the above are has an average 7.90 GPa young's modulus.

#### 4.4.2.3 Basalt with no vesicle and calcite

Table 4.42. Young's Modulus Test Results (sample no: 18)

| Sample No: 18 | | | | | |
|---|---|---|---|---|---|
| Δ.L. (mm) | L (mm) | Strain (E-3) | Load (Kn) | Diam(cm) | Stress (Mpa) |
| 0,05 | 143,2 | 0,349 | 12,2 | 6,15 | 4,109 |
| 0,1 | 143,2 | 0,698 | 26,4 | 6,15 | 8,892 |
| 0,15 | 143,2 | 1,047 | 40,6 | 6,15 | 13,674 |
| 0,2 | 143,2 | 1,397 | 55 | 6,15 | 18,524 |
| 0,25 | 143,2 | 1,746 | 69 | 6,15 | 23,240 |
| 0,3 | 143,2 | 2,095 | 87,9 | 6,15 | 29,605 |
| 0,35 | 143,2 | 2,444 | 107,8 | 6,15 | 36,308 |
| 0,4 | 143,2 | 2,793 | 127 | 6,15 | 42,774 |
| 0,45 | 143,2 | 3,142 | 142 | 6,15 | 47,826 |
| 0,5 | 143,2 | 3,492 | 167,2 | 6,15 | 56,314 |
| 0,55 | 143,2 | 3,841 | 183,7 | 6,15 | 61,871 |
| 0,6 | 143,2 | 4,190 | 189 | 6,15 | 63,656 |
| 0,65 | 143,2 | 4,539 | 192,8 | 6,15 | 64,936 |
| 0,7 | 143,2 | 4,888 | 199,3 | 6,15 | 67,125 |
| 0,75 | 143,2 | 5,237 | 216,4 | 6,15 | 72,885 |
| 0,8 | 143,2 | 5,587 | 239 | 6,15 | 80,497 |
| 0,85 | 143,2 | 5,936 | 258,3 | 6,15 | 86,997 |
| 0,9 | 143,2 | 6,285 | 279,8 | 6,15 | 94,238 |
| 0,95 | 143,2 | 6,634 | 289,2 | 6,15 | 97,404 |

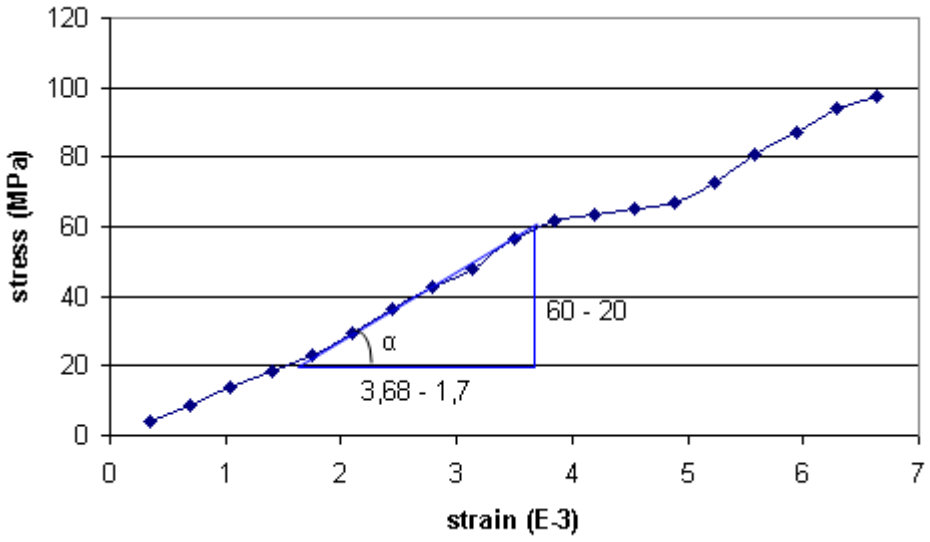


Figure 4.41. Stress-strain diagram (sample no:18)

Figure 4.41 shows the stress-strain diagram of basalt sample with a number 18. Other values which was obtained from the test is given in table 4.42. As can be seen from figure 4.41, uniaxial compressive stress increases as strain increase. From this figure young's modulus of this sample was determined according to Tangent modulus measured at a fixed percentage of ultimate strength. The young's modulus of the sample 18 is 20,20 GPa.

Table 4.43. Young's Modulus Test Results (sample no: 3)

| Sample No: 3 | | | | | |
|---|---|---|---|---|---|
| Δ.L. (mm) | L (mm) | Strain (E-3) | Load (Kn) | Diam(cm) | Stress (Mpa) |
| 0,05 | 149 | 0,336 | 13,7 | 6,13 | 4,644 |
| 0,1 | 149 | 0,671 | 24 | 6,13 | 8,136 |
| 0,15 | 149 | 1,007 | 36,2 | 6,13 | 12,272 |
| 0,2 | 149 | 1,342 | 51,4 | 6,13 | 17,425 |
| 0,25 | 149 | 1,678 | 64,2 | 6,13 | 21,764 |
| 0,3 | 149 | 2,013 | 78,8 | 6,13 | 26,714 |
| 0,35 | 149 | 2,349 | 88,2 | 6,13 | 29,900 |
| 0,4 | 149 | 2,685 | 92,8 | 6,13 | 31,460 |
| 0,45 | 149 | 3,020 | 108,6 | 6,13 | 36,816 |
| 0,5 | 149 | 3,356 | 126,7 | 6,13 | 42,952 |
| 0,55 | 149 | 3,691 | 140,2 | 6,13 | 47,529 |
| 0,6 | 149 | 4,027 | 156,1 | 6,13 | 52,919 |
| 0,65 | 149 | 4,362 | 169,8 | 6,13 | 57,563 |
| 0,7 | 149 | 4,698 | 181 | 6,13 | 61,360 |
| 0,75 | 149 | 5,034 | 189,1 | 6,13 | 64,106 |
| 0,8 | 149 | 5,369 | 192,5 | 6,13 | 65,259 |
| 0,85 | 149 | 5,705 | 194,8 | 6,13 | 66,039 |
| 0,9 | 149 | 6,040 | 196 | 6,13 | 66,445 |

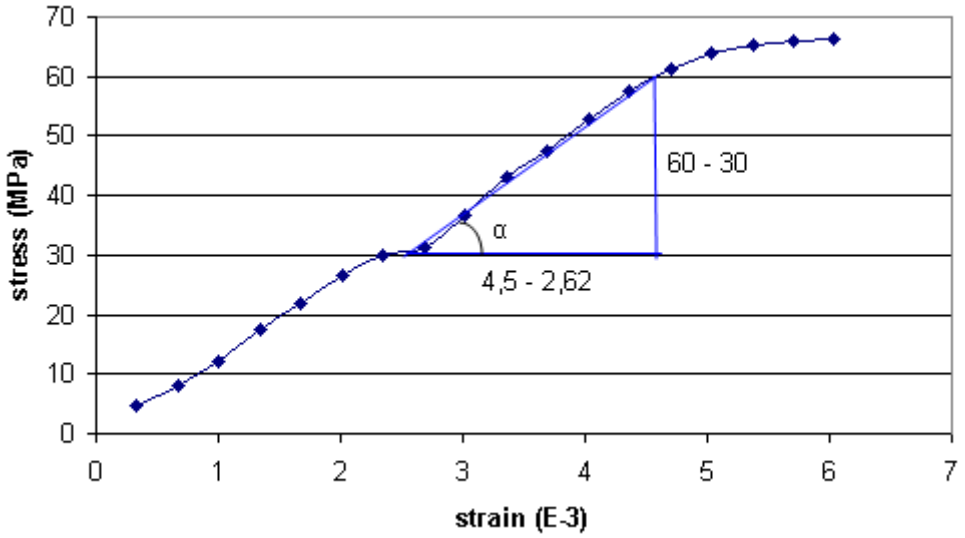


Figure 4.42. Stress-strain diagram (sample no:3)

Figure 4.42 shows the stress-strain diagram of basalt sample with a number 17. Other values which was obtained from the test is given in table 4.43. As can be seen from figure 4.42, uniaxial compressive stress increases as strain increase. From this figure young's modulus of this sample was determined according to Tangent modulus measured at a fixed percentage of ultimate strength. The young's modulus of the sample 18 is 15,96 GPa.

The same two vesicular basalts with  no vesicle and calcite in the above are has an average 18,08 GPa young's modulus.

### 4.5. Visual Variation

#### 4.5.1. Brazil Test

In this part basalt's visual variation was taken into consideration. Basalt specimens were divided into four groups for Brazillian Test to find out their varieties change the graphic or not. (see in figure 4.31). And graphics were drawn one by one for each group for brazillian tensile strength versus ultrasonic velocity. (see is figure 4.32)

- Vesicular basalt
- Basalt with no vesicle and calcite
- Basalt with much calcite-little vesicle
- Vesicular basalt with calcite


Figure 4.43a. Vesicular


Figure 4.43b. No vesicle and calcit


Figure 4.43c. Much calcite-little vesicle


Figure 4.43d. Vesicular with calcit

#### 4.5.1.1. Ultrasonic velocity versus Brazillian tensile strength

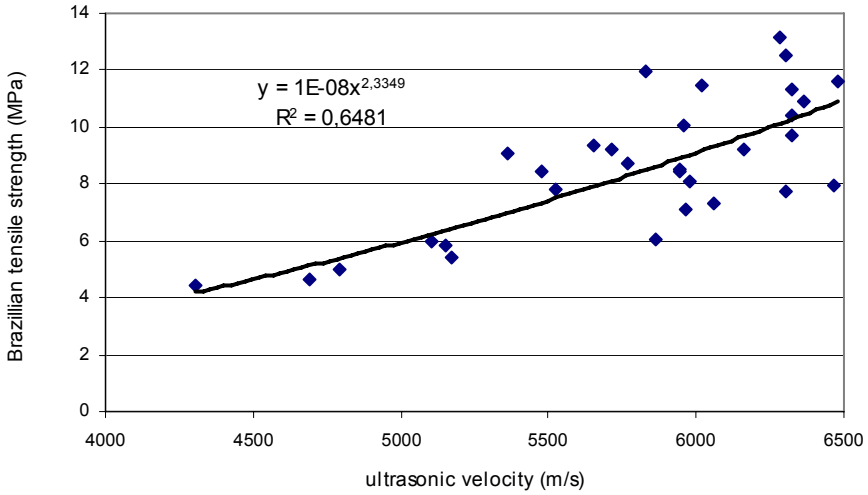


Figure 4.44a. Ultrasonic velocity – Brazillian tensile strength diagram (Vesicular basalt)

Table 4.44. Equation and $R^2$ values for Ultrasonic velocity – Brazillian tensile strength (vesicular basalt)

| TRENDLINE TYPE | $R^2$ | EQUATION |
|---|---|---|
| LINEAR | 0,5614 | $y = 0,0032x - 9,802$ |
| POWER | 0,6481 | $y = 1E\text{-}08x^{2,3349}$ |
| EXPONENTIAL | 0,6398 | $y = 0,7124e^{0,0004x}$ |

Figure 4.44a shows the highest $R^2$ for test results of the ultrasonic velocity of basalts versus Brazillian tensile strength. Other trends of correlation are also given in Table 4.44. It can be seen clearly from figure 4.44a, Brazillian tensile strength of basalt increases as ultrasonic velocity increase. In this graphic the relationship follows an exponential law with a reasonable squared regression coefficient R-square is 0,6398 and equation is $y = 0,7124e^{0,0004x}$.

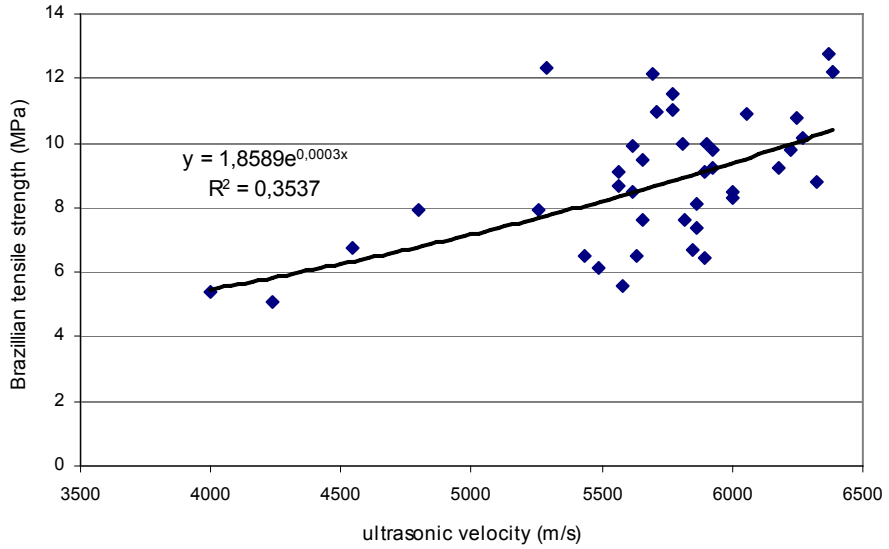


Figure 4.44b. Ultrasonic velocity – Brazillian tensile strength diagram (Basalt with no vesicle and calcite)

Table 4.45. Equation and $R^2$ values for Ultrasonic velocity – Brazillian tensile strength (Basalt with no vesicle and calcite)

| TRENDLINE TYPE | $R^2$ | EQUATION |
|---|---|---|
| LINEAR | 0,3044 | y = 0,0021x - 3,2166 |
| POWER | 0,3525 | $y = 5E\text{-}05x^{1,404}$ |
| EXPONENTIAL | 0,3537 | $y = 1,8589e^{0,0003x}$ |

Figure 4.44b shows the highest $R^2$ for test results of the ultrasonic velocity of basalts versus Brazillian tensile strength. Other trends of correlation are also given in Table 4.45. It can be seen clearly from figure 4.44b, Brazillian tensile strength of basalt increases as ultrasonic velocity increase. In this graphic the relationship follows an exponential law with a reasonable squared regression coefficient R-square is 0,3537 and equation is $y = 1,8589e^{0,0003x}$.

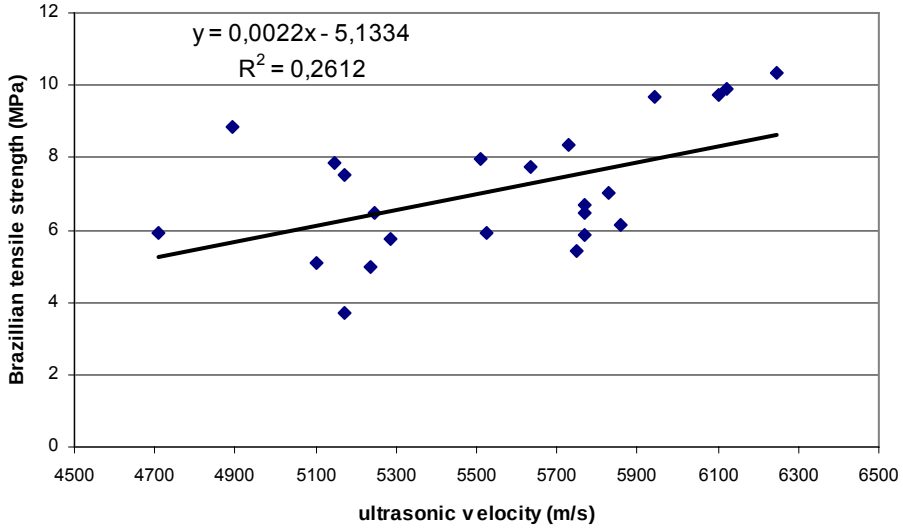


Figure 4.44c. Ultrasonic velocity – Brazillian tensile strength diagram (Basalt with much calcite-little vesicle)

Table 4.46. Equation and $R^2$ values for Ultrasonic velocity – Brazillian tensile strength (Basalt with much calcite-little vesicle)

| TRENDLINE TYPE | $R^2$ | EQUATION |
|---|---|---|
| LINEAR | 0,2612 | y = 0,0022x - 5,1334 |
| POWER | 0,2241 | $y = 6E\text{-}06x^{1,6238}$ |
| EXPONENTIAL | 0,239 | $y = 1,2606e^{0,0003x}$ |

Figure 4.44c shows the highest $R^2$ for test results of the ultrasonic velocity of basalts versus Brazillian tensile strength. Other trends of correlation are also given in Table 4.46. It can be seen clearly from figure 4.44c, Brazillian tensile strength of basalt increases as ultrasonic velocity increase. In this graphic the relationship follows a linear law with a reasonable squared regression coefficient R-square is 0,2612 and equation is y = 0,0022x - 5,1334.

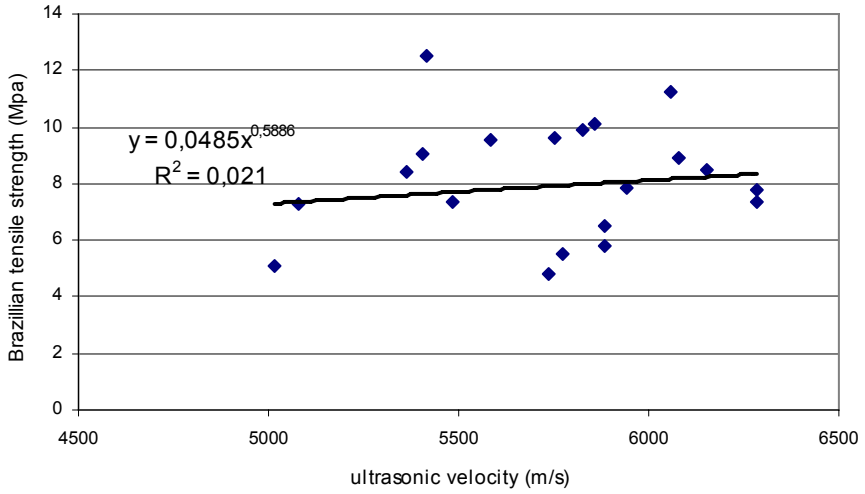


Figure 4.44d. Ultrasonic velocity – Brazillian tensile strength diagram (Vesicular basalt with calcite)

Table 4.47. Equation and $R^2$ values for Ultrasonic velocity – Brazillian tensile strength (Vesicular basalt with calcite)

| TRENDLINE TYPE | $R^2$ | EQUATION |
|---|---|---|
| LINEAR | 0,01 | $y = 0,0006x + 4,9255$ |
| POWER | 0,21 | $y = 0,0485x^{0,5886}$ |
| EXPONENTIAL | 0,019 | $y = 4,4741e^{1E-04x}$ |

Figure 4.44d shows the highest $R^2$ for test results of the ultrasonic velocity of basalts versus Brazillian tensile strength. Other trends of correlation are also given in Table 4.47. It can be seen clearly from figure 4.44d, Brazillian tensile strength of basalt increases as ultrasonic velocity increase. In this graphic the relationship follows a power law with a reasonable squared regression coefficient R-square is 0,21 and equation is $y = 0,0485x^{0,5886}$ .

### 4.5.1.2. Ultrasonic velocity versus dry density

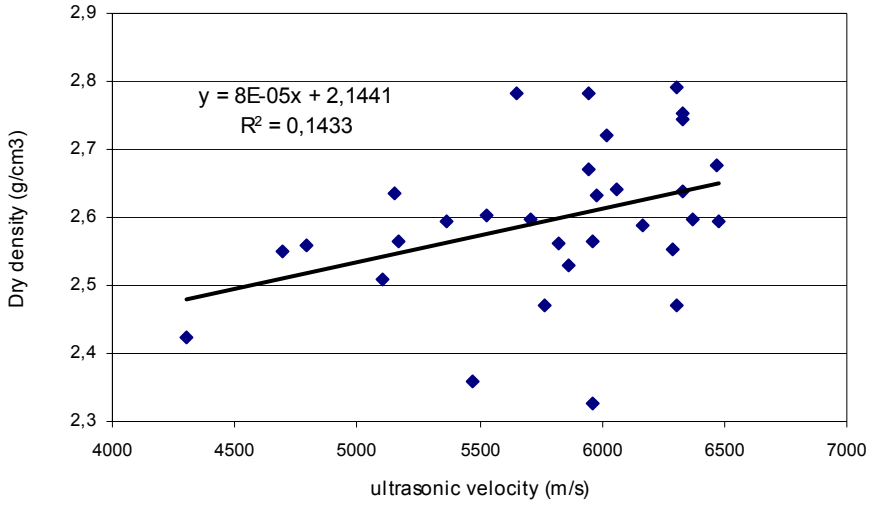


Figure 4.45a. Ultrasonic velocity – Dry density diagram (Vesicular basalt)

Table 4.48. Equation and $R^2$ values for Ultrasonic velocity – Dry density (vesicular basalt)

| TRENDLINE TYPE | $R^2$ | EQUATION |
|---|---|---|
| LINEAR | 0,1433 | y = 8E-05x + 2,1441 |
| POWER | 0,1411 | y = 0,622x0,1649 |
| EXPONENTIAL | 0,1409 | y = 2,1791e3E-05x |

Figure 4.45a shows the highest $R^2$ for test results of the ultrasonic velocity of basalts versus dry density. Other trends of correlation are also given in Table 4.48. It can be seen clearly from figure 4.45a, dry density of basalt increases as ultrasonic velocity increase. In this graphic the relationship follows a linear law with a reasonable squared regression coefficient R-square is 0,1433 and equation is y = 8E-05x + 2,1441.

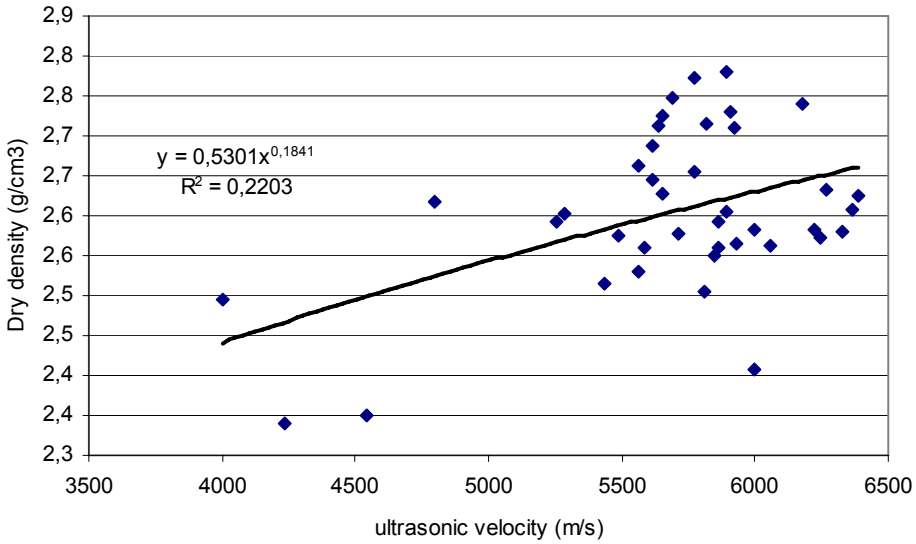


Figure 4.45b. Ultrasonic velocity – Dry density diagram
(Basalt with no vesicle and calcite)

Table 4.49. Equation and $R^2$ values for Ultrasonic velocity – Dry density
(Basalt with no vesicle and calcite)

| TRENDLINE TYPE | $R^2$ | EQUATION |
|---|---|---|
| LINEAR | 0,1938 | y = 9E-05x + 2,1199 |
| POWER | 0,2203 | $y = 0{,}5301x^{0{,}1841}$ |
| EXPONENTIAL | 0,2029 | $y = 2{,}146e^{3E-05x}$ |

Figure 4.45b shows the highest $R^2$ for test results of the ultrasonic velocity of basalts versus dry density. Other trends of correlation are also given in Table 4.49. It can be seen clearly from figure 4.45b, dry density of basalt increases as ultrasonic velocity increase. In this graphic the relationship follows a power law with a reasonable squared regression coefficient R-square is 0,2203 and equation is $y = 0{,}5301x^{0{,}1841.}$

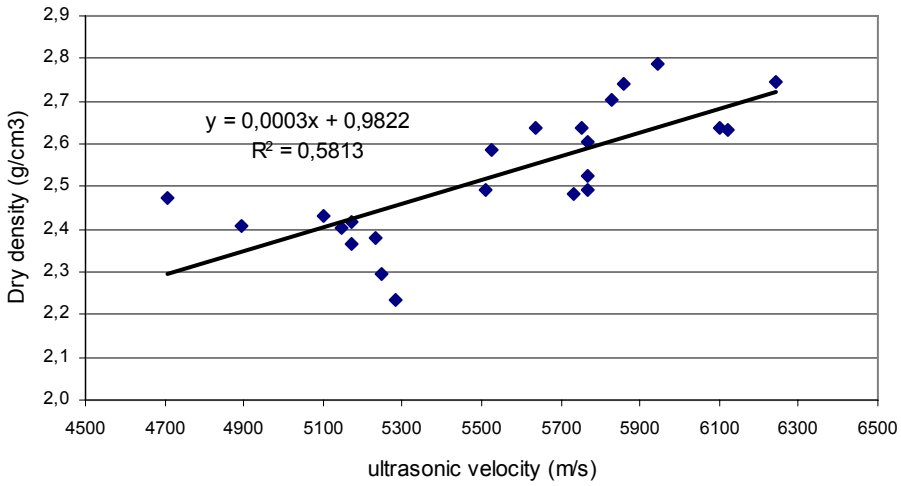


Figure 4.45c. Ultrasonic velocity – Dry density diagram
(Basalt with much calcite-little vesicle)

Table 4.50. Equation and $R^2$ values for Ultrasonic velocity – Dry density (Basalt with much calcite-little vesicle)

| TRENDLINE TYPE | $R^2$ | EQUATION |
|---|---|---|
| LINEAR | 0,5813 | $y = 0,0003x + 0,9822$ |
| POWER | 0,5595 | $y = 0,015x^{0,5945}$ |
| EXPONENTIAL | 0,5746 | $y = 1,3707e^{0,0001x}$ |

Figure 4.45c shows the highest $R^2$ for test results of the ultrasonic velocity of basalts versus dry density. Other trends of correlation are also given in Table 4.50. It can be seen clearly from figure 4.45c, dry density of basalt increases as ultrasonic velocity increase. In this graphic the relationship follows an exponential law with a reasonable squared regression coefficient R-square is 0,5813 and equation $y = 0,0003x + 0,9822$.

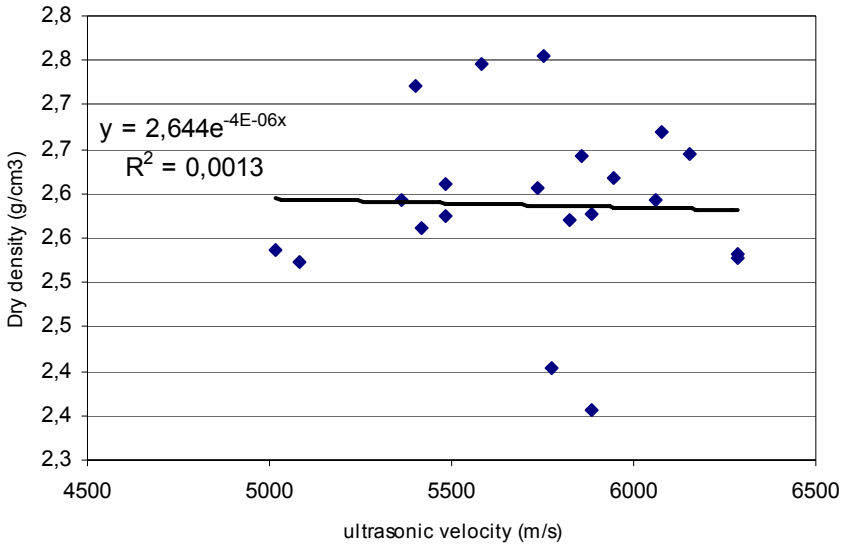


Figure 4.45d. Ultrasonic velocity – Dry density diagram
(Vesicular basalt with calcite)

Table 4.51. Equation and $R^2$ values for Ultrasonic velocity – Dry density
(Vesicular basalt with calcite)

| TRENDLINE TYPE | $R^2$ | EQUATION |
|---|---|---|
| LINEAR | 0,0012 | y = -9E-06x + 2,6431 |
| POWER | 0,0008 | $y = 2,9939x^{-0,0169}$ |
| EXPONENTIAL | 0,0013 | $y = 2,644e^{-4E-06x}$ |

Figure 4.45d shows the highest $R^2$ for test results of the ultrasonic velocity of basalts versus dry density. Other trends of correlation are also given in Table 4.51. It can be seen clearly from figure 4.45d, dry density of basalt increases as ultrasonic velocity increase. In this graphic the relationship follows an exponential law with a reasonable squared regression coefficient R-square is 0,0013 and equation is $y = 2,644e^{-4E-06x}$.

### 4.5.1.3. Ultrasonic velocity versus saturated density

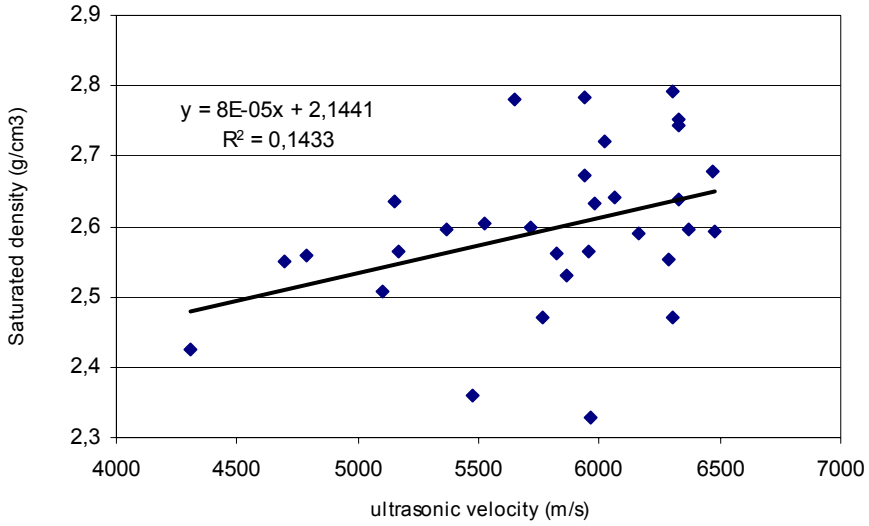


Figure 4.46a. Ultrasonic velocity – Saturated density diagram (Vesicular basalt)

Table 4.52. Equation and $R^2$ values for Ultrasonic velocity – Saturated density (vesicular basalt)

| TRENDLINE TYPE | $R^2$ | EQUATION |
|---|---|---|
| LINEAR | 0,1433 | y = 8E-05x + 2,1441 |
| POWER | 0,1411 | y = 0,622x0,1649 |
| EXPONENTIAL | 0,1409 | y = 2,1791e3E-05x |

Figure 4.46a shows the highest $R^2$ for test results of the ultrasonic velocity of basalts versus saturated density. Other trends of correlation are also given in Table 4.52. It can be seen clearly from figure 4.46a, saturated density of basalt increases as ultrasonic velocity increase. In this graphic the relationship follows a linear law with a reasonable squared regression coefficient R-square is 0,1433 and equation is y = 8E-05x + 2,1441.

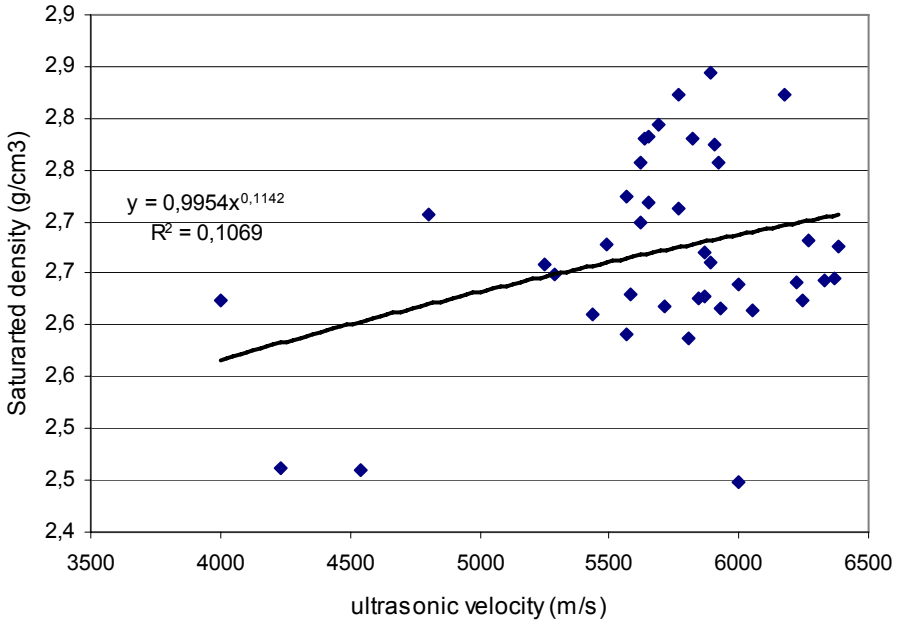


Figure 4.46b. Ultrasonic velocity – Saturated density diagram
(Basalt with no vesicle and calcite)

Table 4.53. Equation and $R^2$ values for Ultrasonic velocity – Saturated density
(Basalt with no vesicle and calcite)

| TRENDLINE TYPE | $R^2$ | EQUATION |
|---|---|---|
| LINEAR | 0,092 | y = 5E-05x + 2,3651 |
| POWER | 0,1069 | $y = 0,9954x^{0,1142}$ |
| EXPONENTIAL | 0,0955 | $y = 2,3731e^{2E-05x}$ |

Figure 4.46b shows the highest $R^2$ for test results of the ultrasonic velocity of basalts versus saturated density. Other trends of correlation are also given in Table 4.53. It can be seen clearly from figure 4.46b, saturated density of basalt increases as ultrasonic velocity increase. In this graphic the relationship follows a power law with a reasonable squared regression coefficient R-square is 0,1069 and equation is $y = 0,9954x^{0,1142.}$

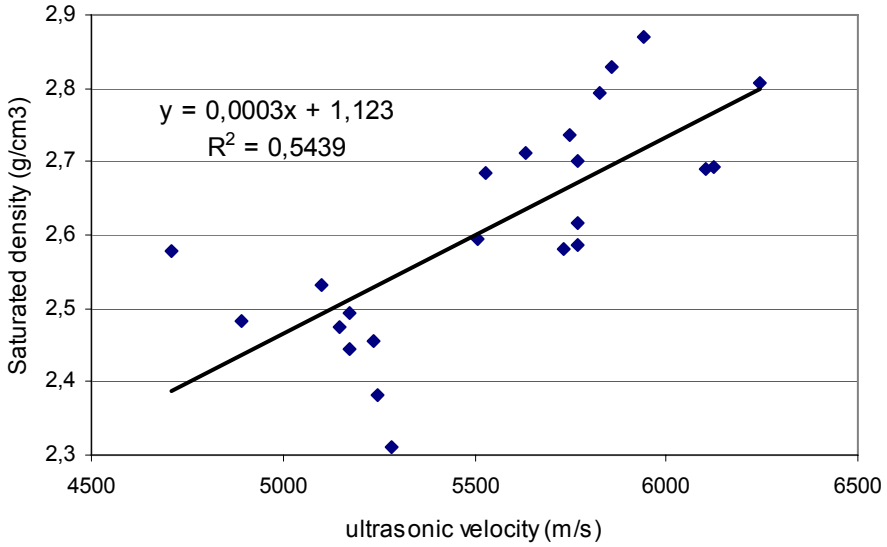


Figure 4.46c. Ultrasonic velocity – Saturated density diagram
(Basalt with much calcite-little vesicle)

Table 4.54. Equation and $R^2$ values for Ultrasonic velocity – Saturated density
(Basalt with much calcite-little vesicle)

| TRENDLINE TYPE | $R^2$ | EQUATION |
|---|---|---|
| LINEAR | 0,5439 | $y = 0,0003x + 1,123$ |
| POWER | 0,5252 | $y = 0,0216x^{0,5564}$ |
| EXPONENTIAL | 0,538 | $y = 1,4743e^{0,0001x}$ |

Figure 4.46c shows the highest $R^2$ for test results of the ultrasonic velocity of basalts versus saturated density. Other trends of correlation are also given in Table 4.54. It can be seen clearly from figure 4.46c, saturated density of basalt increases as ultrasonic velocity increase. In this graphic the relationship follows a linear law with a reasonable squared regression coefficient R-square is 0,5439 and equation $y = 0,0003x + 1,123$.

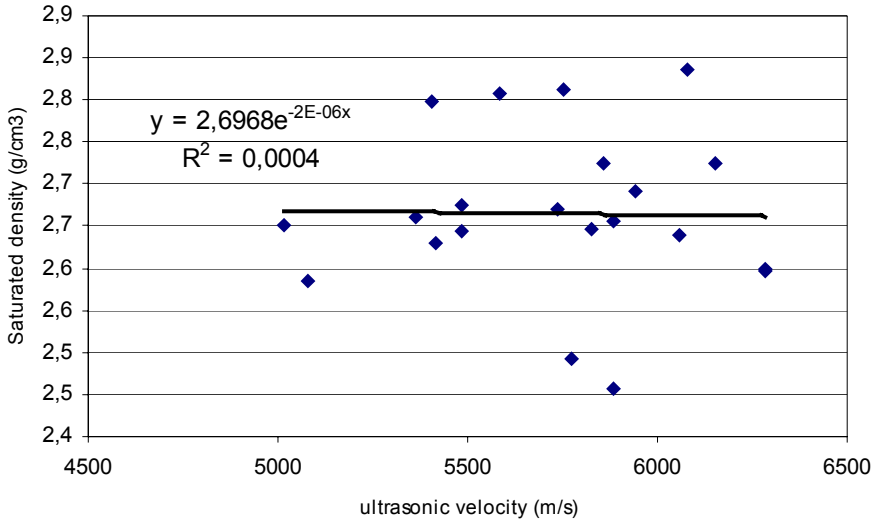


Figure 4.46d. Ultrasonic velocity – Saturated density diagram
(Vesicular basalt with calcite)

Table 4.55. Equation and $R^2$ values for Ultrasonic velocity – Saturated density
(Vesicular basalt with calcite)

| TRENDLINE TYPE | $R^2$ | EQUATION |
|---|---|---|
| LINEAR | 0,0003 | y = -5E-06x + 2,693 |
| POWER | 0,0002 | $y = 2,8606x^{-0,0082}$ |
| EXPONENTIAL | 0,0004 | $y = 2,6968e^{-2E-06x}$ |

Figure 4.46d shows the highest $R^2$ for test results of the ultrasonic velocity of basalts versus saturated density. Other trends of correlation are also given in Table 4.55. It can be seen clearly from figure 4.46d, saturated density of basalt increases as ultrasonic velocity increase. In this graphic the relationship follows an exponential law with a reasonable squared regression coefficient R-square is 0,0004 and equation is $y = 2,6968e^{-2E-06x}$.

### 4.5.1.4. Ultrasonic velocity versus water absorption

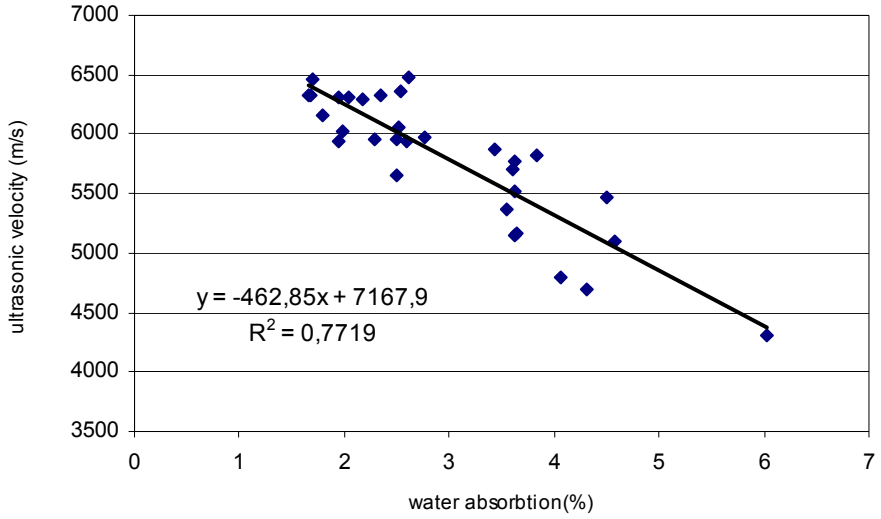


Figure 4.47a. Ultrasonic velocity – Water absorption diagram (Vesicular basalt)

Table 4.56. Equation and $R^2$ values for Ultrasonic velocity – Water absorption (vesicular basalt)

| TRENDLINE TYPE | $R^2$ | EQUATION |
|---|---|---|
| LINEAR | 0,7719 | y = -462,85x + 7167,9 |
| POWER | 0,7102 | $y = 7449x^{-0,2488}$ |
| EXPONENTIAL | 0,7717 | $y = 7409,5e^{-0,0845x}$ |

Figure 4.47a shows the highest $R^2$ for test results of the ultrasonic velocity of basalts versus water absorption. Other trends of correlation are also given in Table 4.56. It can be seen clearly from figure 4.47a, water absorption of basalt increases as ultrasonic velocity decrease. In this graphic the relationship follows a linear law with a reasonable squared regression coefficient R-square is 0,7719 and equation is y = -462,85x + 7167,9.

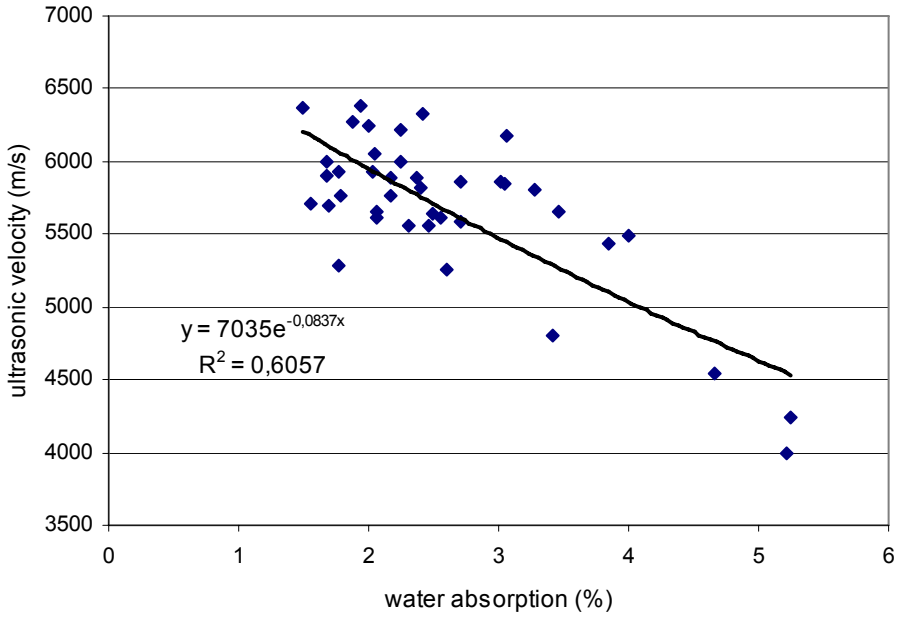


Figure 4.47b. Ultrasonic velocity – Water absorption diagram
(Basalt with no vesicle and calcite)

Table 4.57. Equation and $R^2$ values for Ultrasonic velocity – Water absorption
(Basalt with no vesicle and calcite)

| TRENDLINE TYPE | $R^2$ | EQUATION |
|---|---|---|
| LINEAR | 0,5849 | $y = -428,53x + 6800,9$ |
| POWER | 0,4977 | $y = 6911,8x^{-0,2217}$ |
| EXPONENTIAL | 0,6057 | $y = 7035e^{-0,0837x}$ |

Figure 4.47b shows the highest $R^2$ for test results of the ultrasonic velocity of basalts versus water absorption. Other trends of correlation are also given in Table 4.57. It can be seen clearly from figure 4.47b, water absorption of basalt increases as ultrasonic velocity decrease. In this graphic the relationship follows an exponential law with a reasonable squared regression coefficient R-square is 0,6057 and equation is $y = 7035e^{-0,0837x}$.

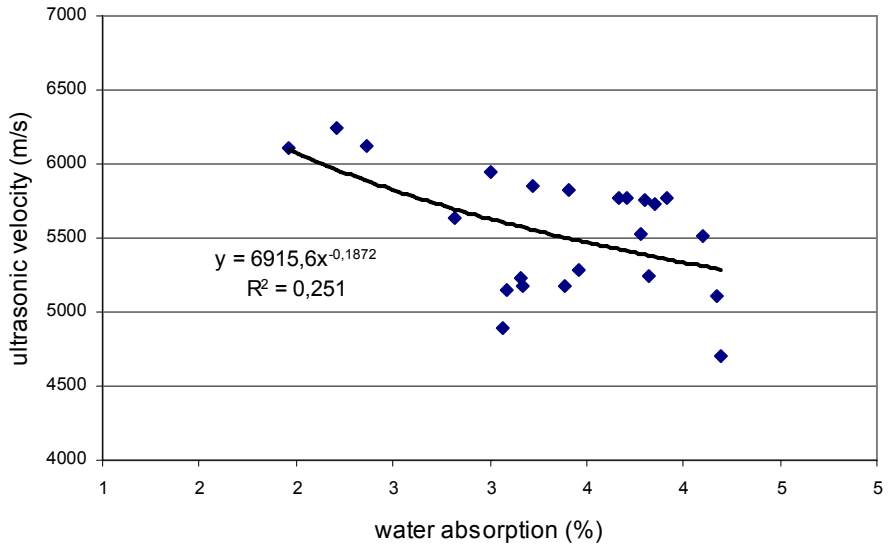


Figure 4.47c. Ultrasonic velocity – Water absorption diagram
(Basalt with much calcite-little vesicle)

Table 4.58. Equation and $R^2$ values for Ultrasonic velocity – Water absorption
(Basalt with much calcite-little vesicle)

| TRENDLINE TYPE | $R^2$ | EQUATION |
|---|---|---|
| LINEAR | 0,2484 | y = -335,96x + 6674,1 |
| POWER | 0,251 | $y = 6915,6x^{-0,1872}$ |
| EXPONENTIAL | 0,2334 | $y = 6753,1e^{-0,0594x}$ |

Figure 4.47c shows the highest $R^2$ for test results of the ultrasonic velocity of basalts versus water absorption. Other trends of correlation are also given in Table 4.58. It can be seen clearly from figure 4.47c, water absorption of basalt increases as ultrasonic velocity decrease. In this graphic the relationship follows a power law with a reasonable squared regression coefficient R-square is 0,251 and equation $y = 6915,6x^{-0,1872}$.

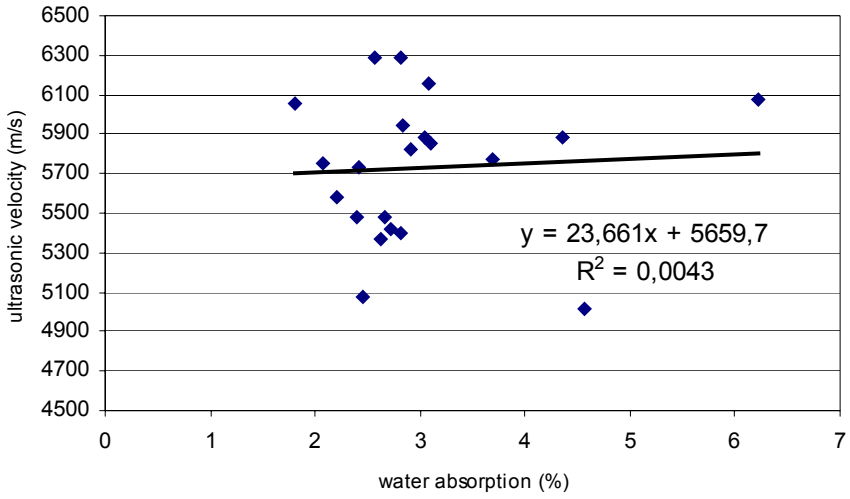


Figure 4.47d. Ultrasonic velocity – Water absorption diagram
(Vesicular basalt with calcite)

Table 4.59. Equation and $R^2$ values for Ultrasonic velocity – Water absorption
(Vesicular basalt with calcite)

| TRENDLINE TYPE | $R^2$ | EQUATION |
|---|---|---|
| LINEAR | 0,0043 | y = 23,661x + 5659,7 |
| POWER | 0,0011 | $y = 5674,1x^{0,0076}$ |
| EXPONENTIAL | 0,0034 | $y = 5656,3e^{0,0037x}$ |

Figure 4.47d shows the highest $R^2$ for test results of the ultrasonic velocity of basalts versus water absorption. Other trends of correlation are also given in Table 4.59. It can be seen clearly from figure 4.47d, water absorption of basalt increases as ultrasonic velocity decrease. In this graphic the relationship follows a linear law with a reasonable squared regression coefficient R-square is 0,0043and equation is y = 23,661x + 5659,7.

#### 4.4.1.5. Ultrasonic velocity versus porosity

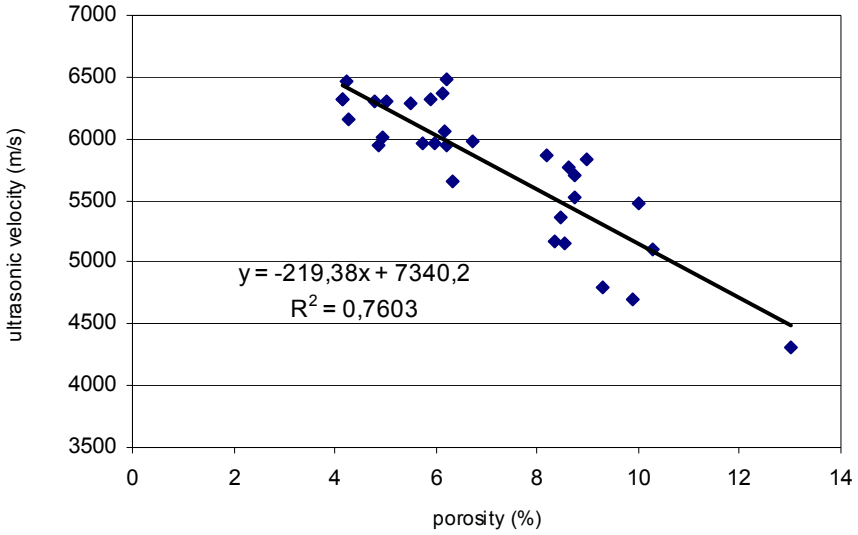


Figure 4.48a. Ultrasonic velocity – Porosity diagram
(Vesicular basalt)

Table 4.60. Equation and $R^2$ values for Ultrasonic velocity – Porosity (vesicular basalt)

| TRENDLINE TYPE | $R^2$ | EQUATION |
|---|---|---|
| LINEAR | 0,7603 | y = -219,38x + 7340,2 |
| POWER | 0,6912 | $y = 9684,8x^{-0,2721}$ |
| EXPONENTIAL | 0,7551 | $y = 7639,2e^{-0,0399x}$ |

Figure 4.48a shows the highest $R^2$ for test results of the ultrasonic velocity of basalts versus porosity. Other trends of correlation are also given in Table 4.60. It can be seen clearly from figure 4.48a, porosity of basalt increases as ultrasonic velocity decrease. In this graphic the relationship follows a linear law with a reasonable squared regression coefficient R-square is 0,7603 and equation is y = -219,38x + 7340,2.

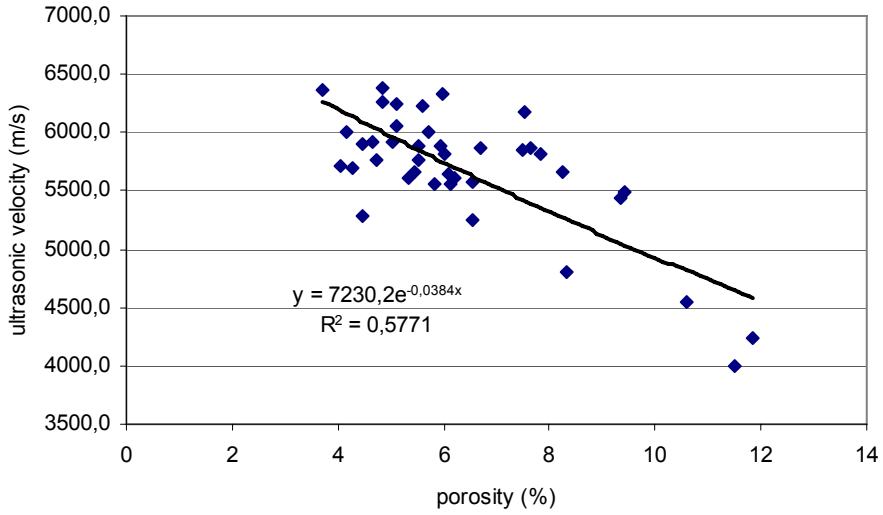


Figure 4.48b. Ultrasonic velocity – Porosity diagram
(Basalt with no vesicle and calcite)

Table 4.61. Equation and $R^2$ values for Ultrasonic velocity – Porosity
(Basalt with no vesicle and calcite)

| TRENDLINE TYPE | $R^2$ | EQUATION |
|---|---|---|
| LINEAR | 0,5614 | $y = -197,2x + 6945,6$ |
| POWER | 0,4825 | $y = 8808,7x^{-0,2442}$ |
| EXPONENTIAL | 0,5771 | $y = 7230,2e^{-0,0384x}$ |

Figure 4.48b shows the highest $R^2$ for test results of the ultrasonic velocity of basalts versus porosity. Other trends of correlation are also given in Table 4.61. It can be seen clearly from figure 4.48b, porosity of basalt increases as ultrasonic velocity decrease. In this graphic the relationship follows an exponential law with a reasonable squared regression coefficient R-square is 0,5771 and equation is $y = 7230,2e^{-0,0384x}$.

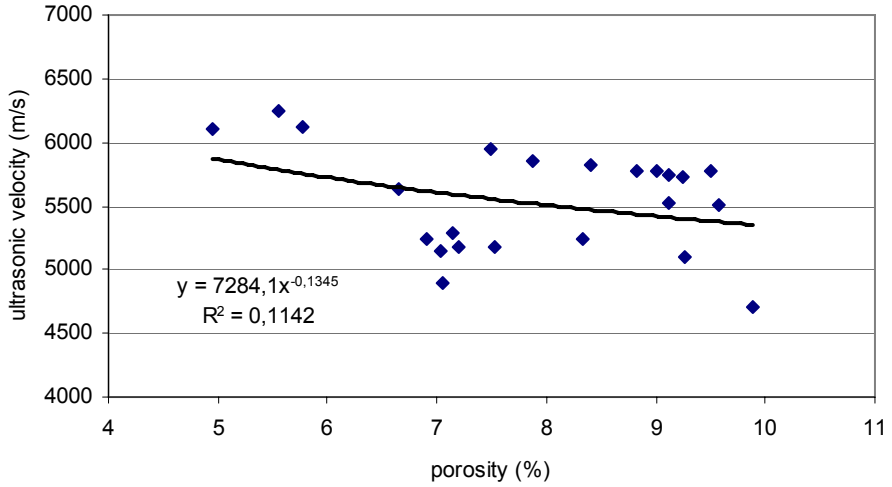


Figure 4.48c. Ultrasonic velocity – Porosity diagram
(Basalt with much calcite-little vesicle)

Table 4.62. Equation and $R^2$ values for Ultrasonic velocity – Porosity (Basalt with much calcite-little vesicle)

| TRENDLINE TYPE | $R^2$ | EQUATION |
|---|---|---|
| LINEAR | 0,1031 | y = -94,798x + 6292 |
| POWER | 0,1142 | $y = 7284{,}1x^{-0{,}1345}$ |
| EXPONENTIAL | 0,095 | $y = 6303{,}8e^{-0{,}0166x}$ |

Figure 4.48c shows the highest $R^2$ for test results of the ultrasonic velocity of basalts versus porosity. Other trends of correlation are also given in Table 4.62. It can be seen clearly from figure 4.48c, porosity of basalt increases as ultrasonic velocity decrease. In this graphic the relationship follows a power law with a reasonable squared regression coefficient R-square is 0,251 and equation $y = 7284{,}1x^{-0{,}1345}$.

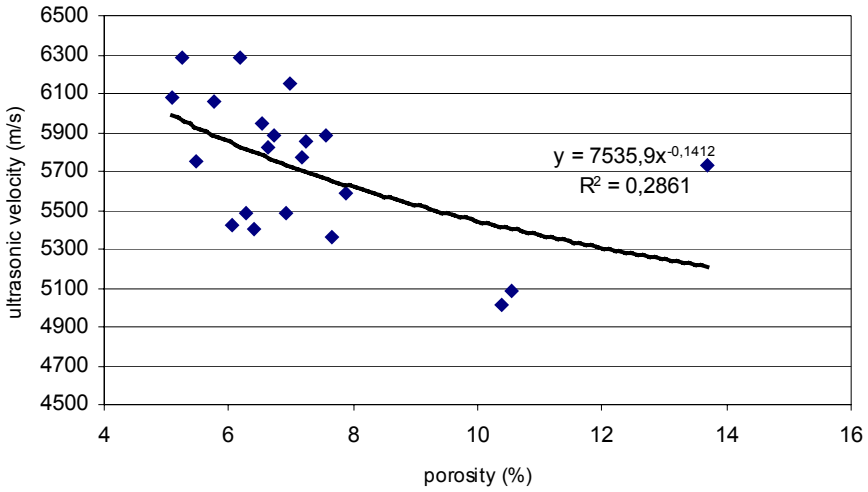


Figure 4.48d. Ultrasonic velocity – Porosity diagram
(Vesicular basalt with calcite)

Table 4.63. Equation and $R^2$ values for Ultrasonic velocity – Porosity
(Vesicular basalt with calcite)

| TRENDLINE TYPE | $R^2$ | EQUATION |
|---|---|---|
| LINEAR | 0,2315 | $y = -84,902x + 6347,4$ |
| POWER | 0,2861 | $y = 7535,9x^{-0,1412}$ |
| EXPONENTIAL | 0,2348 | $y = 6383,7e^{-0,0151x}$ |

Figure 4.48d shows the highest $R^2$ for test results of the ultrasonic velocity of basalts versus porosity. Other trends of correlation are also given in Table 4.63. It can be seen clearly from figure 4.48d, porosity of basalt increases as ultrasonic velocity decrease. In this graphic the relationship follows a power law with a reasonable squared regression coefficient R-square is 0,2861 and equation is $y = 7535,9x^{-0,1412}$.

### 4.5.2. Uniaxial compression test

The same processes were done to basalt specimens as same as above for uniaxial compressive test. For this time basalt specimens were divided into two groups for uniaxial compression test to find out their varieties change the graphic or not. And graphics were drawn one by one for each group for uniaxial compressive strength versus ultrasonic velocity (see in figure 4.33).

- Basalt with no vesicle and calcite
- Vesicular basalt with calcite

#### 4.5.2.1. Ultrasonic velocity versus uniaxial compression strength

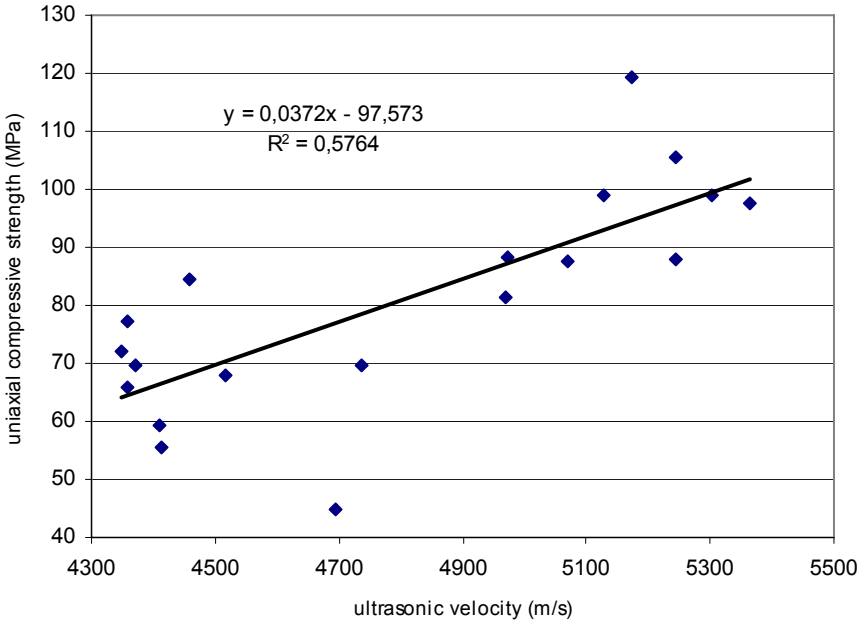


Figure 4.49a. Ultrasonic velocity – Uniaxial compressive strength diagram (Basalt with no vesicle and calcite)

Table 4.64. Equation and $R^2$ values for Ultrasonic velocity – Uniaxial compressive strength (Basalt with no vesicle and calcite)

| TRENDLINE TYPE | $R^2$ | EQUATION |
|---|---|---|
| LINEAR | 0,5764 | y = 0,0372x - 97,573 |
| POWER | 0,5114 | $y = 8E\text{-}07x^{2,1785}$ |
| EXPONENTIAL | 0,5196 | $y = 8,755e^{0,0005x}$ |

Figure 4.49a shows the highest $R^2$ for test results of the ultrasonic velocity of basalts versus uniaxial compressive strength. Other trends of correlation are also given in Table 4.64. It can be seen clearly from figure 4.49a, uniaxial compressive strength of basalt increases as ultrasonic velocity increase. In this graphic the relationship follows a linear law with a reasonable squared regression coefficient R-square is 0,5764 and equation is y = 0,0372x - 97,573.

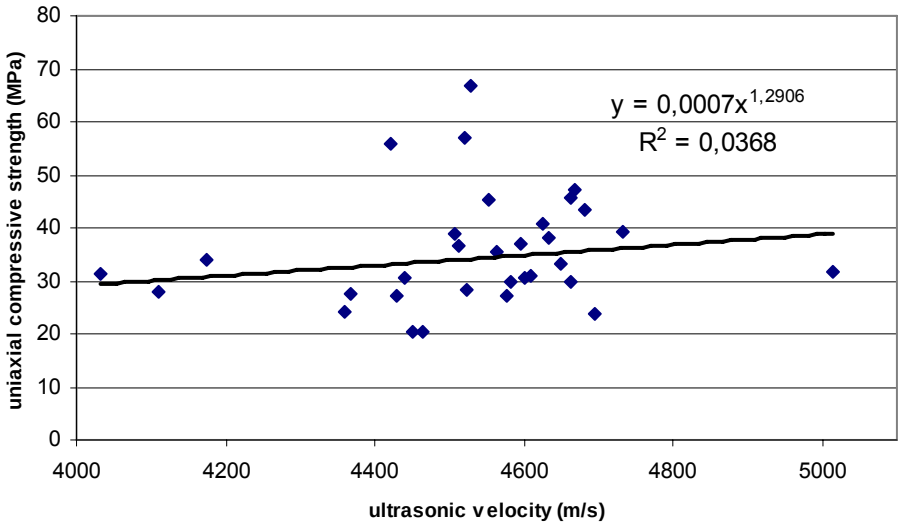


Figure 4.49b. Ultrasonic velocity – Uniaxial compressive strength diagram (Vesicular basalt with calcite)

Table 4.65. Equation and $R^2$ values for Ultrasonic velocity – Uniaxial compressive strength (Vesicular basalt with calcite)

| TRENDLINE TYPE | $R^2$ | EQUATION |
|---|---|---|
| LINEAR | 0,0253 | $y = 0,0091x - 5,6136$ |
| POWER | 0,0368 | $y = 0,0007x^{1,2906}$ |
| EXPONENTIAL | 0,0356 | $y = 9,4019e^{0,0003x}$ |

Figure 4.49b shows the highest $R^2$ for test results of the ultrasonic velocity of basalts versus uniaxial compressive strength. Other trends of correlation are also given in Table 4.65. It can be seen clearly from figure 4.49b, uniaxial compressive strength of basalt increases as ultrasonic velocity increase. In this graphic the relationship follows a power law with a reasonable squared regression coefficient R-square is 0,0356 and equation is $y = 0,0007x^{1,2906}$.

### 4.5.2.2. Ultrasonic velocity versus dry density

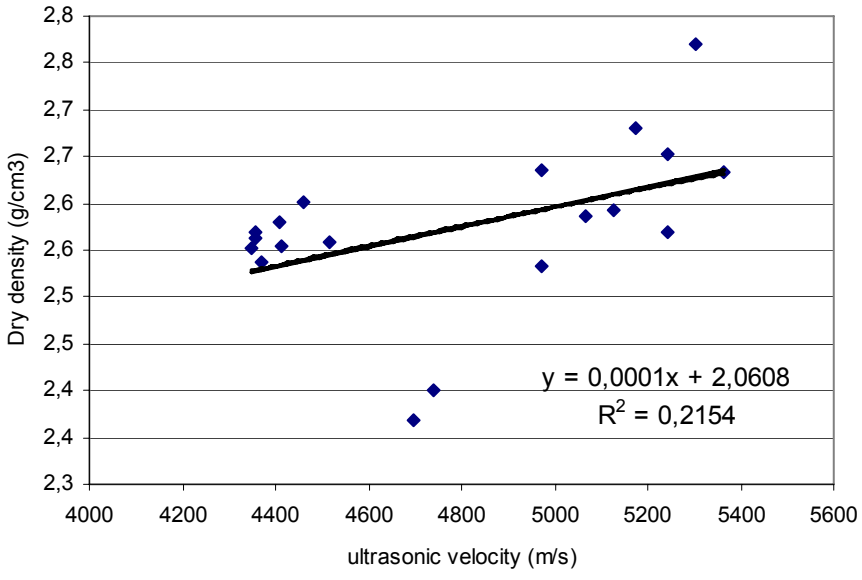


Figure 4.50a. Ultrasonic velocity – Dry density diagram (Basalt with no vesicle and calcite)

Table 4.66. Equation and $R^2$ values for Ultrasonic velocity – Dry density (Basalt with no vesicle and calcite)

| TRENDLINE TYPE | $R^2$ | EQUATION |
|---|---|---|
| LINEAR | 0,2154 | $y = 0,0001x + 2,0608$ |
| POWER | 0,1948 | $y = 0,5061x^{0,192}$ |
| EXPONENTIAL | 0,2058 | $y = 2,1135e^{4E-05x}$ |

Figure 4.50a shows the highest $R^2$ for test results of the ultrasonic velocity of basalts versus dry density. Other trends of correlation are also given in Table 4.66. It can be seen clearly from figure 4.50a, dry density of basalt increases as ultrasonic velocity increase. In this graphic the relationship follows a linear law with a reasonable squared regression coefficient R-square is 0,2154 and equation is y = 0,0001x + 2,0608.

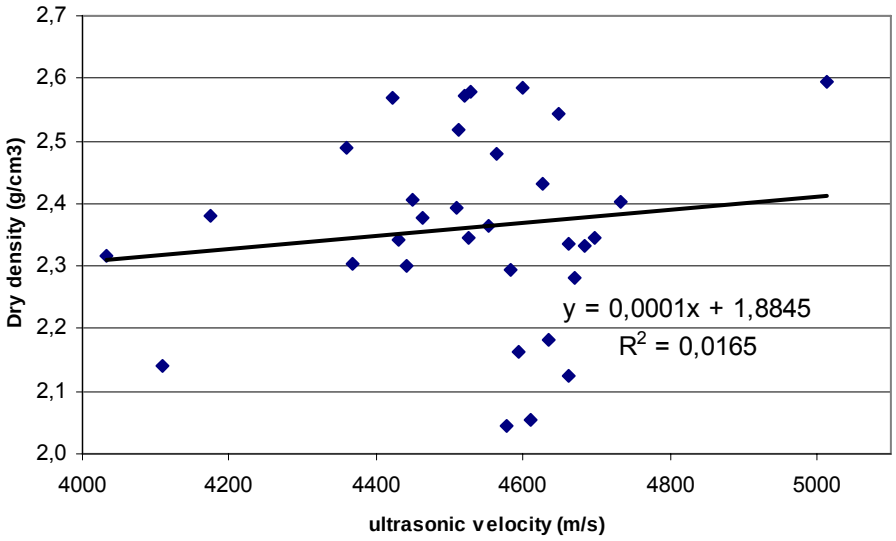


Figure 4.50b. Ultrasonic velocity – Dry density diagram (Vesicular basalt with calcite)

Table 4.67. Equation and $R^2$ values for Ultrasonic velocity – Dry density (Vesicular basalt with calcite)

| TRENDLINE TYPE | $R^2$ | EQUATION |
|---|---|---|
| LINEAR | 0,0165 | $y = 0,0001x + 1,8845$ |
| POWER | 0,014 | $y = 0,4922x^{0,1861}$ |
| EXPONENTIAL | 0,0143 | $y = 1,9475e^{4E-05x}$ |

Figure 4.50b shows the highest $R^2$ for test results of the ultrasonic velocity of basalts versus dry density. Other trends of correlation are also given in Table 4.67. It can be seen clearly from figure 4.50b, dry density of basalt increases as ultrasonic velocity increase. In this graphic the relationship follows a linear law with a reasonable squared regression coefficient R-square is 0,0165 and equation is $y = 0,0001x + 1,8845$.

### 4.5.2.3. Ultrasonic velocity versus saturated density

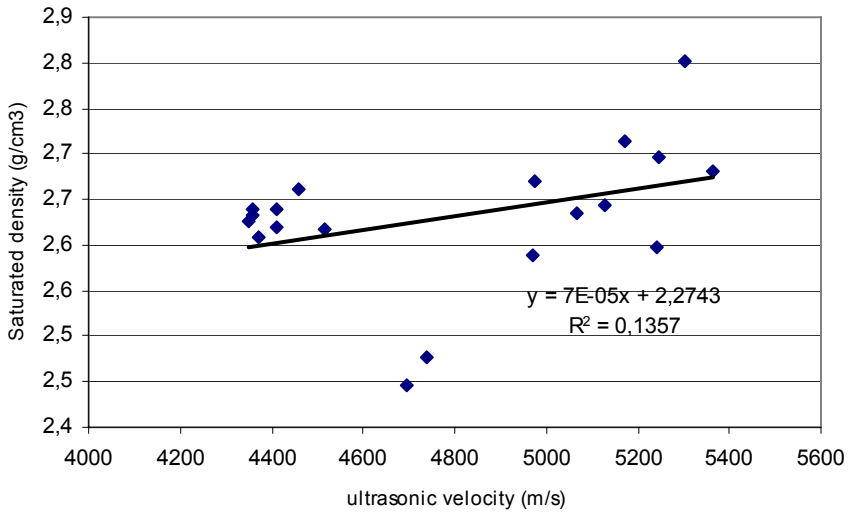


Figure 4.51a. Ultrasonic velocity – Saturated density diagram (Basalt with no vesicle and calcite)

Table 4.68. Equation and $R^2$ values for Ultrasonic velocity – Saturated density (Basalt with no vesicle and calcite)

| TRENDLINE TYPE | $R^2$ | EQUATION |
|---|---|---|
| LINEAR | 0,1357 | y = 7E-05x + 2,2743 |
| POWER | 0,1199 | $y = 0,8834x^{0,1288}$ |
| EXPONENTIAL | 0,1294 | $y = 2,3012e^{3E-05x}$ |

Figure 4.51a shows the highest $R^2$ for test results of the ultrasonic velocity of basalts versus saturated density. Other trends of correlation are also given in Table 4.68. It can be seen clearly from figure 4.51a, saturated density of basalt increases as ultrasonic velocity increase. In this graphic the relationship follows a linear law with a reasonable squared regression coefficient R-square is 0,1357 and equation is y = 7E-05x + 2,2743.

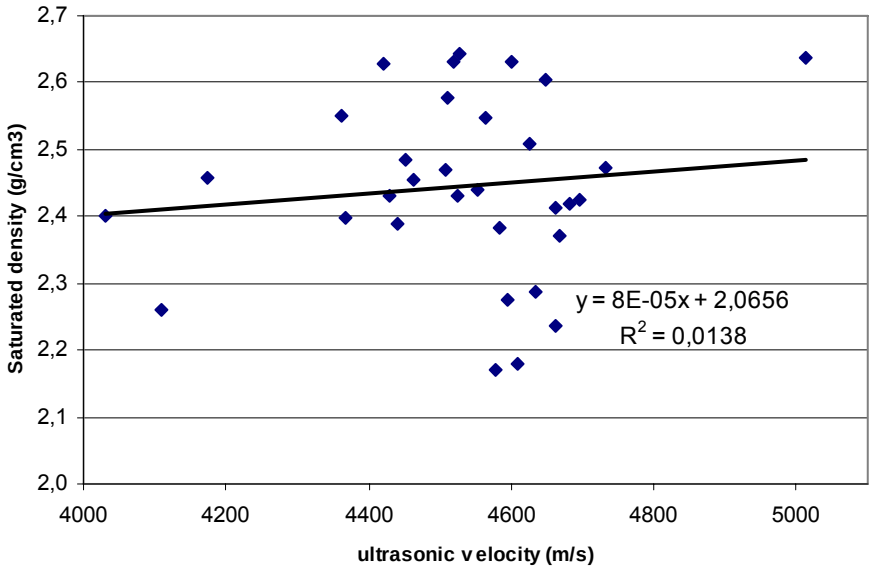


Figure 4.51b. Ultrasonic velocity – Saturated density diagram (Vesicular basalt with calcite)

Table 4.69. Equation and $R^2$ values for Ultrasonic velocity – Saturated density (Vesicular basalt with calcite)

| TRENDLINE TYPE | $R^2$ | EQUATION |
|---|---|---|
| LINEAR | 0,0138 | y = 8E-05x + 2,0656 |
| POWER | 0,012 | $y = 0,7287x^{0,1436}$ |
| EXPONENTIAL | 0,0122 | $y = 2,1068e^{3E-05x}$ |

Figure 4.51b shows the highest $R^2$ for test results of the ultrasonic velocity of basalts versus saturated density. Other trends of correlation are also given in Table 4.69. It can be seen clearly from figure 4.51b, saturated density of basalt increases as ultrasonic velocity increase. In this graphic the relationship follows a linear law with a reasonable squared regression coefficient R-square is 0,0138 and equation is y = 8E-05x + 2,0656.

### 4.5.2.4. Ultrasonic velocity versus water absorption

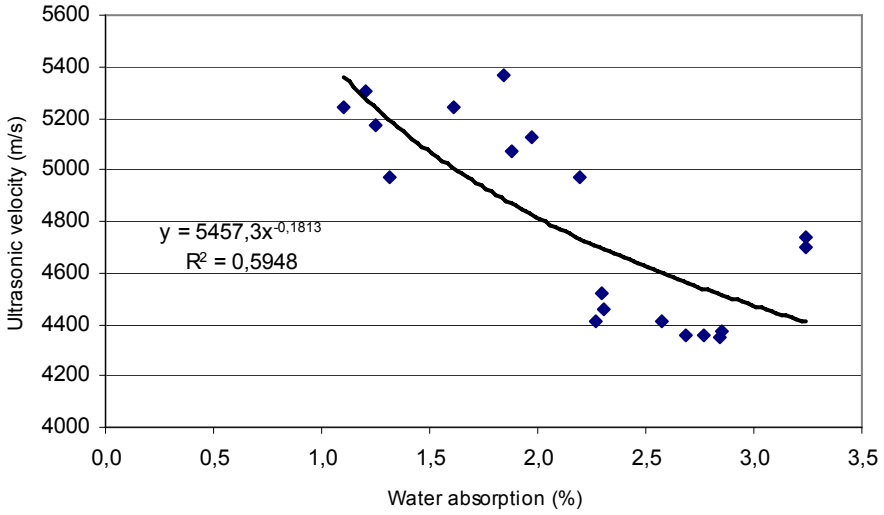


Figure 4.52a. Ultrasonic velocity – Water absorption diagram (Basalt with no vesicle and calcite)

Table 4.70. Equation and $R^2$ values for Ultrasonic velocity – Water absorption (Basalt with no vesicle and calcite)

| TRENDLINE TYPE | $R^2$ | EQUATION |
|---|---|---|
| LINEAR | 0,5869 | y = -434,17x + 5743,4 |
| POWER | 0,5948 | $y = 5457,3x^{-0,1813}$ |
| EXPONENTIAL | 0,5801 | $y = 5818e^{-0,0899x}$ |

Figure 4.52a shows the highest $R^2$ for test results of the ultrasonic velocity of basalts versus water absorption. Other trends of correlation are also given in Table 4.70. It can be seen clearly from figure 4.52a, water absorption of basalt increases as ultrasonic velocity decrease. In this graphic the relationship follows a power law with a reasonable squared regression coefficient R-square is 0,5948 and equation is $y = 5457,3x^{-0,1813}$.

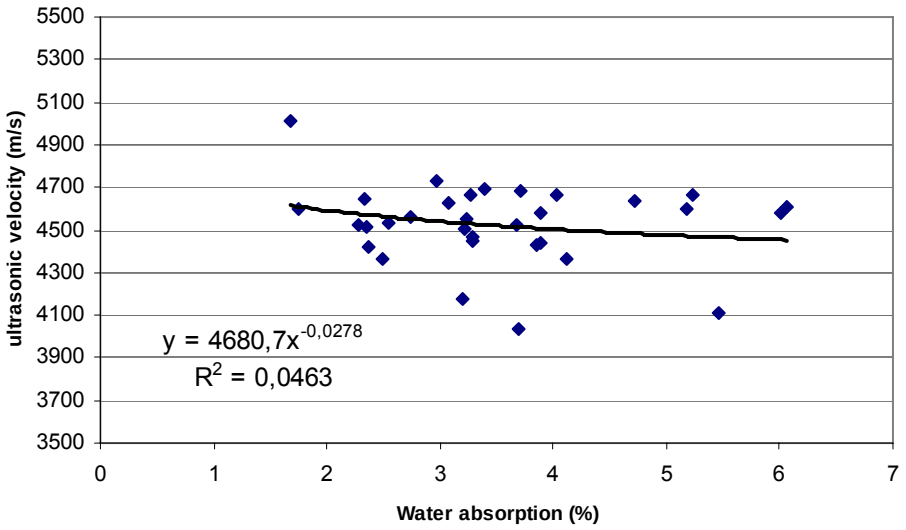


Figure 4.52b. Ultrasonic velocity – Water absorption diagram (Vesicular basalt with calcite)

Table 4.71. Equation and $R^2$ values for Ultrasonic velocity – Water absorption (Vesicular basalt with calcite)

| TRENDLINE TYPE | $R^2$ | EQUATION |
|---|---|---|
| LINEAR | 0,0267 | y = -26,725x + 4624,1 |
| POWER | 0,0463 | y = 4680,7x-0,0278 |
| EXPONENTIAL | 0,0256 | y = 4620,7e-0,0059x |

Figure 4.52b shows the highest $R^2$ for test results of the ultrasonic velocity of basalts versus water absorption. Other trends of correlation are also given in Table 4.71. It can be seen clearly from figure 4.52b, water absorption of basalt increases as ultrasonic velocity deccrease. In this graphic the relationship follows a power law with a reasonable squared regression coefficient R-square is 0,0463 and equation is y = 4680,7x-0,0278.

### 4.5.2.5. Ultrasonic velocity versus porosity

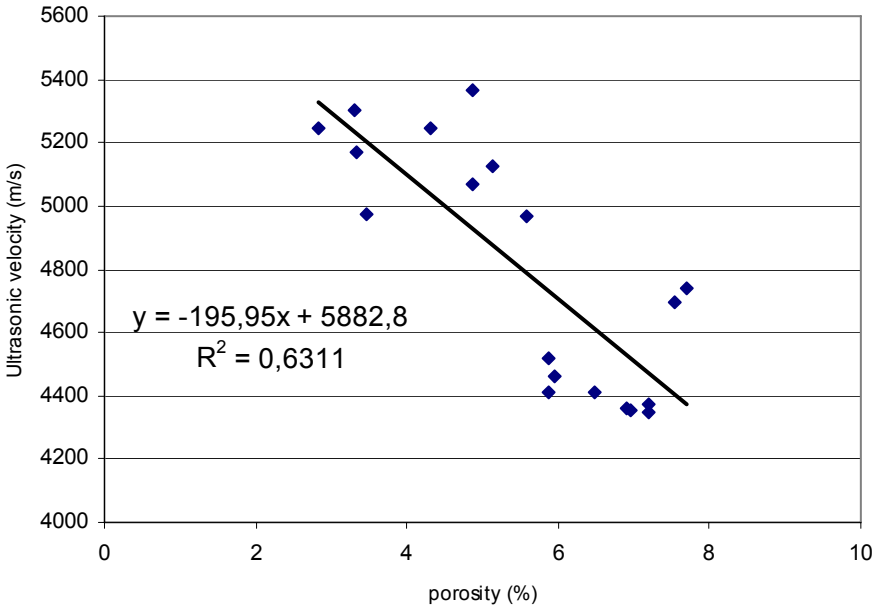


Figure 4.53a. Ultrasonic velocity – Porosity diagram (Basalt with no vesicle and calcite)

Table 4.72. Equation and $R^2$ values for Ultrasonic velocity – Porosity (Basalt with no vesicle and calcite)

| TRENDLINE TYPE | $R^2$ | EQUATION |
|---|---|---|
| LINEAR | 0,6311 | $y = -195,95x + 5882,8$ |
| POWER | 0,6089 | $y = 6680,2x^{-0,2002}$ |
| EXPONENTIAL | 0,6263 | $y = 5991,1e^{-0,0407x}$ |

Figure 4.53a shows the highest $R^2$ for test results of the ultrasonic velocity of basalts versus porosity. Other trends of correlation are also given in Table 4.72. It can be seen clearly from figure 4.53a, porosity of basalt increases as ultrasonic velocity decrease. In this graphic the relationship follows a linear law with a reasonable squared regression coefficient R-square is 0,6311 and equation is y = -195,95x + 5882,8.

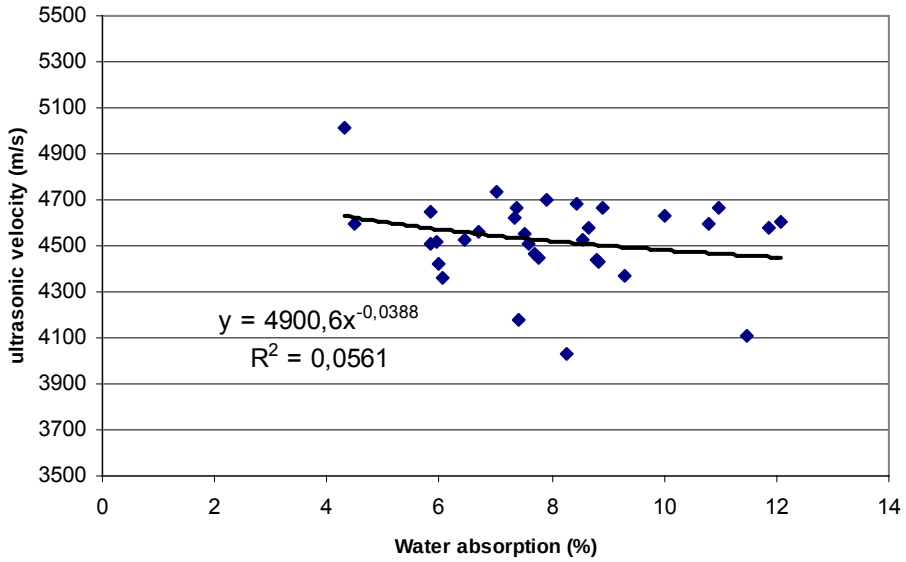


Figure 4.53b. Ultrasonic velocity – Porosity diagram (Vesicular basalt with calcite)

Table 4.73. Equation and $R^2$ values for Ultrasonic velocity – Porosity (Vesicular basalt with calcite)

| TRENDLINE TYPE | $R^2$ | EQUATION |
|---|---|---|
| LINEAR | 0,0392 | $y = -18,561x + 4678,3$ |
| POWER | 0,0561 | $y = 4900,6x^{-0,0388}$ |
| EXPONENTIAL | 0,0375 | $y = 4675,6e^{-0,0041x}$ |

Figure 4.53b shows the highest $R^2$ for test results of the ultrasonic velocity of basalts versus porosity. Other trends of correlation are also given in Table 4.73. It can be seen clearly from figure 4.53b, porosity of basalt increases as ultrasonic velocity deccrease. In this graphic the relationship follows a power law with a reasonable squared regression coefficient R-square is 0,0561 and equation is $y = 4900,6x^{-0,0388}$.

## 4.6. Multiple Regression Analysis

In this section multiple regression analyse were done. In the preceeding sections; determined correlation coefficients of regression are somewhat low, so a multiple analyses are evaluated.

### 4.6.1. Multiple regression analysis for Brazillian tensile strength versus dry density, water absorption and ultrasonic velocity

Table 4.74 Regression Statistics

| | |
|---|---|
| Multiple R | 0,67685661 |
| $R^2$ | 0,458134871 |
| Adjusted $R^2$ | 0,443356731 |
| Standard Error | 1,609507556 |
| Observations | 114 |

For this multiple regression analyses, $R^2$ is determined as 0,46 from the test results and also other values are also given in table 4.74.

Table 4.75 Analize of variance

| | *Df (Degree of Freedom)* | *SS (SumOf Squares)* | *MS (Men Square)* | *F* | *Significance F (Probablity Level)* |
|---|---|---|---|---|---|
| Regression | 3 | 240,9244468 | 80,30815 | 31,00085 | 1,33232E-14 |
| Residual | 110 | 284,9566032 | 2,590515 | | |
| Total | 113 | 525,88105 | | | |

Table 4.76 Coefficients of equation

| | *Coefficients* | *Standard Error* | *t Stat* | *P-value* |
|---|---|---|---|---|
| Intercept | 4,114510914 | 4,520106548 | 0,910269 | 0,364671 |
| Dry density (g/cm$^3$) | 1,307837571 | 1,528298805 | 0,855747 | 0,393998 |
| Water absorption (%) | -1,140487128 | 0,228822082 | -4,98417 | 2,33E-06 |
| Ultrasonic velocity (m/s) | 0,000733592 | 0,000455261 | 1,611367 | 0,109966 |

Table 4.75 shows the analize of variances and detailed coefficients of equation cen be seen in the table 4.76.

The equation of this analyses is :

$$B.\ T.\ S. = 4.11 + 1{,}30\ \delta_{dry} - 1{,}14\ W_{abs.} + 0\ U.\ V.$$

B. T. S. is the Brazillian tensile strength, $\delta_{dry}$ : Dry density, $W_{abs.}$ : Water absorption, U. V. : ultrasonic velocity.

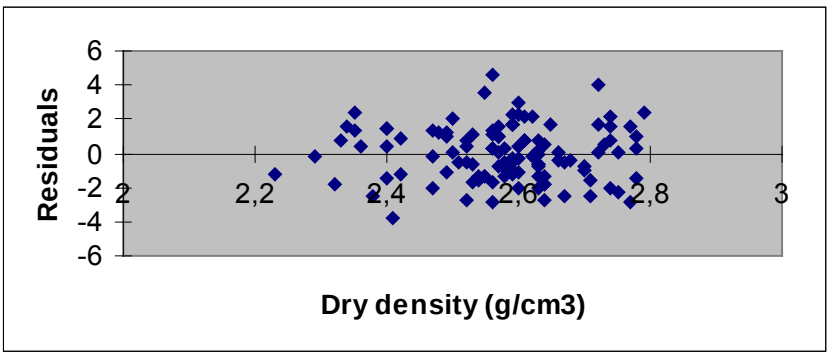


Figure 4.54. Dry density residual plot

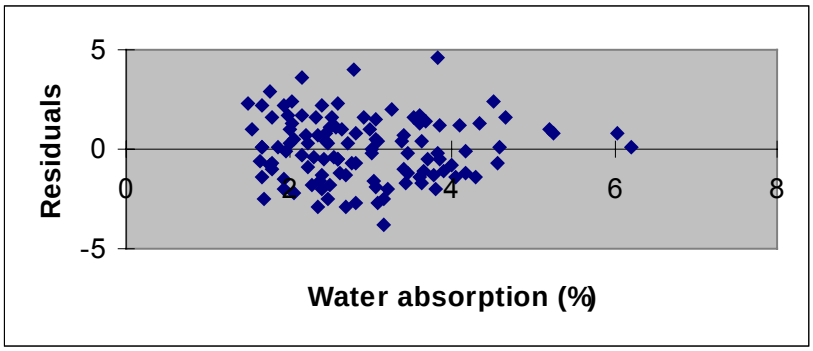


Figure 4.55. Water absorption residual plot

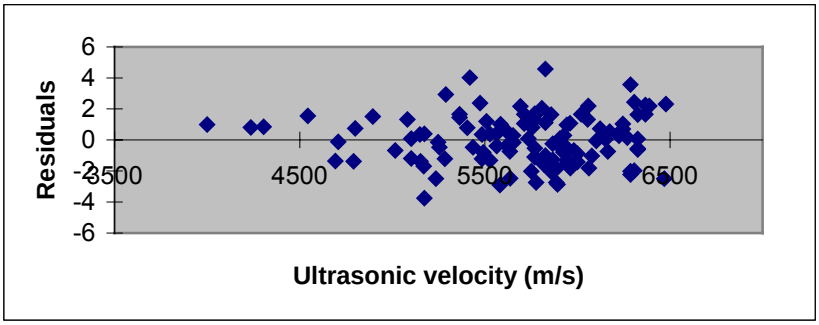


Figure 4.56. Ultrasonic velocity residual plot

The three figures (4.54, 4.55 and 4.56) in the above are shows the dry density –, water absorption –, ultrasonic velocity residuals plot for the samples of Brazillian tensile test, respectively.

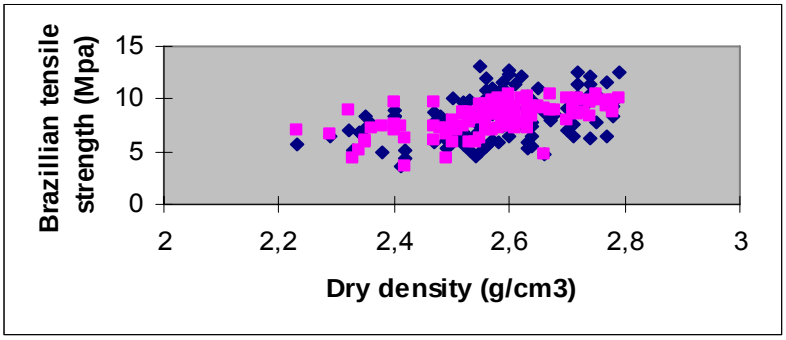


Figure 4.57. Dry density line fit plot

Blue data labels represents Brazillian tensile strength values obtained from equation. Pink data labels represents predicted Brazillian tensile strength values.

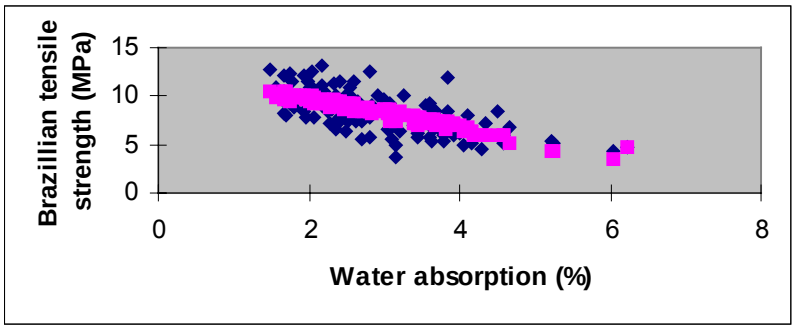


Figure 4.58 Water absorption line fit plot

Blue data labels represents Brazillian tensile strength values obtained from equation. Pink data labels represents predicted Brazillian tensile strength values.

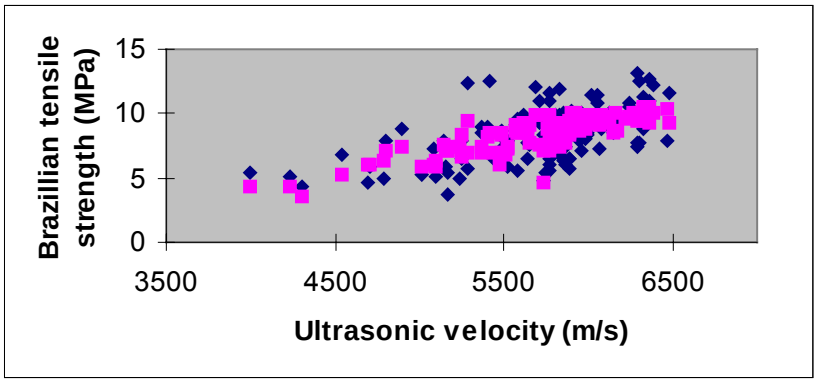


Figure 4.59. Ultrasonic velocity line fit plot

Blue data labels represents Brazillian tensile strength values obtained from equation. Pink data labels represents predicted Brazillian tensile strength values.

The three figures (4.57, 4.58 and 4.59) in the above are shows the dry density – water absorption – ultrasonic velocity line fit plot with the Brazillian tensile strength, respectively.

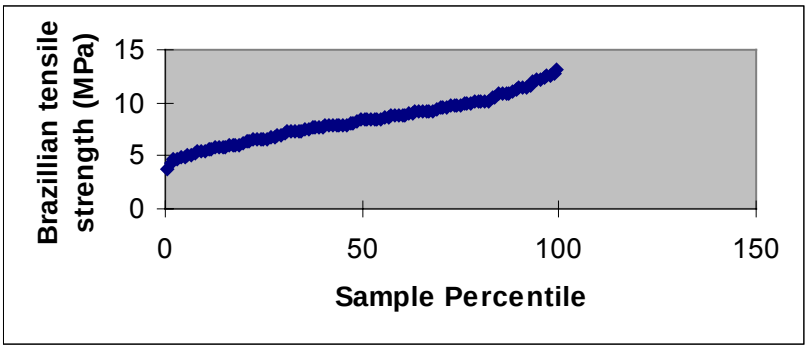


Figure 4.60. Normal probability plot

Figure 4.60 shows the normal probability plot with a Brazillian tensile strength – sample percentile diagram.

### 4.6.2. Multiple regression analysis for ultrasonic velocity versus dry density and water absorption for samples of brazillian tensile test

Table 4.77 Regression Statistics

| | |
|---|---|
| Multiple R | 0,73624151 |
| $R^2$ | 0,54205157 |
| Adjusted $R^2$ | 0,53380024 |
| Standard Error | 335,560736 |
| Observations | 114 |

For this multiple regression analyses, $R^2$ is determined as 0,54 from the test results and also other values are also given in table 4.77.

Table 4.78 Analize of variance

| | *Df (Degree of Freedom)* | *SS (Sum Of Squares)* | *MS (Men Square)* | *F* | *Significance F (Probablity Level)* |
|---|---|---|---|---|---|
| Regression | 2 | 14794124,87 | 7397062 | 65,69268 | 1,49734E-19 |
| Residual | 111 | 12498711,82 | 112601 | | |
| Total | 113 | 27292836,69 | | | |

Table 4.79 Coefficients of equation

| | *Coefficients* | *Standard Error* | *t Stat* | *P-value* |
|---|---|---|---|---|
| Intercept | 4296,86173 | 849,5584313 | 5,057759 | 1,69E-06 |
| Dry density (g/cm$^3$) | 897,92456 | 307,019982 | 2,924645 | 0,004182 |
| Water absorption (%) | -311,919635 | 37,4081959 | -8,33827 | 2,27E-13 |

Table 4.78 shows the analize of variances and detailed coefficients of equation cen be seen in the table 4.79.

The equation of this analyses is :

U. V. = 4296,86 + 1897,92 $\delta_{dry}$ – 311,92 $W_{abs.}$

U. V. is the ultrasonic velocity, $\delta_{dry}$ : Dry density, $W_{abs.}$ : Water absorption.

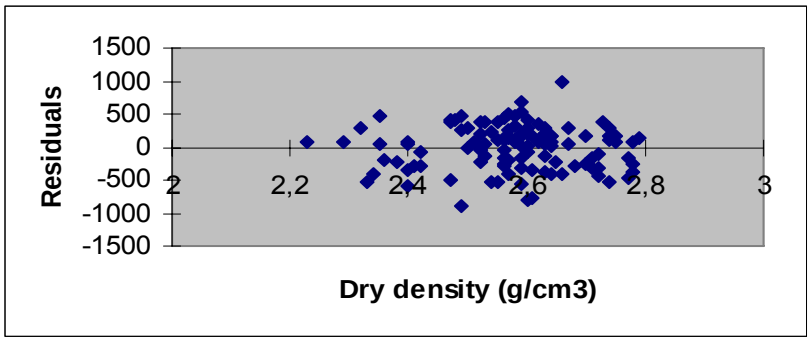


Figure 4.61. Dry density residual plot

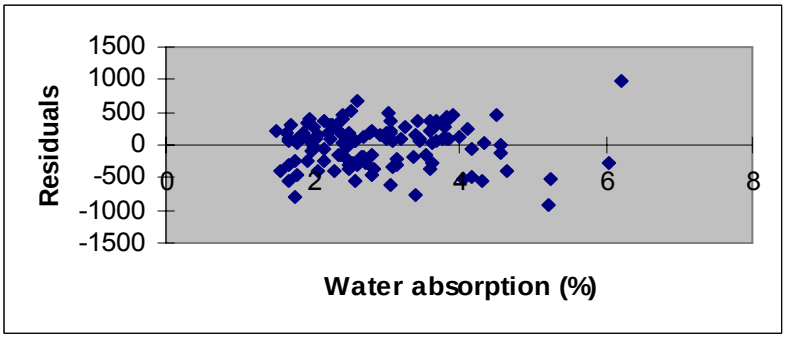


Figure 4.62 Water absorption residual plot

The two figures (4.61 and 4.62) in the above are shows the dry density –, water absorption residuals plot for the samples of Brazillian tensile test, respectively.

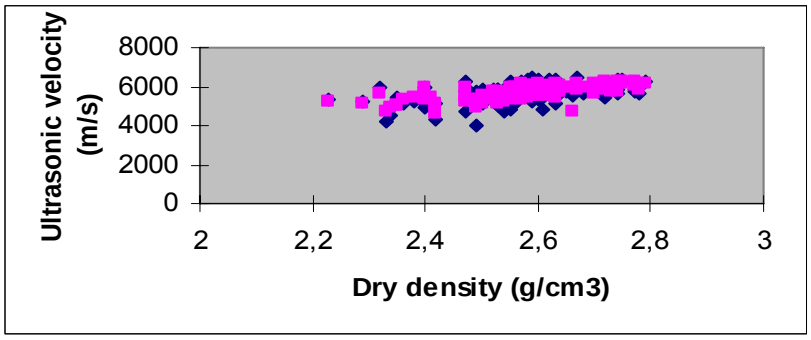


Figure 4.63 Dry density line fit plot

Blue data labels represents ultrasonic velocity values obtained from equation.
Pink data labels represents predicted ultrasonic velocity values.

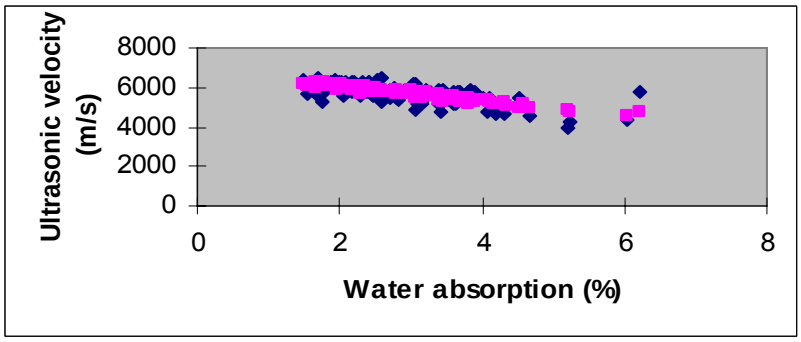


Figure 4.64 Water absorption line fit plot

Blue data labels represents ultrasonic velocity values obtained from equation.
Pink data labels represents predicted ultrasonic velocity values.

The two figures (4.63 and 4.64) in the above are shows the dry density – water absorption line fit plot with the ultrasonic velocity for the samples of Brazillian tensile test, respectively.

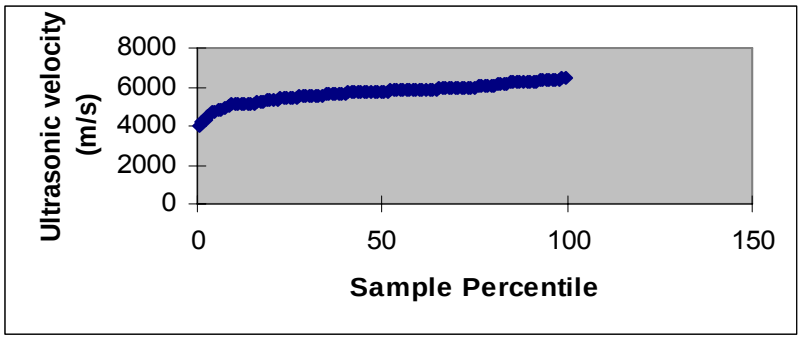


Figure 4.65 Normal probability plot

Figure 4.65 shows the normal probability plot with a ultrasonic velocity – sample percentile diagram for the samples of Brazillian tensile test.

### 4.6.3. Multiple regression analysis for uniaxial compressive strength versus dry density,water absorption and ultrasonic velocity

Table 4.80 Regression Statistics

| | |
|---|---|
| Multiple R | 0,819742455 |
| $R^2$ | 0,671977692 |
| Adjusted $R^2$ | 0,651040098 |
| Standard Error | 15,50869418 |
| Observations | 51 |

For this multiple regression analyses, $R^2$ is determined as 0,67 from the test results and also other values are also given in table 4.80.

Table 4.81 Analize of variance

| | *Df (Degree of Freedom)* | *SS (Sum Of Squares)* | *MS (Men Square)* | *F* | *Significance F (Probablity Level)* |
|---|---|---|---|---|---|
| Regression | 3 | 23157,93325 | 7719,311 | 32,0943126 | 1,93417E-11 |
| Residual | 47 | 11304,42098 | 240,5196 | | |
| Total | 50 | 34462,35423 | | | |

Table 4.82 Coefficients of equation

| | *Coefficients* | *Standard Error* | *t Stat* | *P-value* |
|---|---|---|---|---|
| Intercept | -721,9811169 | 156,2447483 | -4,62083 | 2,993E-05 |
| Dry density (g/cm$^3$) | 0,044492034 | 0,008673995 | 5,129359 | 5,4247E-06 |
| Water absorption (%) | 208,8054418 | 48,99777247 | 4,261529 | 9,6845E-05 |
| Ultrasonic velocity (m/s) | 19,74915268 | 7,271573547 | 2,715939 | 0,00921794 |

Table 4.81 shows the analize of variances and detailed coefficients of equation cen be seen in the table 4.82.

The equation of this analyses is :

B. T. S. $= -721{,}98 + 0{,}04\ \delta_{dry} + 208{,}81\ W_{abs.} + 19{,}75$ U. V.

B. T. S. is the Brazillian tensile strength, $\delta_{dry}$ : Dry density, $W_{abs.}$ : Water absorption, U. V. : ultrasonic velocity.

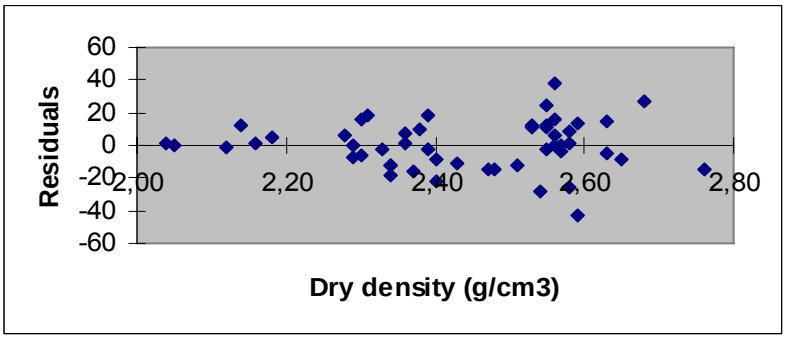


Figure 4.66 Dry density residual plot

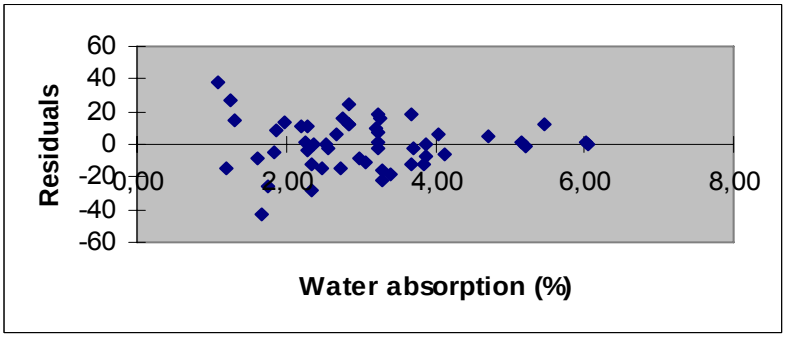


Figure 4.67 Water absorption residual plot

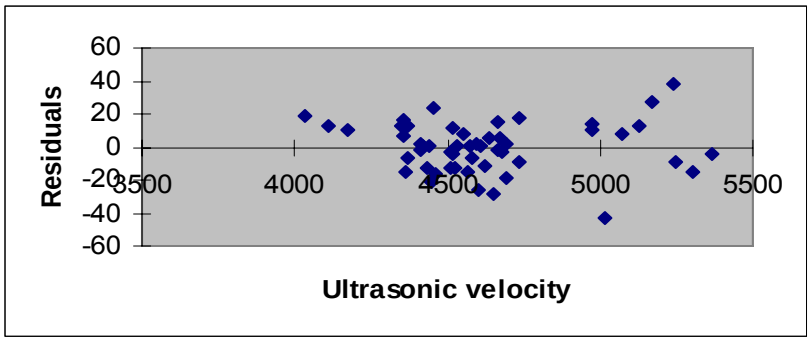


Figure 4.68 Ultrasonic velocity residual plot

The three figures (4.66, 4.67 and 4.68) in the above are shows the dry density –, water absorption –, ultrasonic velocity residuals plot for the samples of uniaxal compressive test, respectively.

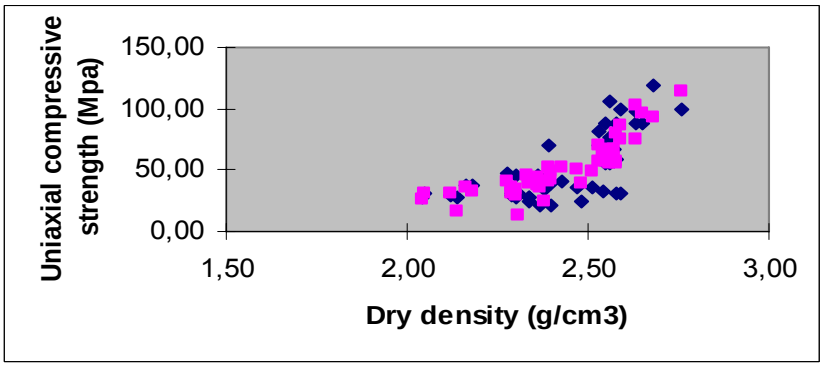


Figure 4.69 Dry density line fit plot

Blue data labels represents uniaxial compressive strength values obtained from equation. Pink data labels represents predicted uniaxial compressive strength values.

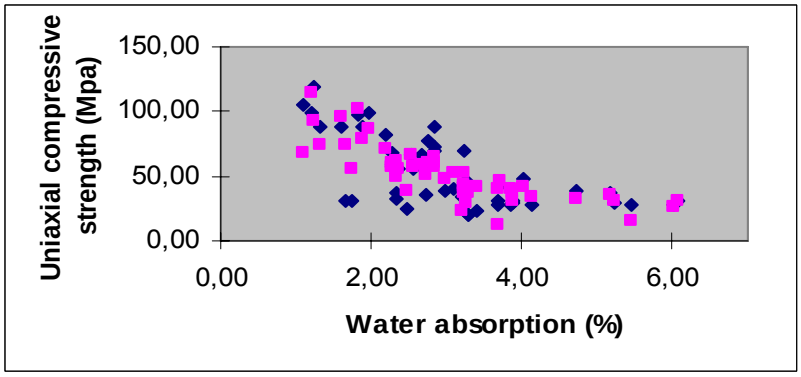


Figure 4.70 Water absorption line fit plot

Blue data labels represents uniaxial compressive strength values obtained from equation. Pink data labels represents predicted uniaxial compressive strength values.

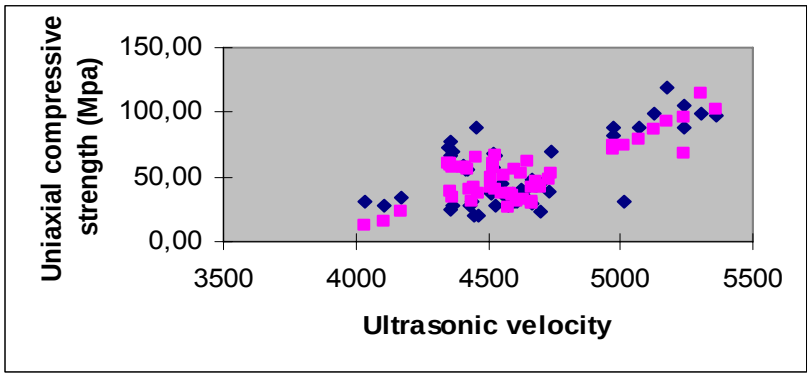


Figure 4.71 Ultrasonic velocity line fit plot

Blue data labels represents uniaxial compressive strength values obtained from equation. Pink data labels represents predicted uniaxial compressive strength values.

The three figures (4.69, 4.70 and 4.71) in the above are shows the dry density – water absorption – ultrasonic velocity line fit plot with the uniaxial compressive strength, respectively.

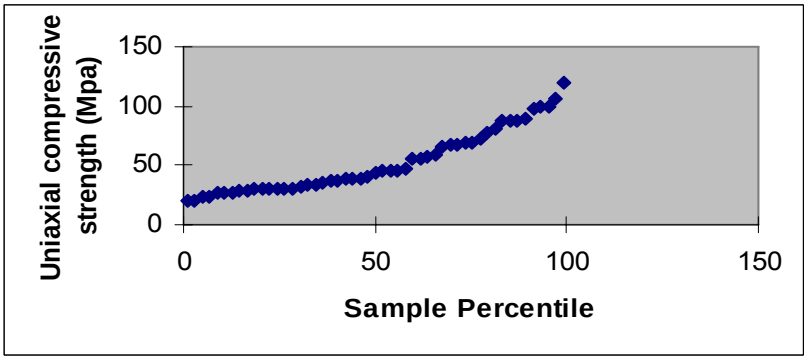


Figure 4.72 Normal probability plot

Figure 4.72 shows the normal probability plot with a uniaxial compressive strength – sample percentile diagram.

### 4.6.4. Multiple regression analysis for ultrasonic velocity versus dry density and water absorption for samples of uniaxial compressive test

Table 4.83 Regression Statistics

| | |
|---|---|
| Multiple R | 0,54838418 |
| $R^2$ | 0,30072521 |
| Adjusted $R^2$ | 0,27158876 |
| Standard Error | 258,068761 |
| Observations | 51 |

For this multiple regression analyses, $R^2$ is determined as 0,30 from the test results and also other values are also given in table 4.83.

Table 4.84 Analize of variance

| | *Df (Degree of Freedom)* | *SS (Sum Of Squares)* | *MS (Men Square)* | *F* | *Significance F (Probablity Level)* |
|---|---|---|---|---|---|
| Regression | 2 | 1374782,74 | 687391,4 | 10,32127 | 0,000186874 |
| Residual | 48 | 3196775,31 | 66599,49 | | |
| Total | 50 | 4571558,049 | | | |

Table 4.85 Coefficients of equation

| | *Coefficients* | *Standard Error* | *t Stat* | *P-value* |
|---|---|---|---|---|
| Intercept | 8994,13252 | 2252,656088 | 3,992679 | 0,000223 |
| Dry density (g/cm$^3$) | -1394,83674 | 790,0885142 | -1,76542 | 0,083854 |
| Water absorption (%) | -319,134748 | 111,8901513 | -2,85221 | 0,006386 |

Table 4.84 shows the analize of variances and detailed coefficients of equation cen be seen in the table 4.85.

The equation of this analyses is :

$$U.V. = 8994{,}13 - 1394{,}84\ \delta_{dry} - 319{,}13\ W_{abs.}$$

U. V. is the ultrasonic velocity, $\delta_{dry}$ : Dry density, $W_{abs.}$ : Water absorption.

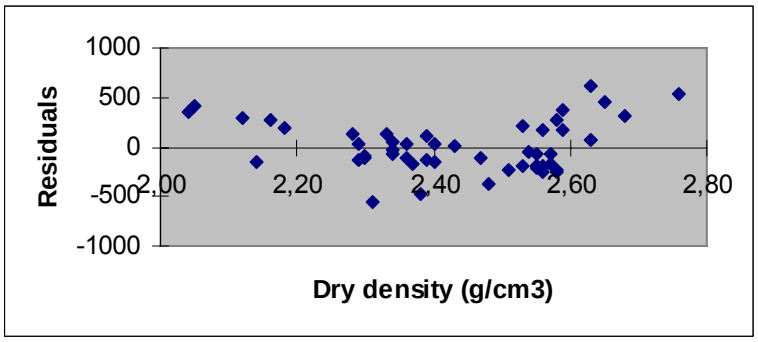


Figure 4.73 Dry density residual plot

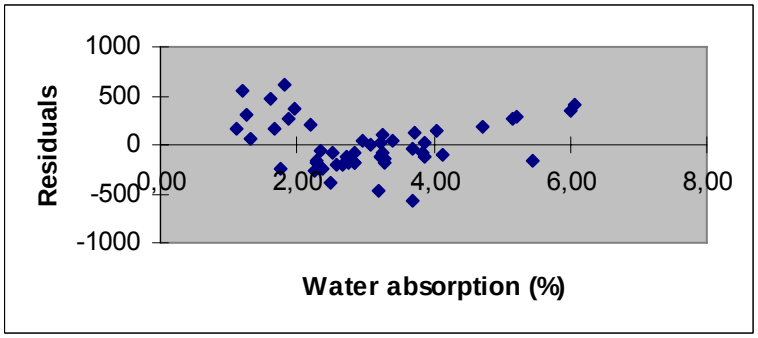


Figure 4.74 Water absorption residual plot

The two figures (4.73 and 4.74) in the above are shows the dry density –, water absorption residuals plot for the samples of uniaxial compression test, respectively.

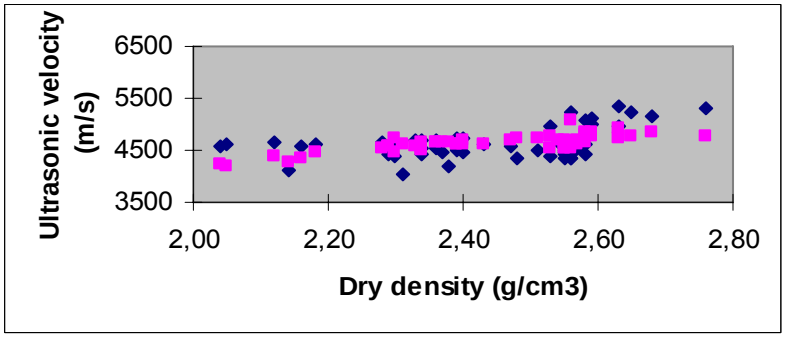


Figure 4.75 Dry density line fit plot

Blue data labels represents ultrasonic velocity values obtained from equation.
Pink data labels represents predicted ultrasonic velocity values.

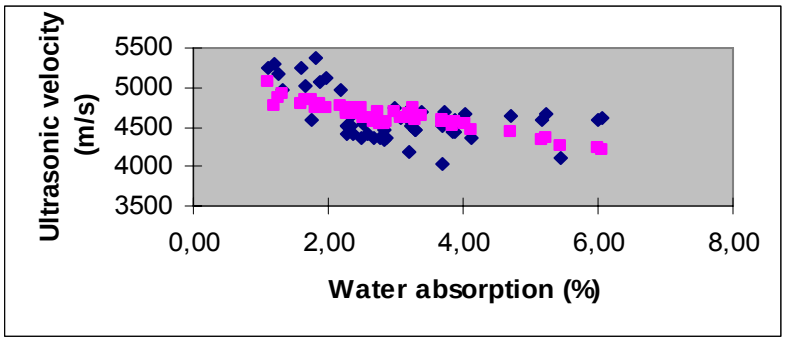


Figure 4.76 Water absorption line fit plot

Blue data labels represents ultrasonic velocity values obtained from equation.
Pink data labels represents predicted ultrasonic velocity values.

The two figures (4.75 and 4.76) in the above are shows the dry density – water absorption line fit plot with the ultrasonic velocity for samples of uniaxial compression test, respectively.

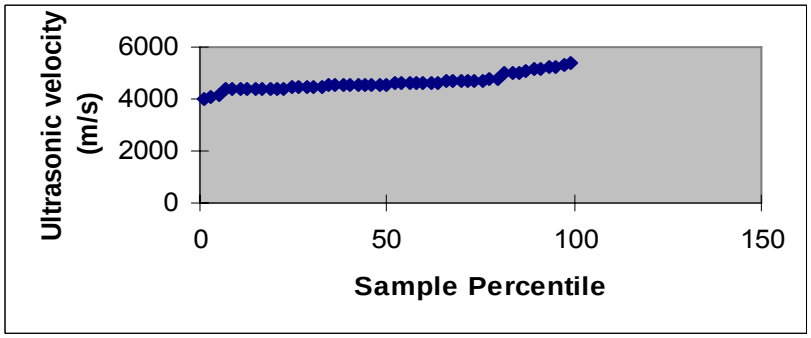


Figure 4.77 Normal probability plot

Figure 4.77 shows the normal probability plot with a ultrasonic velocity – sample percentile diagram for the samples of uniaxial compression test.

# CHAPTER 5

# DISCUSSION

## 5.1. Introduction

In this chapter obtained values are compared to literature values with their reasons to investigate that they are confidental or not.

## 5.2. Review The Obtained Results Based on The Literature Survey

In this study; Indirect (Brazillian) tensile strength-, uniaxial compressive strength-, Shear strength- ultrasonic velocity of Basalt graphics were found using dry cylindrical specimens with the same orientation. Also, index parameters such as dry density, bulk density, water absorbtion and saturated density were determined.

The presence of the vesicles could have caused scatter of the ultrasonic velocity, varying its velocity in all the samples and causing high scattering. It is observed that, for porous igneous rock strength values also decrease linearly with increasing vesicles [31].

The results of this study also demonstrated that ultrasonic velocity is sensitive to changes in vesicles [36]. The longitudinal velocity under dense conditions was always higher than the velocity under porous conditions, in all dimensions. It can be easily said that ultrasonic velocity is not dimension dependent

It was established that the uniaxial compressive strength and Brazillian tensile strength in basalt increase with increasing ultrasonic velocity because of the effect of

pores on the mechanical properties (uniaxial compressive stength, Brazillian tensile strength and young's modulus) and the physical properties (dry density, saturated density, water absorbtion amd saturated density) [1].

It was also established that the parameters dry and saturated density in basalt increase with increasing ultrasonic velocity. Water absorption is inversely related to ultrasonic velocity. The ultrasonic velocities decreased as the water absorption increased. because of the effect of the pores on the physical properties (dry density, saturated density, water absorption) [1].

Bulk density is also increase with increasing ultrasonic velocity. This can be explained by the bulk density changes through changing the amount of air space between the particles of the dry matter and water. Bulk density is increased (greater mass per volume) through compaction (squeezing the particles together as in a bale of hay) or through particle size reduction (allowing smaller particles to fit closer together as in chopping corn) or by increasing the moisture content (filling the air spaces with water). Bulk density is reduced (lesser mass per volume) by adding air space such as fluffing (using a bale buster on the hay) or removing the water through drying [1].

Some basalts' vesicles are filled with calcite and calcite have almost the same ultrasonic velocity value with the basalt [38, 47].

### 5.3. Comparison Literature Values With Obtained Values in This Study

In this section literature values of basalt and Gazianep basalt were compared.

#### 5.3.1. Dry density values

In this thesis dry density of Gaziantep basalt's value was obtained as 2,05 g/cm$^3$ – 2,79 g/cm$^3$. To see the results are confidental or not, literature values are searched and compared to the our test results.

Literaure values:

- Dry density Michigan basalt 2,70 g/cm$^3$ [52].
- Dry density Colorado basalt 2,62 g/cm$^3$ [52].
- Dry density Nevada basalt 2,83 g/cm$^3$ [52].
- Dry density China basalt 2,85 g/cm$^3$ [41].
- Dry density basalt 2,77 g/cm$^3$ [38].
- Mafic igneous rocks 3,00 g/cm$^3$ [47].

### 5.3.2. Bulk density values

In this thesis bulk density of Gaziantep basalt's value was obtained as 1,97 g/cm$^3$ – 2,75 g/cm$^3$. To see the results are confidental or not, literature values are searched and compared to the our test results.

Literaure value:

- Bulk density China basalt 1,70 g/cm$^3$ [41].

### 5.3.3. Water absorbtion values

In this thesis water absorption of Gaziantep basalt's value was obtained as 1,10 % - 6,22 %. To see the results are confidental or not, literature values are searched and compared to the our test results.

Literaure value:

- Water absorption China basalt 0,68 % [41].

### 5.3.4. Brazillian tensile strength values

In this thesis Brazillian tensile strength of Gaziantep basalt's value was obtained as 3,71 MPa – 13,16 Mpa. To see the results are confidental or not, literature values are searched and compared to the our test results.

Literaure values:

- Tensile strenght Michigan basalt 14,6 MPa [52].
- Tensile strenght Colorado basalt 3,2 MPa [52].
- Tensile strenght Nevada basalt 18,1 MPa [52].
- Tensile strength basalt 10 -30 MPa [47].

### 5.3.5. Direct shear strength values

In this thesis direct shear strength of Gaziantep basalt's value was obtained as 4,15 MPa – 15,91 MPa. To see the results are confidental or not, literature values are searched and compared to the our test results.

Literaure value:

- Shear strength basalt 20 - 60 MPa [47].

#### 5.3.5.1. Friction angle values ($\phi$)

In this thesis friction angle of Gaziantep basalt's value was obtained as 43° – 53,5°. To see the results are confidental or not, literature values are searched and compared to the our test results.

Literaure value:

- friction angle of basalt 50°-55° [21].

### 5.3.6.Uniaxial compressive strength values

In this thesis uniaxial compressive strenght of Gaziantep basalt's value was obtained as 20,45 – 119,37 MPa. To see the results are confidental or not, literature values are searched and compared to the our test results.

Literaure values:

Uniaxial compressive strenght Michigan basalt 120 MPa [52].
Uniaxial compressive strenght Colorado basalt 58 MPa [52].
Uniaxial compressive strenght Nevada basalt 48 MPa [52].
Uniaxial compressive strength basalt 100 MPa - 300 MPa [47].
Uniaxial compressive strenght basalt 42 MPa -355 MPa [22].

#### 5.3.6.1. Young's modulus values

In this thesis Young's modulus of Gaziantep basalt's value was obtained as 7,90 GPa – 18,08 GPa. To see the results are confidental or not, literature values are searched and compared to the our test results.

Literaure values:

Young's modulus of Michigan basalt 41 GPa [52].
Young's modulus of Colorado basalt 32,4 GPa [52]
Young's modulus of Nevada basalt 33,9 GPa [52].

### 5.3.7.Ultrasonic velocity values

In this thesis Ultrasonic velocity of Gaziantep basalt's value was obtained as 2939,8 m/s – 6478,3 m/s. To see the results are confidental or not, literature values are searched and compared to the our test results.

Literaure values:

Ultrasonic velocity of basalt 4500 m/s - 6500 m/s [52].
Ultrasonic velocity of basalt 6500 m/s - 7000 m/s [38].
Ultrasonic velocity of calcite 6600 m/s [38].

# CHAPTER 6

# CONCLUSIONS

## 6.1. Conclusion

Indirect (Brazilian) tensile strength, uniaxial compressive strength, Shear strength and ultrasonic velocity of Yavuzeli Basalt in Gaziantep were studied using dry cylindrical specimens with the same orientation. Also, index parameters such as dry density, bulk density, water absorption and saturated density were determined.

Obtained values for Gaziantep basalt are;

**1)** Dry density of Gaziantep basalt's value was obtained as 2,05 g/cm$^3$ – 2,79 g/cm$^3$.

**2)** Bulk density of Gaziantep basalt's value was obtained as 1,97 g/cm$^3$ – 2,75 g/cm$^3$.

**3)** Ultrasonic velocity of Gaziantep basalt's value was obtained as 2939,8 m/s – 6478,3 m/s.

**4)** Brazillian tensile strength of Gaziantep basalt's value was obtained as 3,71 MPa – 13,16 Mpa.

**5)** Direct shear strength of Gaziantep basalt's value was obtained as 4,15 MPa – 15,91 MPa.

**6)** Friction angle of Gaziantep basalt's value was obtained as 43° – 53,5°.

**7)** Uniaxial compressive strenght of Gaziantep basalt's value was obtained as 20,45 – 119,37 Mpa.

**8)** Young's modulus of Gaziantep basalt's value was obtained as 7,90 GPa – 18,08 GPa.

**9)** Water absorption of Gaziantep basalt's value was obtained as 1,10 % - 6,22 %.

It was established that the uniaxial compressive strength in basalt increase with increasing ultrasonic velocity, while the same effect of ultrasonic velocity on Brazilian tensile strength was present.

It was also established that the parameters dry and saturated density in basalt increase with increasing ultrasonic velocity.

Water absorption indices are inversely related to ultrasonic velocity. The ultrasonic velocities decreased as the water absorption increased. The coefficient of determination obtained in the graphics allowing us to state that the variation in velocity and water absorption is not very well.

The presence of the vesicles could have caused scatter of the ultrasonic velocity, varying its velocity in all the samples and causing high scattering. It is observed that, for porous igneous rock strength values also decrease linearly with increasing vesicles.

It is clear from these correlations that the effect of pores on the mechanical properties (uniaxial compressive stength, Brazillian tensile strength and young's modulus) and the physical properties (dry density, saturated density, water absorbtion and saturated density) is beyond dispute.

Some basalts' vesicles are filled with calcite and calcite have almost the same ultrasonic velocity value with the basalt. This influences the ultrasonic velocity of vesicular basalt filled with calcite. They behaves as a solid basalt as measured their ultrasonic velocities. However, calcites has no tensile or compressive strength capacity. This results; The correlation between uniaxial compressive strength and Brazillian strength or parameters between ultrasonic velocity is somewhat weaker in the graphics.

The results of this study also demonstrated that ultrasonic velocity is not sensitive to changes in vesicles of Gaziantep basalt. The longitudinal velocity under dense conditions was always somewhat higher than the velocity under porous conditions, in all dimensions. It can be easily said that ultrasonic velocity is not dimension dependent

The results of this study allow that lineer squared regression coefficients are low in most correlations.

The results of this study allow that lineer squared regression coefficients are low in most correlations.

The results of this study allow to state that the nondestructive method using ultrasound can not be used to reliably evaluate the mechanical properties of basalt with structural dimensions.

## 6.2 Recommendations for Future Work

Further investigation of this study is detailed correlations for obtained results. Additional to this study experiment will be performed using wet cylindrical specimens with the same orientation to see the effect of the moisture.

## REFERENCES


**1.** Al-Harthi, A.A., Al-Amri, R.M., Shehata,W.M. (23 March 1999) *The porosity and engineering properties of vesicular basalt in Saudi Arabia* .Department of Engineering Geology, Faculty of Earth Sciences, King Abdulaziz University, P.O. Box 1744, Jeddah 21441, Saudi Arabia.

**2.** Amadei B. and Robinson M. J. (1986). *Strength of rock in multiaxial loading conditions. In Proc*. 27th U.S. Symp. Rock Mech., Tuscaloosa, AL (Edited BY H. L. Hartman), pp. 47-55.

**3.** Atkinson R. H. and Ko H.-Y. A (1973). *Fluid cushion, multiaxial cell for testing cubical rock specimens.* Int. J. Rock Mech. Min. Sci. & Geomech. Abstr. Pp.10, 351-361.

**4.** Bell F.G., Haskins D.R. (1997). *A geotechnical overview of Katse Dam and Transfer Tunnel Lesotho, with a note on basalt durabilit.* Department of Geology and Applied Geology, University of Natal, Durban, 4041, South Africa. Engineering Geology 175 -198.

**5.** Bieniawski Z. T. (1968). *Propagation of brittle fracture in rock*. In Proc. 10th U.S. Symp. Rock Mech., Austin, TX (Edited by K. E. Gray), pp. 409-427.

**6.** Brace W. F. and Martin R. J. (1968). *A* test of the law of effective stress for crystalline rocks of low porosity. Int. J. Rock Mech. Min. Sci.pp.5, 415-426.

**7.** Brown E. T. (1974). *Fracture of rock under uniform biaxial compression*. In Proc. 3rd Int. Congr. Rock Mech., Denver, Vol. 2, pp. 111-117.

**8.** Brown, E. T. (1981). *Rock characterization testing and monitoring* ISRM suggested methods.Royal School of Mines. Imperial Colloge of Science and technology, London, England.

**9.** Çanakcı, H., Çabalar, A.F., Kılınç, E. (June 06-08-2002) *Geotechnical Properties of Yavuzeli Basalt Occuring in GAZİANTEP*, Harran University Faculty of Engineering, Proceedings of the Fourth GAP Engineering Congress Volume 2.

**10.** De Freitas, M. H. B.Sc., F.G.S. F. Blyth, G. H. Ph.D.,D.I.C., F.G.S. *A Geology for Engineers.* 6th edition Formerly Reader in Engineering Geology, Imperial College of Science and Technology, London Lecturer in Engineering Geology, Imperial College of Science and Technology, London. pp. 130 – 131, 148 – 149. 171 – 173, 189 – 191.

**11.** Dusseault M.B., Rothenburg L. and Mraz D. Z. (1987). *The desing of openings in saltrock using a multiple mechanism viscoplastic law.* Proc. 28th U.S. symp. Rock Mech., Tuscon, AZ (Edited by I. W. farmer, J.J.K. Daemen, C. S. Desai, C.E. Glass and S. P. Neuman ), pp. 633-642.

**12.** Friedman M., Handin J.,Higgs N.G. and Lantz J. R. (1979). *Strength and ductility of four dry igneous rocks at low pressures and temperatures to partial melting*. In. Proc. 20th U.S. Symp. Rock Mech., Austin, TX, pp. 35 – 43.

**13.** Freidman M., Handin J. and Bauer S. J. (1982). *Deformation mechanisms in granodiorite at effective pressures to 100 MPa and temperatures to partial melting* .In Proc. 23rd U.S. Symp. Rock Mech., Berkely, CA (Edited by R. E. Goodman and F. E. Heuze), pp. 279 – 290.

**14.** Garg S. K. and Nur A. (1973). *Effective stress laws for fluid-saturated porous rocks*. J. Geophys. Res.pp. 78, 5911-5921.

**15.** Goodman R. E. (1980). *Introduction to Rock Mechanics*, pp. 478. Wiley, New York.

**16.** Gupta A.S., Seshagiri K. R. (2000). *Weathering effects on the strength and deformational behaviour of crystalline rocks under uniaxial compression state* Department of Civil Engineering, Indian Institute of Technology Delhi, Hauz Khas, New Delhi 110016, India. Engineering Geology 56 257–274.

**17.** Herbert L. Brodie. (January-February 1997). *Extension Agricultural Engineer.* Biological Resources Engineering Topics bulk density measurements better compositing school greenhouse barns for dairy housing.

**18.** Hilsdorf H. K. (1965). *Die Bestimmung der zweiachsigen Festigkeit von Beton*. In Proc. Deutscher A+usschuss fur Stahlbeton, pp. 173.

**19.** Hoek, E., Marinos, P. and Benissi, M.(1998).*Applicability of the Geological Strength Index (GSI) Classification for Very Weak and Sheared Rock Masses*. The case of the Athens Schist Formation. 3034 Edgemont Boulevard, P.O.Box 75516, North Vancouver, British Columbia,Canada,V7R 4X1.

**20.** Hoek E. (1983). *Strength of jointed rock masses* – 23rd Rankine Lecture. Geotechnique pp.33, 187-223.

**21.** Housen, K. (Feb. 7-9, 2003). Effects *of Material Properties on Cratering* The Boeing Co. MS 2T-50 P.O. Box 3999 Seattle, WA 98124 *Bridging the Gap between Modeling and Observation* Lunar & Planetary Institute, Houston, TX pp.33.

**22.** Hudson, J. A. (Editor-in-Chief). (1993). *Comprehensıve Rock Engineering.* Principles, Practice & Projects Imperial College of Science, Technology & Medicine, London, UK Volume 3 Rock Testing and Sıte Characterization Imperial College of Science, Technology & Medicine, London, UK. pp. 73, 79.

**23.** Hudson J. A., Brown E. T. and Fairhurst C. (1971). *Shape of the complete stress-strain curve of the rock.* In Proc. 13th U.S. Symp. Rock Mech., Urbana, IL (edited by E. J. Cording), pp. 773-795.

**24.** Hudson J. A., Crouch S. L. and Fairhurst C. (1972). *Soft, stiff and servo-controlled testing machines: a review with reference to rock failure*. Eng. Geol. Amsterdam pp.6, 155 – 189.

**25.** Hudson J. A., (Editor-in-Chief). (1993). *Comprehensıve Rock Engineering.* Principles, Practice & Projects Imperial College of Science, Technology & Medicine, London, UK Volume 1 Rock Testing and Sıte Characterization Imperial College of Science, Technology & Medicine, London, UK. pp. 256 - 258.

**26.** Jaeger J. C. and Cook N. G. W. (1976). *Fundamentals of Rock Mechanics*, 2nd edn., pp.585 Chapman and Hall, London.

**27.** Johnson B., Freidman M., Hopkins T. W. and Bauer S. J. (1987). *Strength and microfracturing of Westerly granite extended wet and dry at temperatures to $800^0$ and pressures to 200 MPa*. In Proc. 28th U.S.Symp. Rock Mech., Tucson, AZ (Edited by I. W. Farmer, J. J. K. Daemen, C. S. Desai, C. E. Glass and S. P. Neuman), pp. 399 – 412.

**28.** Kjellman W. (1936). *Report on an apparatus for consummate investigation of the mechanical properties of soils*. In Proc. 1st Int. Conf. Soil Mech. Found. Eng., Boston, pp. 16-20.

**29.** Lama R. D. and Vutukuri V. S. (1978). *Handbook on Mechanical Properties of Rock,* Vol. 2, Trans. Tech., Berlin.

**30.** Lama R. D. and Vutukuri V. S. (1978). *Handbook on Mechanical Properties of Rock,* Vol. 4, Trans. Tech., Berlin.

**31.** Lumb, P., 1983. Engineering properties of fresh and decomposed igneous rocks from Hong Kong. Eng. Geol. 19,81-94.

**32.** Maso J. C. and Lerau J. (1980). *Mechanical behaviour of Darney sandstone in biaxial compression.* Int. J. Rock Mech. Min. Sci. & Geomech. Abstr. pp.17, 109-115.

**33.** Militky J., Kovacic V., Rubnerova J. (2002) *Influence of thermal treatment on tensile failure of basalt fibers* Faculty of Textile Sciences, Technical University of Liberec, Halkova 6, Liberec CZ 461 17, Czech Republic. Engineering Fracture Mechanics 69 1025 –1033.

**34.** Moore J. G. (30 May 2001). *Density of basalt core from hilo drill hole, Hawaii.*. US Geological survey. MS 910, 345 Middlefield Road. Menlo Park CA 94025, USA. Journal of Volcanology and Geothermal Research 221 – 230.

**35.** Obert L. and Duvall W. I. (1967).Rock *Mechanics and the design of structures in Rock*, pp. 650. Wiley, Newyork .

**36.** Oliveira, F. G. R., Candian, M., Francieli F. Lucchette, Salgon, J.L., Sales, A.(Mar. 2005). *Moisture content effect on ultrasonic velocity in Goupia glabra.* University of São Paulo, São Carlos SP, Brazil. Department of Civil Engineering, UFSCar, Federal University of São Carlos, São Carlos - SP, Brazil.

**37.** Pan Y., Christensen N. I., Batiza R., Coleman T.L. (1998). *Velocities of a natural mid – ocean ridge basalt glass.* Department of Geology and Geophysics, University of Hawaii, 2525 Correa Road USA. Tectonophysics. 171 – 180.

**38.** Richard E. Goodman. *Introduction to Rock Mechanics.* (1989). Second Edition University of California at Berkeley. pp. 33, 40 – 41.

**39.** Saliya S. S., Vutukuri V. S. and Lama R. D. (1974). *Handbook on Mechanical Properties of Rocks*, Vol. 1, Trans. Tech., Berlin.

**40.** Serafim J. L. (1979). Influence *of interstitial water on the behaviour of rock masses*. In Rock Mecchanics in Engineering Practice (Edited By K. G. Stagg and O. C. Zienkiewicz), pp. 55-97. Wiley, London.

***41.*** Shaopeng Wu, Yongjie Xue and Wenfeng Yang. *Experimental Evaluation of Stone Matrix Asphalt Mixtures Performance Using Blast Oxygen Furnace Steel Slag as Aggregate* The Key Laboratory of Silicate Materials Science and Engineering of Ministry of Education, Wuhan University of Technology, Wuhan 430070, Hubei, P. R China.

**42.** Stagg, K. G. and Zienkiewicz, O. C.. *Rock Mechanics in Engineering Practice.*Division of Civil Engineering, School of Engineering, University of Wales, Swansea. pp 113 – 114.

**43.** Stowe R. L. and Ainsworth D. L. (1968). *Effect of rate of loading on strength and Young's modulus of elasticity of rock*. In. Proc. 10th U.S. Symp. Rock. Mech., Austin, TX (Edited by K. E. Gray), pp 33-34.

**44.** Vutukuri V. S. and Lama R. D. (1978). *Handbook on Mechanical Properties of Rock,* Vol. 3, Trans. Tech., Berlin.

**45.** Weibull W. (1951).*A statistical distribution function of wide applicability*. J. Appl. Mech., pp.18, 293-297.

**46.** http://www.findstone.com/tibasalt.htm (arrival date : 15.05.2005)

**47.** http://geology.bgsu.edu/Onasch/GEOL_615/Some%20Useful%20Numbers.doc. (arrival date : 21.05.2005)

**48.** http://www.jktech.com.au/LabServices/ucs_tests.htm#results2
(arrival date : 06.06.2005)

**49.** http://manuals.dot.state.tx.us/dynaweb/colbridg/geo/@Generic__BookTextView/5105;cs=default;ts=default;pt=5105. (arrival date : 06.06.2005)

**50.** http://mta.gov.tr (arrival date : 21.06.2005)

**51.** http://www.rocscience.com/hoek/pdf/Chapter 4 of Rock Engineering.pdf (arrival date : 22.05.2005)

**52.** http://www.usace.army.mil/inet/usace-docs/eng-manuals/em1110-2-2901/c-8.pdf (arrival date : 15.06.2005)

**53.** http://users.ntua.gr/marinos/downloads/applicability.pdf (arrival date: 15.06.2005)